OPTOACOUSTIC FREQUENCY STABILIZATION OF A CARBON DIOXIDE LASER

A thesis presented for the Degree of Doctor of Philosophy
at the University of Keele

by

Mohammad Ibrahim Abdallah Abu-Taha, B.Sc.,M.Sc.

Department of Physics
University of Keele
Staffordshire, U.K.

June, 1987

In the name of Allah, the Beneficent, the Merciful.

بِسْمِ اللّٰهِ الرَّحْمٰنِ الرَّحِيْمِ ○

* 35. Allah is the Light of the heavens and the earth. The similitude of His light is as a niche wherein is a lamp. The lamp is in a glass. The glass is as it were a shining star. (This lamp is) kindled from a blessed tree, an olive neither of the East nor of the West, whose oil would almost glow forth (of itself) though no fire touched it. Light upon light, Allah guideth unto His light whom He will. And Allah speaketh to mankind in allegories, for Allah is Knower of all things.

اَللّٰهُ نُوْرُ السَّمٰوٰتِ وَالْاَرْضِ ؕ مَثَلُ نُوْرِهٖ كَمِشْكٰوةٍ فِيْهَا
مِصْبَاحٌ ؕ اَلْمِصْبَاحُ فِيْ زُجَاجَةٍ ؕ اَلزُّجَاجَةُ كَاَنَّهَا كَوْكَبٌ
دُرِّيٌّ يُّوْقَدُ مِنْ شَجَرَةٍ مُّبٰرَكَةٍ زَيْتُوْنَةٍ لَّا شَرْقِيَّةٍ
وَّلَا غَرْبِيَّةٍ ۙ يَّكَادُ زَيْتُهَا يُضِيْٓءُ وَلَوْ لَمْ تَمْسَسْهُ نَارٌ ؕ
نُوْرٌ عَلٰى نُوْرٍ ؕ يَهْدِى اللّٰهُ لِنُوْرِهٖ مَنْ يَّشَآءُ ؕ وَيَضْرِبُ
اللّٰهُ الْاَمْثَالَ لِلنَّاسِ ؕ وَاللّٰهُ بِكُلِّ شَيْءٍ
عَلِيْمٌ ۝٣٥

LIGHT

SŪRAH XXIV/35.

صَدَقَ اللّٰهُ الْعَظِيْمُ.
سورة النور ٢٤/الآية ٣٥.

* The English is a word by word translation of verse 35, Surah(24); reproduced from: The meaning of the glorious Qur'an, an explanatory translation by M. Pickthall, Taj Company, 3151 Turkman Gate, New Delhi, 1983.

Acknowledgements

The author would like to express his thanks to his supervisor, Dr. D.C. Lainé for his continuous encouragement, constructive guidance and useful suggestions throughout the period of study; Professor W. Fuller for the provision of the laboratory facilities; Mr. D. James of the University Workshop for the precise engineering in the construction of the laser system and accessories; Mr. M. Wallace and the Departmental Workshop staff for their technical help; Mr. B. Minshull and Mr. M. Davies for their assistance with electronic equipment; Mr. M. Daniels for the preparation of the photographs for this thesis; Mr. F. Rowerth, Mr. W. Robinson, Mr. S. Cartledge and the rest of the technical staff of the Physics Department for their assistance; Mr. C. Cork for the construction of the pyrex laser tubes; Mrs. K. Merifield for typing this thesis.

Thanks are also due to the administration of the College of Science and Technology at Abu Deis-Jerusalem, the Arab Student Aid International and the ORS Committees for their financial support, which made it possible for me to carry out this study. Special thanks must go to my parents and wife for their support.

Abstract

In this thesis a study has been made of the design, construction and, in particular, frequency stabilization of a d.c. excited carbon dioxide laser. The outline of the theory of the carbon dioxide laser is presented as a prelude to a detailed study of optogalvanic and optoacoustic effects. Experimental investigations have been made of both of these phenomena, and the results used for frequency stabilization of a conventional large tube diameter flowing gas type of carbon dioxide laser. A special feature of the work is intra-cavity optoacoustic detection of laser power by carbon dioxide gas absorption within the laser tube itself but outside the plasma region, for a new method of frequency stabilization. It is shown experimentally that this novel method is superior to the well established optogalvanic technique of frequency stabilization, in terms of signal to noise ratio and short response time.

Extension of the intra-cavity optoacoustic method to both d.c. and r.f. excited waveguide lasers is discussed.

CONTENTS

Chapter 1

Introduction

For many years carbon dioxide lasers have been a very useful tool in numerous applications. Their utility has been enhanced by the great number of spectral lines that support laser oscillations, as many as 590 lines in all, involving seven isotopic species (Freed, Bradley and O'Donnell 1980). In addition, other important beam properties, often shared with other types of lasers, are of interest too, such as monochromaticity, coherence, directionality, frequency tunability, power and ability to be focused to a very small spot.

Carbon dioxide lasers can be constructed in two forms: conventional and waveguide. The conventional laser dates from 1964 (Patel 1964B). The advent of waveguide lasers some time later (1971) has led to an increase in gain per unit length over conventional types, but high power is usually obtainable from the latter types. An important feature of waveguide lasers is their frequency tunability (Abrams 1972; Degnan 1973; Degnan 1976 and Lyszyk, Herlemont and Lemaire 1977).

In many applications it is necessary that the laser is frequency stabilized. For example, in optically pumped far infrared lasers (Busse, Basel and Pfaller 1977 and Boscolo, Passaseo and Bernardini 1986) it is essential to use a frequency stabilized CO_2 laser. Likewise, far infrared generation using metal-insulator-metal (MIM) diodes (Hocker, Sokoloff, Daneu, Szoke and Javan 1968) require two frequency stabilized lasers for reliable power mixing. In trace gas analysis (Shtrikman and Slaltkine 1977) with its capability of detecting absorptions as small as 3×10^{-10} cm^{-1}, frequency stable lasers should be used. Low pressure, highly stabilized CO_2 lasers have been used as an absolute frequency

reference grid in the 28 THz range (Clairon, Lerberghe, Brêant, Salmon, Camy and Bordé 1981). By locking two lasers oscillating at two adjacent line wavelengths, whose radiation output is readily absorbed by a heavy molecule such as OsO_4 and subsequent mixing the two laser beams on a MIM diode it is possible to determine the exact difference in frequency between the two lines. These are just a few examples of important applications of frequency stabilized CO_2 lasers.

Frequency stabilization is one of the most difficult problems facing laser researchers. As an example, consider a carbon dioxide laser oscillating on the P(20) line of the ($00^0 1$-$10^0 0$) branch with a cavity length of 1.8 m. This length should be kept constant within 0.06 μm for its frequency to be constant within 1 MHz (see Chapter 7, eqn. 7.2). This is not a trivial problem, since the CO_2 laser needs an accurate and complete control of all the parameters involved in laser action, together with cavity length stabilization and control of environmental conditions as well.

Existing methods of frequency stabilization can be divided into two categories. The first category includes schemes that employ gas absorption in a cell placed either externally (for example Ouhayoun and Bordé 1977) or internally (for example Kunikane, Ohtsu, Nakamura and Tako 1984) with respect to the laser cavity. The second category monitors variations of the laser power directly, e.g. by the use of a pyro-electric detector. In the following, examples of some techniques employed in laser frequency stabilization will be presented. One of the early techniques used was the saturated fluorescence method, in which a cell containing CO_2 is placed in the laser cavity at pressures within the range 0.005-0.8 torr (Freed and Javan 1970). The intensity of 4.3 μm fluorescence radiation from the $00^0 1$ level to the ground state was then monitored through a sapphire window in the cell side using a liquid nitrogen cooled InSb detector. This is

quite a sensitive method, but is rather awkward and is also expensive. Goldberg and Yusek (1971) have used the inverted lamb dip method with an extra-cavity SF_6 absorption cell for laser frequency stabilization. Frequency modulation was achieved by doppler 'dithering' of the laser beam employing an external moving mirror after which it enters the absorption cell, thereby avoiding internal frequency modulation of the laser. Their result was a 53 kHz drift in 15 min. Saturated absorption stabilization in SF_6 achieved three parts in 10^{11} stability (Ouhayoun and Bordé 1977). In an absorption cell many techniques are available for the purpose of stabilization, e.g. via Stark resonances detected using a pyro-electric detector (Hall, Jenkins and Gorton 1978; Okajima, Yamanaka, Nishizawa, Makino, Kondo, Kon and Fujita 1985 and Nussmeir and Abrams 1974). An advantage can be gained by Stark cell stabilization where the modulation can be applied to the Stark cell rather than to the laser (Nussmeir et al. 1974 and Okajima et al. 1985). A stability better than ± 100 kHz was possible with gas Stark cell stabilization (Nussmeir et al. 1974). A more direct method involves detection of gas absorption in a cell without the Stark electrode, again using a pyro-electric detector (Mingozzi and Tonelli 1977). A further technique is to use a microphone to detect absorption in an external optoacoustic cell (Kavaya, Menzies and Oppenheim 1983). This method achieved a long term frequency drift of ±1 MHz. Lamb dip stabilization using optoacoustic detection has been used by Souilhac and Gundjian (1982). Using a molecular beam, narrow spectral lines have been obtained (~23 kHz) through the reduction of the first order doppler width of the spectral lines, especially using the technique of optical Ramsey fringes at 10.6 μm. This approach employs a supersonic seeded beam of 7% SF_6 in He, illuminated by a CO_2 laser radiation in spatially separated field zones (Bordé, Avrillier, Lerberghe, Salmon, Bassi and Scoles 1981). High frequency stability can be obtained by frequency locking a

CO_2 laser to the peak of the central fringe of the Ramsey pattern.

Simpler, less precise methods that do not involve an external cell include detection of the frequency dependent power variation using a thermopile power meter (Lund, Cogan and Davis 1979) or using a pyro-electric detector for more sensitive monitoring of laser power variations (Shanahan and Heckenberg 1984). These two experiments gave a result of ±3 MHz and ±2 MHz respectively. One of the widely used methods is opto-galvanic (OG) frequency stabilization in which variations in the laser tube impedance are used to fingerprint CO_2 gas resonances within the plasma tube. A long term stability of ±1 MHz has been achieved (Moffatt and Smith 1981) and even a stability of ± 50 kHz/h drift has been claimed by Skolnick (1970).

Every stabilization method has its own limitations and problems. For example in methods where an expensive pyro-electric detector is used, the cost may be too high and the experimentor is faced with the problems of cooling or burning out of expensive detectors. Other methods necessitate alignment and the need for expensive optical components and windows, especially in gas absorption systems. Intensity fluctuations can be problematic in methods relying on fluorescence intensity detection. Even the accurate technique of Lamb dip stabilization suffers from the fact that the centre of the gas resonance is subject to pressure shifts, or, if detected in a discharge tube, the dip centre might shift in frequency because of the ambipolar field set up as a result of the difference between electron and ion mobilities (Wallard 1973). In most of the above mentioned frequency stabilization systems the frequency stability is ~±1 MHz, so it is worthwhile looking for a yet more conventional approach. Apart from the OG method all the above techniques mentioned so far involve windows and detectors with the latter often of a special type. This makes frequency stabilization techniques not only expensive but also introduces

practical problems associated with the alignment of the laser beam with a gas absorption cell as mentioned in the examples given above. This makes the task of manufacturing a compact frequency stabilized laser system difficult. The optogalvanic method has proved to be an inexpensive and simple approach to CO_2 laser frequency stabilization in respect of the fact that no addition need be made to the plasma tube, apart from the necessary optogalvanic sensing circuit. This method, however, does have its problems. Firstly the OG signal is often detected with difficulty due to the fact that the plasma is sustained by a high value of D.C. voltage. Secondly, even in the absence of laser oscillations, plasma fluctuations produce electrical noise. Thus although optogalvanic signals are of large amplitude, they are also rather noisy (Moffatt et al. 1981). This necessitates a larger modulation depth to give a satisfactory signal to noise ratio in a frequency stabilization system. Frequency modulation, in turn, causes spectral broadening of the CO_2 laser power output. In addition to the above mentioned problems, harmonics of the mains electrical supply can be quite strong, and contribute to the average noise level.

Although the OG technique (and its variations) has been considered to be the most convenient method in practice for CO_2 laser frequency stabilization, its limitations in the area of signal to noise ratio indicates a need for a new approach. Any alternative technique should be simple, inexpensive and should offer a better electrical performance. It should also offer a compactness comparable to the OG method. The approach taken in this thesis is that of using optoacoustics. It is possible to detect the optoacoustic signals created by laser beam absorption using a microphone placed outside the plasma region, although within the laser tube itself. This technique will be shown to be simple, avoids discharge noise, and needs no additional optical components. Signal detection and processing, in common with the OG method, is of course still necessary.

This thesis is concerned with the problem of frequency stabilization of CO_2 lasers, including both conventional and waveguide types. Before a detailed discussion of each system is undertaken a brief resume is given of the theoretical background of CO_2 lasers in general in Chapter 2. The constructional and experimental details of both conventional and waveguide lasers are outlined in Chapter 3. A brief study of the optogalvanic effect is given in Chapter 4 and the theory of the optoacoustic absorption method given in Chapter 5. In this same chapter, details of optoacoustic cells used in the study of this thesis and ultimately in an operational frequency stabilization scheme are given. In Chapter 6 a comparison is made between optogalvanic and optoacoustic (OA) methods. The frequency stabilization of the conventional CO_2 laser is given with examples of successful results in Chapter 7 comparing optogalvanic and optoacoustic approaches. In Chapter 8, the last Chapter, conclusions stemming from the work carried out to date are presented and work suggested for the future is put forward.

This thesis is concerned with the problem of frequency stabilization of CO_2 lasers, including both conventional and waveguide types. Before a detailed discussion of each system is undertaken a brief resume is given of the theoretical background of CO_2 lasers in general in Chapter 2. The constructional and experimental details of both conventional and waveguide lasers are outlined in Chapter 3. A brief study of the optogalvanic effect is given in Chapter 4 and the theory of the optoacoustic absorption method given in Chapter 5. In this same chapter, details of optoacoustic cells used in the study of this thesis and ultimately in an operational frequency stabilization scheme are given. In Chapter 6 a comparison is made between optogalvanic and optoacoustic (OA) methods. The frequency stabilization of the conventional CO_2 laser is given with examples of successful results in Chapter 7 comparing optogalvanic and optoacoustic approaches. In Chapter 8, the last Chapter, conclusions stemming from the work carried out to date are presented and work suggested for the future is put forward.

Chapter 2

Theoretical background of the CO_2 laser

2.1 Introduction:

To have a laser system that emits at wavelengths of a few microns, atomic systems should in general be avoided (Patel 1968). To achieve such wavelengths, the atoms have to be excited to energy levels very close to the onset of ionization which results in low energy and quantum efficiencies. The former quantity is the capability of the laser system to convert the input energy into laser power. The latter quantity, defined as $(E_u - E_L)/E_u$ in a laser system, where E_u is the energy of the upper laser level and E_L the energy of the lower laser level, does not normally reach a high value in a laser system. In CO_2 lasers the theoretical quantum efficiency is equal to 38% while the practical energy efficiency is of the order 15-20% (Sasnett 1984). These efficiencies are high for CO_2 lasers, relative to lasers in general and are due to vibrational energy levels being close to the ground state which ensures efficient excitation. Following the first CO_2 laser to be operated (Patel 1964B), CO_2 laser systems have undergone many improvements either as a result of theoretical studies (Tychinskiĭ 1967 and Sobolev and Sokovikov 1967), or through experimental work (e.g., see Table 2.1). One particularly successful outcome has been the development of the waveguide lasers (Bridges, Burkhardt and Smith 1972 and Ioli, Morruzzi and Strumia 1980). In this Chapter the basic theory of CO_2 lasers will be discussed. A brief introductory account of waveguide lasers is also given.

2.2 Vibrational-rotational levels of the CO_2 molecule:

Carbon dioxide is an asymmetric triatomic molecule with three degrees of freedom v_1, v_2 and v_3 (Patel 1968). As Fig. 2.1 shows, v_1 represents the symmetrical vibration, v_2 the asymmetric bending and finally v_3 the asymmetric stretch mode. So the state of the molecule can be described by $CO_2(v_1, v_2, v_3)$. A transition from $CO_2(000)$to the upper laser level $CO_2(00^01)$ is equivalent in energy to 2349.3 cm^{-1}. Other situations are shown on the energy level diagram of Fig. 2.2 (Lengyel 1971). The transition (10^00)-(00^00) is forbidden in the infrared region of the spectrum, but can be detected in the Raman spectrum (Sobolev et al. 1967). The transition of the (01^10) and (00^01) levels to the ground state (000) occur at 15.6 μm and 4.3 μm respectively. It should be mentioned that the possibility of a Fermi resonance between the (10^00) and (02^00) levels will result in a reduction of the separation between (01^10) and (02^00) levels to 618 cm^{-1} instead of 667 cm^{-1} (Sobolev et al. 1967). Each vibrational level has sub-rotational levels and as far as selection rules are concerned, vibrational-rotational transitions occur according to the following rules (Lengyel 1971): $\Delta v=0$, no change in vibrational state; pure rotational spectrum; $\Delta v=1$, molecular excitation to another vibrational-rotational level; $\Delta v=-1$ emission of radiation as one of the vibration-rotation spectra. The rotational quantum number (J) follows the selection rules: $\Delta J=1$, rotation from the P-branch band; $\Delta J=0$*, rotation from the Q-branch band; $\Delta J=-1$, rotation from the R-branch. Usually the line is related to the J value of the lower level. For example a transition from the J'=10 to J=11, with the latter associated with the lower vibrational level, will be called P(11).

---

* This is a forbidden transition (Patel 1964A).

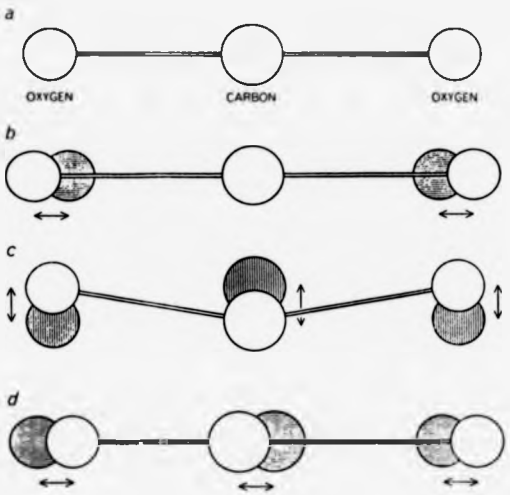

Fig. 2.1 : Schematic diagram to show the 3-degrees of freedom of the CO_2 molecule (a) CO_2 asymmetric linear
(b) Symmetrical vibration (v_1)
(c) Asymmetrical bending (v_2)
(d) Asymmetric sketch (v_3)
(After Patel 1968).

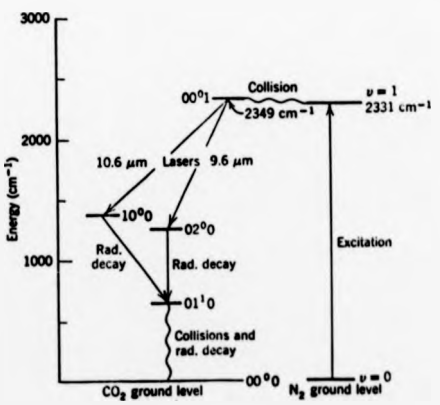

Fig. 2.2 : Energy level diagram of CO_2 and N_2 molecules
(After Lengyel 1971).

2.3 Requirements for the laser medium:

In this section the requirements for the molecular laser medium are discussed and wherever possible examples concerning the CO_2 laser will be given.

2.3.1 General considerations:

High working efficiency can be ensured if the laser medium satisfies certain conditions. Tychinskiĭ (1967) in his review of powerful gas lasers applied the conditions proposed by Gould (1965) for atomic lasers to molecular gas lasers. The upper laser level lifetime is assumed to be long, say $\sim 10^{-4}$ s, compared with that of the lower laser level which should be an order of magnitude smaller, say $\sim 10^{-6}$ s, to ensure a high level of population inversion. Good laser media have a high stimulated emission probability of the order $\bar{P}/Nh\nu \geq 10^5\ s^{-1}$, where $\bar{P}$ is the generated power density, N the population of the upper laser level and $h\nu$ is the transition energy which is related to the saturation flux I_s by the formula (Hotz and Austin 1967):

$$\sigma \tau I_s = h\nu \qquad (2.1)$$

where σ is the stimulated emission cross-section, τ is the inversion rise time which is inversely proportional to the pressure of the active medium (Hocker, Kovacs, Rodes, Flynn and Javan 1966). As the carbon dioxide pressure is increased, a high saturation flux is needed to achieve the same population at the new pressure. It is useful to know (Hotz et al. 1967) that:

$$I_s \tau = \text{constant} \qquad (2.2)$$

for all tubes having gain at a wavelength of 10.6 μm. This implies that as I_s is increased, τ is decreased, i.e. the population required for laser

operation is obtained in a shorter time. For a tube 12 mm diameter and 1 m long at a total pressure of 20 torr of gas mixture (N_2-He-CO_2), τ was found ~ 0.3 ms and $\sigma \sim 3 \times 10^{-18}$ cm^2. The knowledge of σ and the inversion density (N_1) gives an estimate of the output power, P_{out}, proportional to $N_1 \sigma$. For the upper laser level it should not decay greatly by inelastic collisions with molecules in the system or with the walls of the container (Tychinskiĭ 1967). The lower laser level should be depleted quickly so as to be ready for upper state laser excitation. If these levels lie close to the ground state, it is difficult for depletion to occur by radiative decay and they will only be depleted by inelastic collisions at a colliding particle potential energy of $\Delta E \leq kT_{gas}$. The rotational energy is given by the formula (Herzberg 1945):

$$E_r = hc\, F(J) \tag{2.3}$$

where F(J) is the rotational term given by:

$$F(J) = B\, J(J+1) \tag{2.4}$$

Here J is the rotational quantum number and B is the rotational constant equal to:

$$B = \frac{h}{8\pi^2 cI} \tag{2.5}$$

where I is the moment of inertia of the molecule about the axis of rotation and c is the speed of light. At room temperature ($300^{o}K$ ~ 208 cm^{-1}) most of the molecules are expected to be in the ground vibrational level (v=0) (Lengyel 1971). This is not the case for rotational levels as they are more closely spaced; some will be expected to be occupied, especially those in the ground vibrational (v=0) level. At equilibrium, for a given vibrational level (v), molecules will be

distributed over the rotational levels according to the following relation (see, for example, Herzberg 1945 or Patel 1964A):

$$N_{v,J} = N_v(hcB/kT_r)(2J+1)\exp(-F(J)hc/kT_r) \qquad (2.6)$$

where T_r is the temperature of the rotational level which will be assumed to be equal to T_{gas} when the rotational levels are in thermal equilibrium. The question which may be asked is 'can thermal equilibrium between the vibrational levels be achieved?'. The thermal equilibrium lifetime t_{ther} for vibrational levels is about $\sim 10^{-3}$ s whereas for rotational levels of the same vibrational level the lifetime is of the order $\sim 10^{-7}$ s. From this large lifetime difference it can be concluded that there is a near thermal equilibrium within each vibrational level. For transitions to occur even at small optical gain from state n to m, the following condition must be satisfied (Lengyel 1971):

$$N_n/g_n > N_m/g_m \qquad (2.7)$$

where g_n, g_m are the respective statistical weights. Now consider the distribution of rotational levels in two vibrational levels v and $v' = v+1$. Here the distribution is exponential and is proportional to $g_n\exp(-E_n/kT)$ for state n. It is readily seen from Fig. 2.3 that the population of J=19 in level (00^01) is larger than the population of J=20 in level (10^00) and the transition condition given by Lengyel (1971) is satisfied:

$$N_{v',J-1/2J-1} > \frac{N_{v,J}}{2J+1} \qquad (2.8)$$

This condition might be met even if there is no complete population inversion, or what is known as partial inversion. Using eqn. (2.6), condition (2.8) can be written as follows:

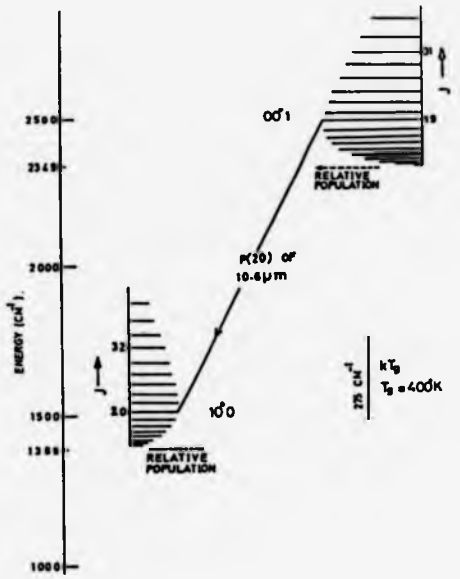

Fig. 2.3 : Sub-rotational level population of upper and lower laser levels
(After Patel 1971).

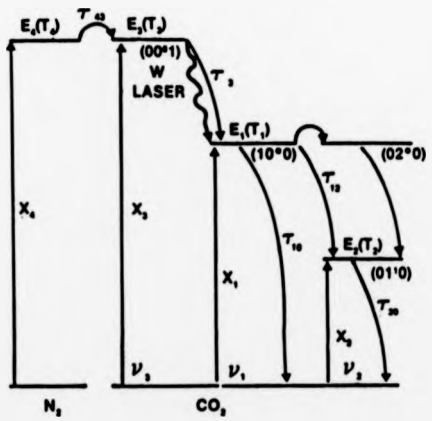

Fig. 2.4 : Energy level diagram showing the different excitation processes of CO_2 and N_2 molecules
(After Scott et al. 1984).

$$N_{v'} \exp\left[\frac{-F(J-1)hc}{kT_r}\right] > N_v \exp\left[\frac{-F(J)hc}{kT_r}\right] \qquad (2.9)$$

Assuming $\gamma = Bhc/kT_r$ and using eqn. (2.3) condition (2.9) leads to:

$$J > \frac{1}{2\gamma} \log_e \left(\frac{N_v}{N_{v'}}\right) \qquad (2.10)$$

This is true for all values of J in the case of complete inversion and some of the J states for partial inversion. Another important point is that this condition for the R and Q branches require complete inversion for gain, i.e. $N_{v'} > N_v$ (Patel 1964A). If $T_r = 400^oK$ then $kT_r \simeq 275\ cm^{-1}$ and $B_{00^0 1} = 0.3866\ cm^{-1}$ (Tychinskiĭ 1967). Assuming the measured value of $N_v/N_{v'} = 1.05$, substitution in condition (2.10) yields $J > 8$. For $N_v/N_{v'} = 1.1$, $J > 15$ and for $N_v/N_{v'} = 1.13$, $J > 19$, showing that as $N_{v'}$ becomes smaller than N_v, emission will occur at higher values of J. R-transition shows gain only for $N_{v'}/N_v > 1.02$ (Patel 1964A). It was reported (Crocker, Clack and Butcher 1981) that P(20) is the strongest line. In the case of full inversion it can be easily shown by differentiation of eqn. (2.6) that the optimum value of J (Tychinskiĭ 1967) is:

$$J_{opt} = 0.95\sqrt{T_{gas}} - \tfrac{1}{2}, \quad \text{at } T_{gas} \sim 400\ K;$$
$$J' = 19, \quad \text{i.e. the P(20) line.}$$

If the laser is cooled efficiently, low J value transitions are enhanced (Tychinskiĭ 1967).

2.3.2 Rate equations:

Recently Scott and Myers (1984) reported a model which can be used to predict the performance of a slow (or zero) flow CW CO_2 laser. In Fig. 2.4, E_1, E_2 and E_3 are the energy densities in the CO_2 symmetrical

stretching mode ($10^0 0$), the doubly degenerate bending mode ($02^0 0$) and the asymmetrical stretching mode ($00^0 1$), respectively. E_4 is the energy density in the N_2 stretching mode. This model was derived for the steady state situation based on the equation given by Manes and Seguin (1972) leading to the following set of equations:

$$N_e N_{CO_2} hf_1 X_1 - \frac{E_1 - E'_1(T)}{\tau_{10}(T)} - \frac{E_1 - E'_1(T_2)}{\tau_{12}(T_2)} + \left(\frac{hf_1}{hf_3}\right)\left[\frac{E_3 - E'_3(T,T_1,T_2)}{\tau_3(T,T_1,T_2)}\right] + hf_1 \Delta N W I_\nu = 0 \qquad (2.11)$$

$$N_e N_{CO_2} hf_2 X_2 + \frac{E_1 - E'_1(T_2)}{\tau_{12}(T_2)} - \frac{E_2 - E'_2(T)}{\tau_{20}(T)} + \left(\frac{hf_2}{hf_3}\right)\left[\frac{E_3 - E'_3(T,T_1,T_2)}{\tau_3(T,T_1,T_2)}\right] = 0 \qquad (2.12)$$

$$N_e N_{CO_2} hf_3 X_3 - \frac{E_3 - E'_3(T,T_1,T_2)}{\tau_3(T,T_1,T_2)} + \frac{E_4 - E'_4(T_3)}{\tau_{43}(T)} - hf_3 \Delta N W I_\nu = 0 \qquad (2.13)$$

$$N_e N_{N_2} hf_4 X_4 - \frac{E_4 - E'_4 (T_3)_3}{\tau_{43}(T)} = 0 \qquad (2.14)$$

$$-\frac{I_\nu}{\tau_c} + chf_L \Delta N(WI_\nu + S) = 0 \qquad (2.15)$$

where I_ν is the intracavity optical intensity, E_1, E_2, E_3, E_4, I_ν and the translational temperature T are six unknowns in five equations. Other quantities assumed known are: N_e, electron number density, N_{CO_2} and N_{N_2} are the densities of the molecular species CO_2 and N_2 respectively.

X_1, X_2, X_3 and X_4 are the excitation rates of the different vibrational modes as shown on Fig. 2.4. hf_1, hf_2, hf_3 and hf_4 are the energy spacings of the vibrational modes; and f_L the laser frequency. W in eqn. 2.15 is the stimulated emission rate at the line centre given by:

$$[\lambda_L^2 g(f)F]/8\pi hf_L \tau_{sp},$$

where g(f) is the line shape function; F the filling factor, or fraction of discharge volume filled by oscillating mode. T_1 ... T_4 are the effective temperatures of the corresponding vibrational modes; τ represents the various relaxation times discussed in the following section. Thus $\tau_3(T,T_1,T_2)$ signifies that τ_3 is a function of the unknown T, E_1 and E_2. The spontaneous emission term S in eqn. (2.15) can be neglected for CW lasers, so eqn. (2.15) becomes:

$$\frac{-1}{\tau_c} + chf_L W\Delta N = 0 \qquad (2.16)$$

where τ_c is the photon lifetime. At this stage another equation (the sixth) is needed to allow for the solution for the six unknowns using eqns. (2.11) to (2.14) with eqn. (2.16). This additional necessary equation can be the energy balance equation derived as follows. The electrical energy supplied will be consumed as heat dissipated via the laser walls and removed by laser tube cooling and through the gas flowing through the discharge tube. Some of the input power is also removed when excited molecules are swept out before they emit and finally some of the input power will be removed by the output coupled optical power. Using the above argument, the energy balance equation can take the form:

$$IV = \frac{48}{11}\pi kL(T_w-T_b) + \pi C_p \rho \mu R_d^2 (T_b-T_i) + \sum_{j=1}^{4} (E_j-\tilde{E}_i)(\pi R_d^2 \mu) + I_\nu A_m \left(\frac{L}{c\tau_c}\right) \qquad (2.17)$$

where:

k : thermal conductivity of the gas.

L : length of the discharge tube.

T_w : temperature of the laser tube wall.

T_b : bulk temperature of the gas.

C_p : specific heat of the gas at constant pressure.

ρ : density of the gas.

μ : gas flow velocity.

T_i : initial gas temperature.

R_d : discharge radius.

E_j : energy density in mode j after passing through the discharge.

$\tilde{E}_j$: initial energy density in mode j.

A_m : cross sectional mode area.

With eqn. (2.17), the model is complete and eqns. (2.11) to (2.14), (2.16) and (2.17) are now a complete set of six equations with six unknowns, E_1, E_2, E_3, E_4, I_ν and T, which can be solved to predict the performance of a carbon dioxide laser.

2.4 Vibrational relaxation times:

From Section 2.3 it is understood that it is most important for laser action, to populate the (00^01) level and avoid all processes that lead to a loss of molecules of the (00^01) level, other than via laser action. Furthermore, molecules should not be allowed to accumulate in the lower laser level (10^00). This latter level is worrying to laser researchers as it has previously been shown in Section 2.2 that the transition (10^00) to (000) is forbidden. Instead, the (10^00) level decays to the two levels (01^10) and (02^00). This will leave two levels to be considered which should be depleted quickly so that the molecules will be

ready for excitation to the $(00^0 1)$ level. Exact knowledge of the relaxation times of the different levels is vital for setting up the right conditions for laser action. Relaxation times used in the rate equations of Section 2.3.2 can be calculated from the formula of Manes et al. (1972) as follows:

$$\tau_{12} = \frac{1}{N_{CO_2} A_{12}} \left[\frac{\exp(hf_2/kT_2) - 1}{\exp(hf_2/kT_2) + 1} \right] \tag{2.18}$$

Here τ_{12} is the relaxation time associated with the transfer of energy between the CO_2 symmetric stretching mode and the bending modes; A_{12} is a constant, T_2 the effective temperature of CO_2 bending mode and hf_2 the quantum of energy of the bending mode. The relaxation time of the antisymmetric mode τ_3 is given by the following relation:

$$\tau_3(T,T_1,T_2) = \left[\exp(\frac{hf_1}{kT_1}) - 1 \right] \left[\exp(\frac{hf_2}{kT_2}) - 1 \right]$$
$$\left[N_{CO_2} A_3 (\exp(\frac{hf_1}{kT_1} + \frac{hf_2}{kT_2} + \frac{hf_3 - hf_2 - hf_1}{kT}) - 1) \right]^{-1} \tag{2.19}$$

where A_3 is a constant, T_1 the effective temperature of the CO_2 antisymmetric stretching mode, and N_{CO_2} the number of CO_2 molecules/cm^3; hf_1, hf_2 and hf_3 are the quantum energy of one symmetric stretching mode, bending mode and antisymmetric stretching mode, respectively. Taylor and Bitterman (1969) gave a relation from which the different relaxation times were obtained as function of temperature and pressure of the different CO_2 gas mixtures:

$$\tau_{ij}(T) = \left[N_{CO_2} k_{ij_{CO_2}}(T) + N_{N_2} k_{ij_{N_2}}(T) + N_{He} k_{ij_{He}}(T) \right]^{-1} \tag{2.20}$$

where k_{ij} is called the kinetic rate constant whose value is given for various ij values by Manes et al. (1972). Experimental measurements of the lifetimes of the $(00^0 1)$ and $(10^0 0)$ levels (Crafer, Gibson, Kent and

Kimmit 1969) gave values of (0.93 ± 0.05) ms and (90 ± 20) μs respectively. An estimation of these values by Tychinskiĭ (1967) was of the order of 1 ms and 0.3 ms respectively. Crafer et al. (1969) found that the addition of helium gas does not change the measured value of the (00^01) level lifetime significantly and that the N_2 - CO_2 transfer time was about 0.3 ms. Volume quenching of the (00^01) level as measured by Hocker, Kovacs, Rodes, Flynn and Javan (1966) was of the order 385 $s^{-1}mm^{-1}$ corresponding to a cross section of (3.3 ± 0.3) x 10^{-19} cm^2. They also found that molecules in the level (00^01) could be lost by collisions with the other molecules CO_2* (00^01) or N_2*(v=1) and the result led to the formation of CO_2*$(00v_3)$. Vibrational states up to v_3 = 4 were found to be populated. The time in which the (00^01) level could be excited again after it was depleted was of the order of 10^{-15} s (Sobolev et al. 1967). The question which should be asked at this stage is what happens to the other laser levels (10^00), (01^10) and (02^00)? At P_{CO_2} = 1 torr and operation at room temperature, the CO_2-CO_2 collision cross section is ~ 1.6 x 10^{-15} cm^2, i.e. a collision rate of ~ 1.15 x 10^7 s^{-1} (Sobolev et al. 1967). At least 5 x 10^2 collisions of molecules in the CO_2 (10^00) level with other molecules were needed to transfer these to the (01^10) level. Simple calculation gave a relaxation time of the (10^00) level of about 4.3 x 10^{-5} s. Sobolev and Sokovikov (1967) concluded from the measured collision rate of 1.15 x 10^7 s^{-1} at one torr pressure of CO_2 at room temperature, that molecules themselves were the main agents of the relaxation process from the lower laser level. The presence of CO at small pressures ~ 0.5 torr reduced the relaxation time to 4 x 10^{-6} s. This value was an order of magnitude smaller than for the calculated CO_2-CO_2 collision process. Also He in amounts similar to that of CO, and somewhat less in the case of H_2O, resulted in a decrease of relaxation times (Sobolev et al. 1967). It was necessary for the (01^10) level to be

depleted effectively, otherwise a decrease in the population inversion occurred as CO_2 molecules were expected to accumulate in this level (Patel 1968). The lifetime of this level was determined using the formula (Sobolev et al. 1967):

$$\frac{1}{\tau_{01^10}} = \frac{P_{CO_2}}{\tau_{CO_2\text{-}CO_2}} + \frac{P_{tot.} - P_{CO_2}}{\tau_{CO_2\text{-}M}} \qquad (2.21)$$

where $\tau_{CO_2\text{-}CO_2}$ gave the relaxation time as a result of collision of CO_2-CO_2 molecules. Here, $\tau_{CO_2\text{-}M}$ was the relaxation time as a result of a CO_2 molecule and an atom in the discharge. $P_{tot.} = P_{CO_2} + P_M$. In fact, N_2 at 2.5 torr was seen to lead to a decrease of relaxation time of the (01^10) level to $\sim 4 \times 10^{-5}$ s. NO or a CO introduced even at small pressures, also greatly reduced the relaxation time.

2.5 Laser action in pure CO_2:

Laser action in pure CO_2 gas was first reported by Patel (1964B) and later by Howe (1965) who found that in an electrical discharge it was possible to excite molecules to the vibrational level (00^01) and even to the higher equally spaced levels (00^0v_3) (Patel 1968). Following this, a collisional reaction of the form:

$$CO_2(00v_3) + CO_2(000) \rightarrow CO_2(00v_3\text{-}1) + CO_2(001),$$

was shown to be possible. It was not possible to rely on this reaction as a means of populating the upper laser level, since the highly excited electrons in the discharge were few. Dissociation of the CO_2 molecules was expected. As the dissociation energy of CO_2 was low (2.8 eV) an appreciable number of CO molecules were expected to be formed (Sobolev et al. 1967). These were shown to play a role similar to that of N_2 in CO_2 lasers, but with lower efficiency. This is due to the energy difference

between the vibrational level of CO and the upper laser level of CO_2 ~170 cm^{-1}, whereas for N_2 the difference is only ~18 cm^{-1}. The amount of CO molecules formed depends on the discharge parameters of pressure, discharge current, gas flow rate and presence of other gases within the discharge. Carbon dioxide dissociation ratios up to 85% can be expected (Smith 1969). High ratios of dissociation are harmful and may be reduced according to Smith (1969) by the addition of ~0.2 torr H_2O vapour. Attention should also be given to the lower laser level (100) and (020), since for effective laser action these must be depleted. Accordingly, the following reactions might be possible (Patel 1968):

$$CO_2(100) + CO_2(000) \rightarrow CO_2(010) + CO_2(010)$$

$$CO_2(010) + \text{foreign atom} \rightarrow CO_2(000) + \text{foreign atom} + \text{K.E.}$$

The last reaction is non resonant and can cause what Patel (1968) called a 'bottleneck' in the process of excitation-de-excitation in CO_2 lasers. Accumulation in the (010) level might arise if foreign atoms are not available.

2.6 Effect of other gases on laser performance:

Addition of other gases to the CO_2 laser often (but not always) influences the output power in a beneficial way (Patel 1965; Howe 1965 and Moeller and Rigden 1965). In this section the effect of other molecules such as N_2, He, CO, O_2, H_2O, air and other gases used experimentally by various researchers will be discussed.

N_2

Nitrogen is a diatomic molecule with one degree of freedom N(v=1) with an energy difference of 18 cm^{-1} from the $CO_2(00^01)$ level, so a collision with the two molecules will result in $CO_2(00^01)$ population.

Here, the collision is considered near-resonant (Patel 1964B). The nitrogen molecule has a zero permanent dipole moment so electric dipole radiation cannot occur. This means that all the excited N_2*(v=1) molecules participate in the CO_2 excitation process. In addition to the importance of nitrogen in level populating processes of the upper laser level, it also reduces the lifetime of the lower laser level. At P_{N_2} = 1 torr, N_2(v=1) has a lifetime ~14.5 - 16 ms (Tychinskiĭ 1967). P_{N_2} must be several times that of CO_2 in order that the outcome of the reaction:

$$CO_2 + N_2^* \rightleftarrows CO_2^* + N_2$$

will give high concentrations of CO_2* since the reaction is reversible (Tychinskiĭ 1967). The importance of N_2 in enhancing P_{out} has been confirmed experimentally by many researchers. For example Howe (1965) found that P_{out} was increased by a factor of three when N_2 was added. Furthermore, no nitrogen oxides were detected (Smith 1968).

He

It is known that helium can increase the diffusion time of CO_2 molecules to the container walls which is about 0.7 ms and therefore less than the radiative lifetime (Moeller and Rigden 1965). These authors also explained the importance of He in thermalization of the rotational levels of excited CO_2 molecules without de-exciting them, since He has a very good thermal conductivity (k) compared with other gases (Tychinskiĭ 1967): $k_{He} = 0.344 \times 10^{-3}$ cal $s^{-1}deg^{-1}$, $k_{N_2} = 0.057 \times 10^{-3}$ cal $s^{-1}deg^{-1}$ and $k_{CO_2} = 0.034 \times 10^{-3}$ cal $s^{-1}deg^{-1}$. Helium also assists the relaxation of the lower laser level to the ground state (Woods and Joliffe 1976). Patel et al. (1965) showed that the following reaction is expected:

$$He^*(2^3S_1) + 2N_2 \rightarrow He + 4N - \Delta E, \quad \Delta E < 0.1 \text{ eV}.$$

This means that this reaction is near-resonant. When nitrogen atoms recombine, a vibrationally excited N_2 molecule is formed in a high lying vibrational level. This decays via two processes:
(i) collision with another N_2 molecule which gains one quantum and the excited N_2 loses one; (ii) collision with a CO_2 molecule which consequently will be excited and $N_2^*(v)$ loses one quantum of vibrational energy.

CO_2-He mixtures gave more power than CO_2-N_2 mixtures in flowing gas systems and the best result was obtained with all three mixed together at the following pressures: 2.7 torr CO_2, 7.8 torr He and 3.5 torr N_2 (Moeller et al. 1965). P_{out} was found to be four times greater than the power with the CO_2-N_2 mixture.

H_2O

When water vapour was added to the laser mixture of CO_2-N_2-He at pressures lower than 9 torr total presure of the mixture, an increase in P_{out} by a factor of two to three times was gained for a partial pressure of water vapour of 0.25 torr. At higher pressures than this, H_2O proved to be harmful to laser operation (Smith 1969).

CO and O_2

As mentioned before the existence of CO can be beneficial; it plays a similar role to N_2, but with lower efficiency (see Section 2.5). However with the presence of N_2, CO de-excites $N^*(v=1)$, thereby decreasing the possibility of CO_2 excitation (Smith 1969). The existence of O_2 is not helpful at all. A pressure of 0.1 torr of O_2 will result in a reduction of between 10-15% of P_{out}. This was also confirmed by Howe (1965) who obtained a reduction of P_{out} by one half after adding O_2. Oxygen also excites CO_2 to the (10^00) and (02^00) levels and therefore

reduces the population inversion. At P_{O_2} = 1 torr the O_2(v=1) relaxation time is ~2.4 s (Tychinskiĭ 1967). In situations where the CO_2 dissociation is high with the presence of N_2, experimental solutions must be found to inhibit this, for example by increasing the rate of flow (Smith 1968) or by adding H_2 as suggested by Woods et al. (1976). Other techniques such as the introduction of a 12 cm platinum wire heated to 850°C in the discharge region acts as a catalyst in the reaction:

$$2CO + O_2 \rightarrow 2CO_2$$

which results in a decrease in CO_2 loss (Taylor, Lambert and Eppers 1967). Other gases were also tested, such as H_2, but without any change in P_{out} (Howe 1965). Howe (1965) also tested air which gave an increase in P_{out} by a factor of 2.6, N_2O gave a reduction by a factor of 0.5 and C_2H_2 or C_2H_4 was explained by Tychinskiĭ (1967) as being due to absorption of P_{out} at 10.6 μm which with the fact of its small vibrational relaxation time makes it act as a deactivating gas. Ar and Ne do not improve the performance of the CO_2-N_2 laser; in fact P_{out} decreases at P_{Ar} or P_{Ne} = 7 to 8 torr (Patel et al. 1965). Xe showed an effect of decreasing the electron temperature (Woods et al. 1976). Some of the above mentioned gases have an effect on the relaxation lifetimes of the CO_2 laser levels (see Section 2.4).

2.7 Waveguide CO_2 laser:

The idea for a waveguide laser was first proposed by Marcatili and Scheltzer (1964). Actual construction and operation was later carried out by Smith (1971) and Bridges et al. (1972) for a He-Ne and a CO_2 laser system, respectively. From the point of view of conventional lasers, Smith's resonator was unstable and laser action could be explained only in terms of waveguiding effects (Hall 1979). Since the gain per unit length

is proportional to the inverse of tube diameter, large gains can be obtained by using small bore discharge tubes (Smith 1971). Other properties, such as tunability, also provoked researchers to investigate the physics of waveguide lasers, because pressure line broadening permits a larger linewidth to be obtained than is possible with Doppler broadening alone, which leads to a greater range of tunability (Abrams 1974). In a gas discharge at $T = 400^{o}K$, pressure broadening of CO_2 is about 4.5 MHz per torr. So a pressure in the range 200-300 torr is needed for GHz tunability (Abrams 1974). In fact the increase in the gain from a waveguide laser is not due to the increase in pressure as this is compensated by pressure broadening linewidth (Bridges et al. 1972). It may be attributed to the associated temperature decrease since a reduction of $10^{o}C$ in waveguide laser temperature produced a 20% increase in P_{out} (Carter and Marcus 1979). The temperature gradient between the centre of gas and the inner wall of the optical waveguide is expected to be lower than in conventional lasers. Even in waveguides a temperature difference $\sim 100^{o}C$ was found to exist between the capillary and the coolant liquid (Bridges et al. 1972). It seems that capillary wall thickness ~2.7 mm was one of the reasons for the high temperature difference actually measured. Another important property of the laser beam which is sought after by laser researchers is single mode operation. This is greatly affected by temperature and gain variations (Crocker, Clack and Butcher 1981). A solution can be found by discrimination against off-axis modes which according to Crocker et al. (1981) produce efficiency limitations and alignment problems. Trying to solve these problems by other methods, means conflicting practical requirements are faced, since short cavities (10-60 cm) are needed for good mode separation and tunability. This will be limited by the need for a minimum allowable length in order to have reasonable gain on the required CO_2 line (Ioli et al. 1980). A compromise

between these requirements can be handled by a reduction on the waveguide bore which is faced in turn by the need for diameters to be large enough for reasonable spot size on the grating. Some of these practical points together with other material concerning waveguide lasers will be discussed in detail in Chapter 3.

Table 2.1: Examples of previous experimental work with CO_2 lasers

No.	Author/ year	Laser tube L=length d=diameter	Window/ material	Mirror R=radius of curvature T=transmission %	Discharge v=voltage Kv I=current mA	Mixture/ Pressure torr	Power/ Efficiency %	Lines detected
1.	Bridges et al. 1965B	L=1m d=10.5mm	Potassium chloride 5mm thick	R_1=10m convex R_2=3m concave	v=7-11 I=5-10		52w/cc of gas discharge 15%	
2.	Moeller et al. 1965	L=96cm d=2.1cm		R_1=3m gold R_2=3m Irtran-2 T=12%		He+CO_2 +N_2 $P_{tot.}$=14	18 watts 4%	Strong line at 10.6 m
3.	Patel et al. 1965	L=230cm d=7.7cm		R=50.8m 1.5cm hole for output coupling	v=8.6 I=200	P_{CO_2}=0.33 P_{He}=7 P_{N_2}=1.2	45-61 watts 6.2%	P(20) and P(24)

4.	Moeller et al. 1966	L=6m sectionalized for 1m for discharge purposes d=2.2cm		R=20m T_1 2% grating 70L/mm	Ac 60cps source		> 130 watts	$(00^0 1\text{-}10^0 0)$ 50 lines $(001\text{-}02^0 0)$ 53 lines
5.	Witteman 1966	L=2m d=2.5cm	Ge window	R_1=2.4m R_2=2.4m gold mirrors	v=11 I=15	CO_2 1 N_2 2.5 H_2O 0.1 $P_{tot.}$ 3.6	20 watts 12%	P(20) P(22) P(24)
6.	Hotz et al. 1967	L=1m d=1.2cm		R_1=3m gold R_2=6m Ge with 4mm coupling hole	v=0-20 I=0-140 Rectified unsmoothed	20 torr total of N_2+He + CO_2	10 watts	
7.	Tyte 1970	L=10cm d=7mm and 1.5cm quartz		R_1=1m gold R_2=1m Ge T=11.5%		95 torr total pressure	20 watts	

8.	Woods et al. 1976	L=80cm d=8mm fused-silica	Potassium chloride 5mm thick	R_1 plane G mirror R_2=5mm gold coated quartz mirror		CO_2 2 N_2 1.8 He 8 H_2 .2 Xe .5 $P_{tot.}$ 12.5	25 watts	
9.	Ioli et al. 1980	20 cm two sections d=3mm pyrex			3 electrode discharge v=5 I=15	80 torr total pressure	6.5 watts 11%	P(6)-P(46) R(4)-R(46)
10.	Crocker et al. 1981	L=1m d=.4cm pyrex	Two ZnSe windows	R=1m Ge mirrors	-20Kv on cathode 15Kv on anode 800KΩ ballast	CO_2:N_2:He 1:1.1:2.5		60 lines
11.	Thiebeaux et al. 1981	L=1.4m d=10mm	ZnSe window	R_1=6m ZnSe mirror T=30% 150 L/mm grating	12Kv 15mA	(low pressure operation) CO_2 0.2 N_2 0.2 He 0.6 $P_{tot.}$ 1 torr		

12.	Boscolo et al. 1986	L=2m d=8.5mm to 11.5mm used	ZnSe window	R_1=10m T=22% grating 150 L/mm	30Kv and 40 mA supply used	25 total pressure	40 watts on 9P(36)

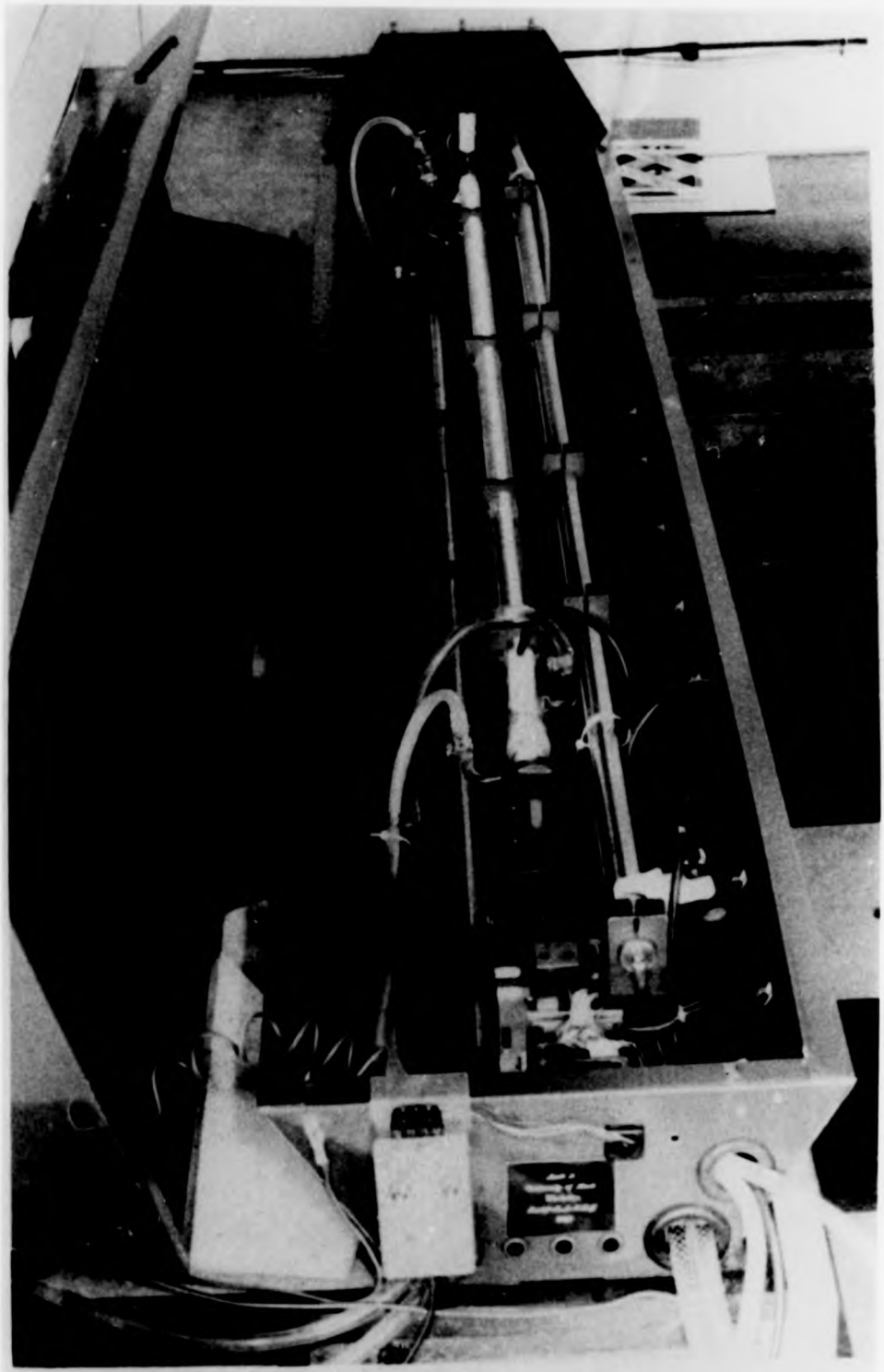

Fig 3.1 The completed CO_2 laser : conventional type.

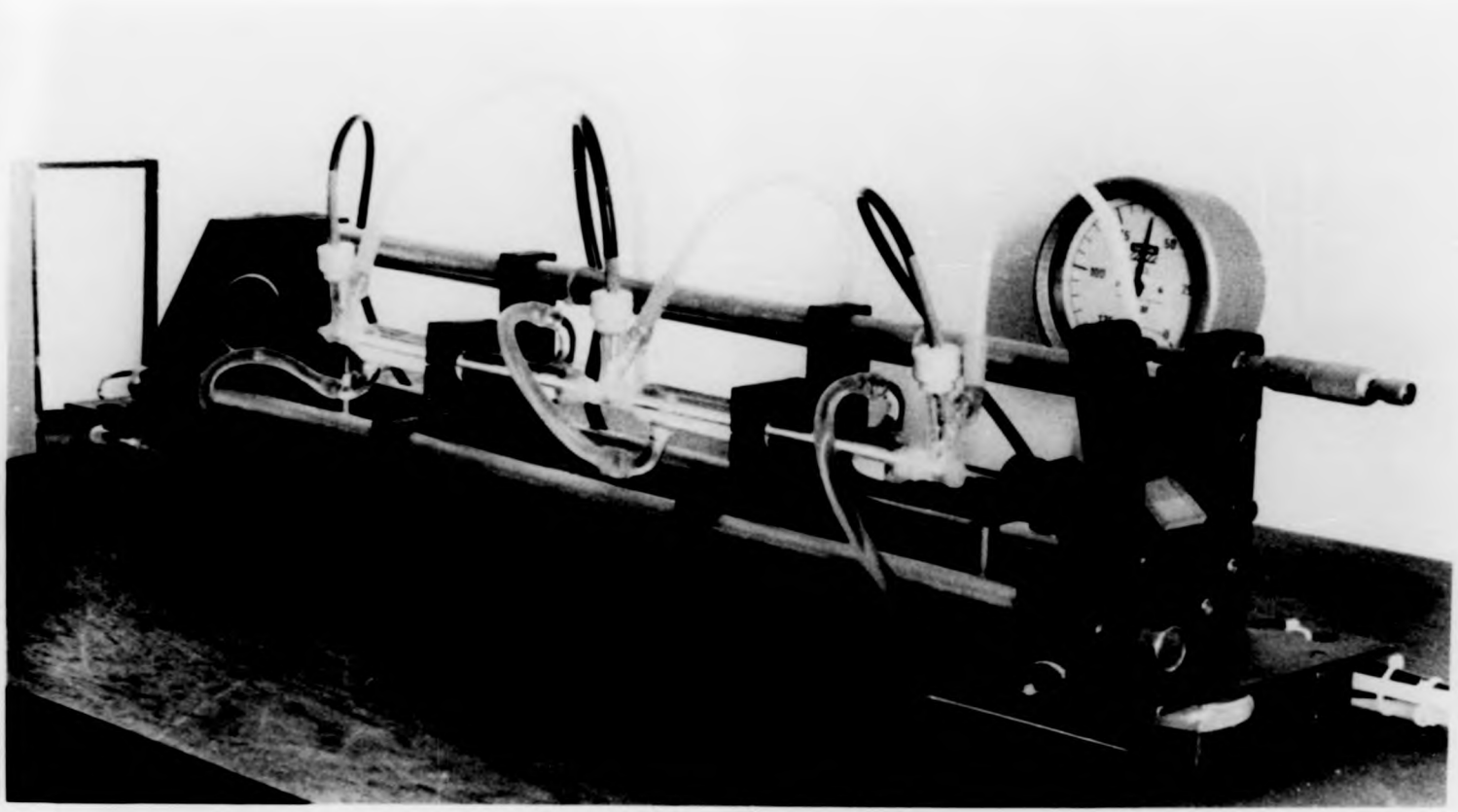

Fig 3.2 The completed CO_2 waveguide laser system.

Chapter 3

Construction and design details of both conventional and waveguide lasers

3.1 Introduction:

In this chapter details of the two lasers constructed will be given. A conventional laser with a power of 30 watts or more and a waveguide laser of 3 watts capability are described. The waveguide laser was constructed from an adaptation of a design of the University of Nijmegen, Holland.

In the following sections the different parameters involved in the design of both lasers will be discussed. Some aspects are the same for both types and will therefore only be discussed once. The two complete systems are shown separately in Fig. 3.1 and Fig. 3.2.

3.2 Laser power:

3.2.1 Conventional lasers : power output:

Usually CO_2 laser designers aim to get the laser oscillating on the fundamental TEM_{00} mode with maximum power output and consider this as a first indication of laser design success. In practice the laser power depends on most of the parameters involved in laser design, which include laser tube (length and diameter), gas discharge temperature and current, gas pressure, mirror reflectivities and so on. Laser designers often use empirical equations, which although sometimes not very accurate, can be used as a helpful guide. A carbon dioxide laser can be constructed to operate either in the sealed or in the gas flow form depending on whether the laser is operated in the slow or fast flow mode (Sasnet 1984). In the

slow flow rate mode of operation the predictor equation gives the power as:

$$P_{out} = 70\ L \tag{3.1}$$

where L is the laser plasma length in meters to give P_{out} in watts. In the fast flow rate mode of operation the power takes the form:

$$P_{out} = 120\ vA\rho \text{ watts} \tag{3.2}$$

where ρ is the gas density gr/cm^3, v is the gas velocity cm/s and A is the laser tube cross-sectional area in cm^2. In this section and those that follow, the results of Fahlen (1973) will be discussed and used. Although the theoretical study was performed for a sealed CO_2 laser it can be used for slow flow on the assumption the flow rate is optimized to sustain an optimum pressure in the laser. It is particularly useful for the selection of parameters not affected by flow rate such as optimum mirror transmission and TEM_{00} mode selection. In practice the operational conditions favour flow lasers relative to sealed lasers. In sealed CO_2 lasers the power can be written as (Fahlen 1973):

$$P = K A_T I_o \tag{3.3}$$

where I_o is the effective output intensity; A_T is the cross-sectional area of the tube and K is an empirically determined factor which is approximately 0.8 for TEM_{00} mode operation. To see how the power varies with other parameters it is important to introduce the saturation intensity (I_s) into eqn. (3.3). I_s is dependent on gas flow and gas mixture, plasma excitation current and tube diameter. Equation (3.3) can be written in the form:

$$P = K A_T \left(\frac{I_o}{I_s}\right) I_s \tag{3.4}$$

A good approximation for I_s at a tube diameter (D_T) in the range 4 to 20 mm is as follows:

$$I_s = (72/D_T^2) \tag{3.5}$$

This gives I_s in units of watts/cm^2 where D_T is in cm. This approximation was established from the results of many experiments. Substituting eqn. (3.5) and the above value for K into eqn. (3.4), then:

$$P = 14.4\pi(I_o/I_s) \tag{3.6}$$

An expression for (I_o/I_s) has been given by Fahlen (1973) quoting Rigrod (1965):

$$\frac{I_o}{I_s} = \frac{(1-L)^{\frac{1}{2}}T[g_oL_A + \ln[(1-L)(1-L-T)]^{\frac{1}{2}}]}{[(1-L)^{\frac{1}{2}} + (1-L-T)^{\frac{1}{2}}][1-[(1-L)(1-L-T)]^{\frac{1}{2}}]} \tag{3.7}$$

where L is the intra-cavity loss; T is the mirror transmission; (g_oL_A) is the single pass gain; L_A is the active laser plasma length and g_o is the unsaturated laser gain which can be estimated for CO_2 lasers using the following approximation:

$$g_o = 0.012 - 0.0025\ D_T \tag{3.8}$$

This approximation holds good for tube diameters in the range $0.4 \leq DT \leq 3.4$ cm. Fahlen combined eqn. (3.7) with eqn. (3.6) and generated many curves of P_{out} versus mirror transmission, at different values of intra-cavity loss and gain values (see Fig. 3.3). It is clear from these curves that increasing the loss lowers the output power even if the mirror transmission is at the optimum value. These curves help to estimate the power if the mirrors are to be changed or replaced by a more lossy optical component, such as a grating. If a certain power is needed from the laser then a particular optimum transmission value ($T_{opt.}$) of the mirror should be selected. To do this, a given output power is chosen using Fig. 3.4(a)

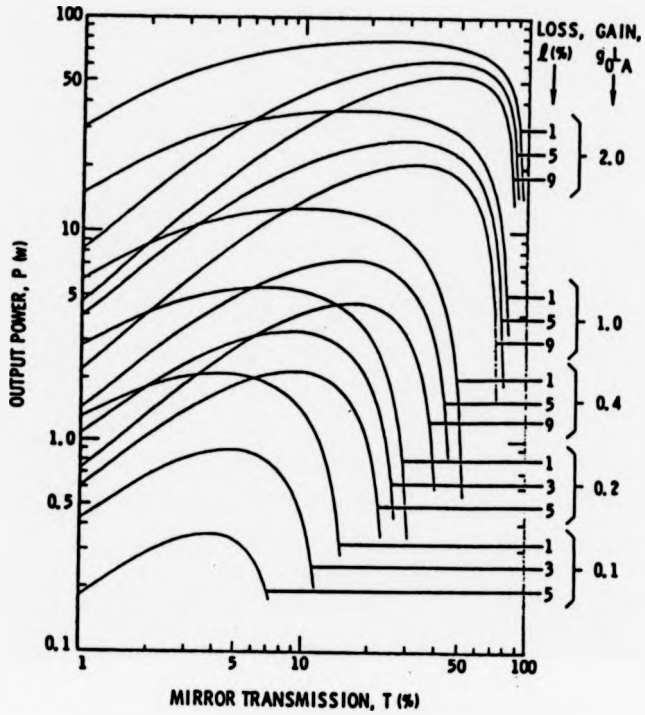

Fig. 3.3 : Laser output power versus mirror transmission at different gain and loss values. Reproduced from Fahlen (1973).

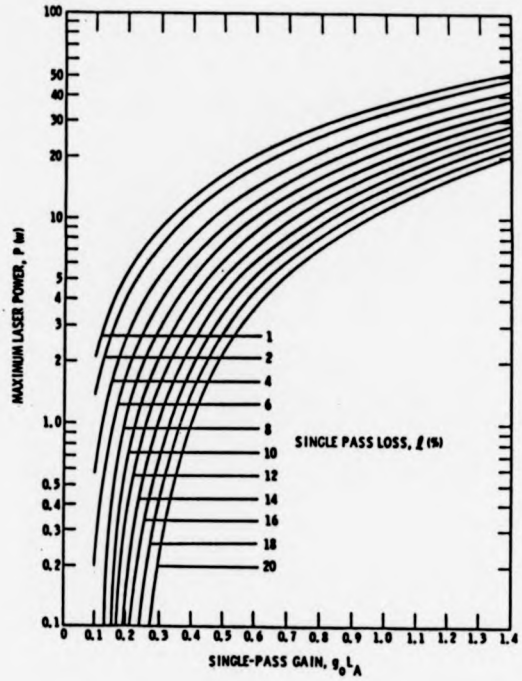

(a)

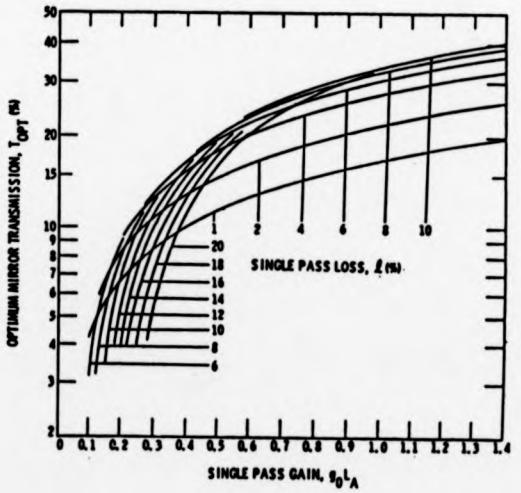

(b)

Fig. 3.4 : Useful maps for $T_{opt.}$ determination:
(a) Laser power vs. single pass gain.
(b) $T_{opt.}$ vs. single pass gain.
(After Fahlen 1973).

and the corresponding gain per pass ($g_o L_A$) found. Then using Fig. 3.4(b) a value of $T_{opt.}$ can be established. Upon estimation of g_o using eqn. (3.8), an approximate value for L_A can be found which is necessary to give that chosen power. In summary it is advisable to start with a specified output power value and then optimize the other parameters accordingly. Since most laser parameters are in some way or another related to laser power they too will need to be taken into account later. As an example for the conventional laser described in this thesis a power of 30 watts output is needed. Referring to Fig. (3.4) and considering a moderate single pass loss of 6%, the gain $g_o L_A$ is approximately 1.3. If g_o is approximated to the value $\sim 9.5 \times 10^{-3}$ cm^{-1}, the active laser length is found to be approximately 135 cm and $T_{opt.}$ is about 30%.

3.2.2 Waveguide lasers: power output:

The key to optimum maximum power from a waveguide laser is a proper mirror arrangement. By choosing an appropriate mirror radius of curvature, diameter and placing the mirror at a suitable distance from the waveguide entrance, losses of the low loss hybrid mode (EH_{11}) can be minimized. If high power is an aim in itself then the advice is to build a conventional laser. However waveguide lasers have other important features which make them attractive. For example they have 98% of energy contained in the central lobe of the output radiation (Degnan and Hall 1973), high gain per unit length and wide range tunability (Degnan 1976 and Abrams 1972). The optimum conditions for EH_{11} coupling will be discussed in Section 3.3.2. In general, the design procedure for a waveguide laser starts by specifying the laser power and using the maps generated by Hall (1980), assuming the resonator losses designated as A. A value of ($g_o L$) can be found from Fig. 3.5(a). Then using Fig. 3.5(b) the necessary values for gas pressure, bore size and guiding losses may be obtained. As an

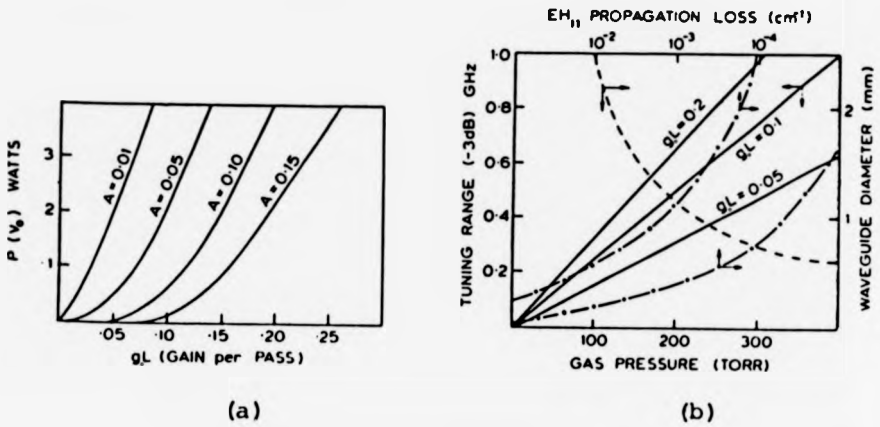

Fig. 3.5 : Waveguide laser design maps.
(After Hall 1980).

example: if a power of 3 watts is wanted from a waveguide laser assuming the losses A = 0.05, Fig. 3.5(a) will give a value ~ 0.1 for $g_o L$. From Fig. 3.5(b) it can be seen that a waveguide of bore 2 mm will give an EH_{11} propagation loss of 10^{-4} cm^{-1} and a tunability 0.3 GHz when operated at 150 torr total gas pressure.

3.3 Single mode operation:

3.3.1 Single mode in a conventional CO_2 laser:

For many laser operations the TEM_{00} mode is desirable as it makes it possible to focus the beam to a very small spot (Sasnet 1984). So laser operation in the fundamental mode TEM_{00} is an optimum target for a good laser system. Knowledge of the diffraction loss of the different modes is the key to mode selection because by making the intra-cavity losses large for higher order modes, it is possible to prevent them from oscillating (Fahlen 1973). Two important phenomena should be looked at carefully at this point. The first is that for homogeneously broadened lines, all atoms participate in the gain of a single mode and further increase in pump power will increase the mode power. The second is that because the intensity of the TEM_{00} mode is at a maximum value on the laser axis, gain saturation tends to lower the gain at the axis which makes the gain of higher order modes large enough for oscillation. This makes determination of the exact value of loss for only TEM_{00} oscillation difficult. In any case, diffraction losses must be chosen without upsetting the fundamental mode power. Single mode operation can be achieved in a conventional laser by choosing a tube diameter (D_T) in such a way that only the mode TEM_{00} oscillates. As a rough guide this occurs at tube diameters of the order 3.5 ω, where ω is the laser beam spot size (Bloom 1968). Calculation of (ω) will be discussed later. The idea behind this rule is that by

restricting the diameter to a certain value, higher order modes are sufficiently lossy such that they do not oscillate. For a diameter larger than 3.5 ω a "doughnut" mode is expected which is the pair of TEM_{01} and TEM_{10} modes oscillating simultaneously but 90^{o} out of phase. In the laser cavity there are two types of losses. Those associated with absorption and scattering of radiation (L_m) by the mirrors which can be easily measured. Their value is expected to be in the range 0.5 - 1%. The other type is the corresponding TEM_{pq} losses (L_{pq}). The latter is due to diffraction losses. The total loss of the cavity can be written as:

$$L = L_m + L_{pq} \tag{3.9}$$

To estimate diffraction losses, cavity length L_c, mirror radius of curvature R and tube diameter D_T need to be known for the sake of calculating the g-factor given as follows:

$$g = 1 - L_c/R \tag{3.10}$$

The value of the g-factor can be used together with the curves given earlier by Li (1965) to yield a plot of the TEM_{00} power losses versus Fresnel number (N) through the following formula:

$$N = D_T/4\lambda L_c \tag{3.11}$$

TEM_{00} power losses curves were reproduced by Fahlen (1973) for half symmetric cavities based on Li's work. From these curves diffraction losses of TEM_{00} and TEM_{10} modes can be obtained for different values of g (see Fig. 3.6). For the laser studied in this thesis the cavity length L_c = 180 cm, mirror radius of curvature R = 10 m, D_T = 10 mm, g = 0.82 and N = 1.3. Using Fig. 3.6 it can be found that the losses of TEM_{00} and TEM_{10} are 5% and 18% respectively. If a mirror of 5 m radius of curvature is used the losses associated with the TEM_{00} will be ~3% and that of the

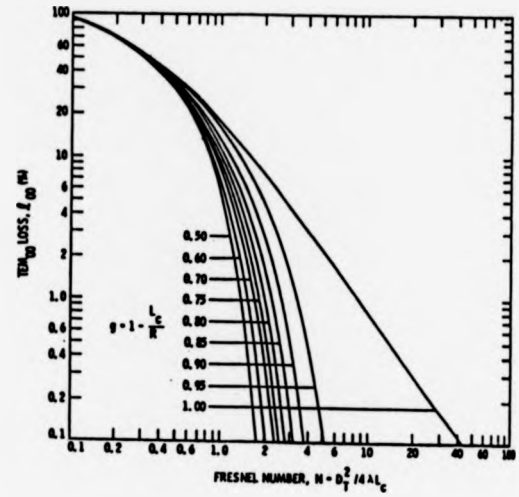

(a)

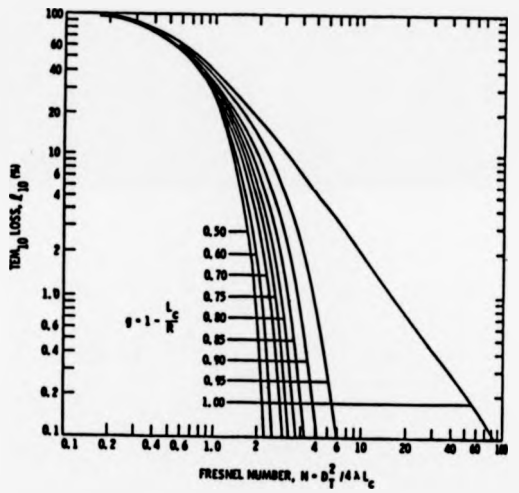

(b)

Fig. 3.6 : Average single pass mode loss for half symmetric cavity:
(a) for TEM_{00} mode
and (b) for TEM_{10} mode.
Reproduced from Fahlen (1973).

TEM_{10} mode ~ 10%. If an 8 mm tube diameter is used with the R = 10 m focal length mirror, the results will be ~ 12% and 35% respectively which indicates that the tube diameter is of greater significance for diffraction losses than mirror curvature. Calculation showed that changing L_c does not have a greater effect than changing D_T. To combine the diffraction losses with other parameters to guarantee successful single mode operation Fahlen (1973) developed a criterion for mode selection. This was based on selecting a value of the total loss (L) that makes the ratio between the effective output intensity (I_o) and the saturation intensity (I_s) equal to zero, i.e. $I_o/I_s = 0$. The value of the ratio I_o/I_s has been derived by Rigrod (1965) (see eqn. 3.7). According to this criterion the loss ratio between TEM_{00} and TEM_{10} modes is equal to

$$\frac{L_{10}}{L_{00}} = \frac{1 - L_m - (T_{opt.}/2) - [(T_{opt.}^2/4) + \exp(-2g_oL_A)]^{\frac{1}{2}}}{L - L_m} \qquad (3.12)$$

Here, g_oL_A and $T_{opt.}$ must be chosen so as to make L_{10} big or the ratio $\frac{L_{10}}{L_{00}}$ large enough to prevent the TEM_{10} mode from oscillating. A thermal image plate illuminated with an ultraviolet lamp was used to display the oscillating TEM modes. By proper adjustment of the mirrors, PZT voltage and sometimes the gas pressure, it was possible to obtain single mode operation of the fundamental mode TEM_{00}. Usually the doughnut mode is very hard to eliminate if it appears. An adjustable camera type of iris was also used in the process of single mode selection which proved to be very effective in discriminating against higher order modes.

3.3.2 Waveguide laser: single mode operation:

A waveguide laser is distinguished from the conventional laser by the fact that radiation is guided by the waveguide for at least some distance in the laser cavity (Degnan 1976; Hall 1980). For the waveguide

laser design most of the decisive parameters will be given in this section. In a waveguide laser there are three types of modes that propagate in the guide (Marcatili and Schmeltzer 1964; Degnan 1976 and Hall 1980). These have been categorized as follows: transverse circular electric TE_{0m} modes, transverse circular magnetic TM_{0m} modes and the hybrid EH_{nm} modes, where n is a positive or negative integer whose absolute value gives the number of nodal diameters in the field distribution and m is a positive integer indicating the number of nodal minima. Approximate field components of these modes have been derived (Marcatili et al. 1964; Degnan 1974 and Degnan 1976). Of all the above mentioned modes, the EH_{11} hybrid one has the lowest loss. When this mode is excited in laser operation, 98% of the energy is contained in the central lobe (Degnan and Hall 1973, and Hall 1980). Because of this it is very important to arrange the mirrors in a waveguide laser in favour of exciting the EH_{11} mode. There are three low loss arrangements which can be used (Degnan et al. 1973; Degnan 1976 and Hall 1980) as follows.

I) The first arrangement uses a flat mirror placed very close to the waveguide (Degnan 1976). A large radius of curvature mirror can be used instead of the flat mirror (Degnan and Hall 1973). Mirrors also can be placed on plungers so that they can be moved in or out of the guide for frequency tunability (Degnan 1976). In these mirror arrangements the distance (d) of the mirror from the end of the guide is very important in order to minimize losses.

II) A mirror with a large radius of curvature may be placed at a distance in such a way that the centre of curvature lies at the waveguide entrance.

III) A mirror with a small radius of curvature placed at a distance half the radius of curvature from the waveguide may also be used.

Coupling efficiency has been described (Degnan et al.1973) in terms of different parameters; $\alpha \equiv \frac{ka^2}{c}$, $\beta \equiv d/c$, $\gamma = b/a$ and $k = \frac{2\pi}{\lambda}$ (see Fig. 3.7), where a is the waveguide radius, c is the mirror radius of curvature, k is the propagation constant, d is the distance between mirrors and the waveguide, λ is the radiation wavelength and b is the mirror radius. In Fig. 3.7, γ has been taken to be 11 based on the results of many experiments. From Fig. 3.7 it can be seen that maximum coupling occurs at $\beta = 0$ for $\alpha = 0.296$, which is case (I). For case (III) maximum efficiency obtained at $\beta = 0.5$ at $\alpha = 2.415$ and for case (II), $\beta = 1$ at $\alpha = 0.296$. Very high efficiency could be achieved using case (I); but degradation of mode strength is due to increase in the distance from the guide or using a small radius of curvature mirror (Degnan et al. 1973). In practical laser systems it is difficult sometimes to close the laser system, especially in CO_2 lasers where a grating is required. In this case a small distance is kept between mirrors and guide. It is thought that loss occurs in this situation (Abrams 1972) as a result of imperfect coupling of the radiation to the guide after propagating to the mirrors and back. The losses can then be related to two reasons:

(i) The field is spread out and does not re-enter the guide after reflection from the mirror.

(ii) Some of the energy is converted to higher order waveguide modes.

It was shown by Abrams (1972) that for an optimum value $(\omega_o/a) = 0.6435$, 98% of the energy will be contained in the lowest order gaussian mode, where ω_o is the 1/e value of the mode radius amplitude. From Abrams' study it is concluded that for mirrors of radius of curvature (c), the lowest loss value suffered by the mode can be achieved by placing the mirror at a distance (d) from the guide, calculated from the following

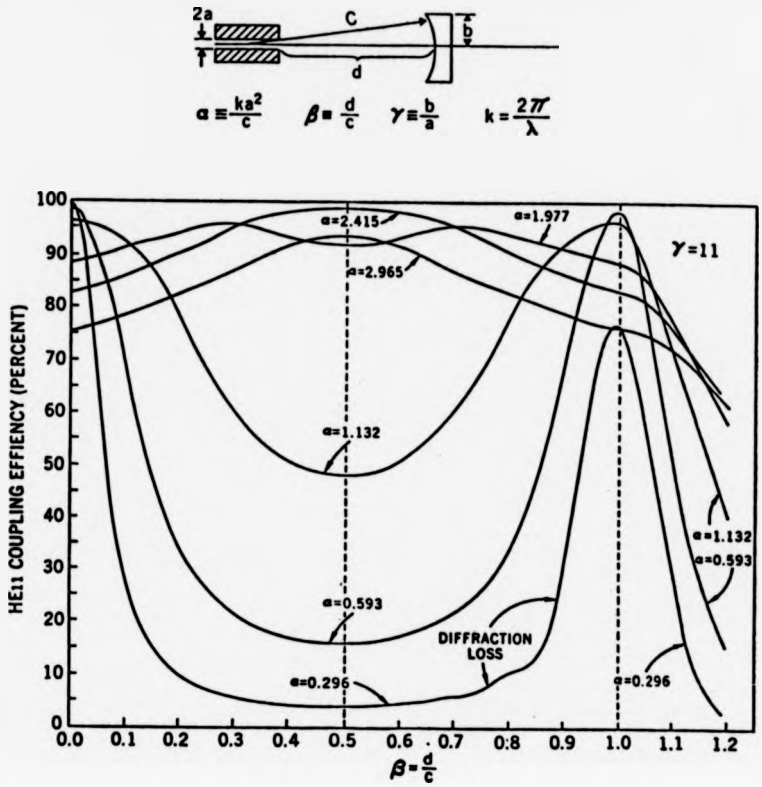

Fig. 3.7 : Coupling efficiency of EH_{11} vs. β.
HE_{11} (Snitzer 1961) is equivalent to EH_{11} of Marcatili et al. (1964).
Reproduced from Degnan et al. (1973).

relation:

$$c = \left(\frac{\pi\omega_o^2}{\lambda}\right)\left[\frac{\pi\omega_o^2}{\lambda d} + \frac{\lambda d}{\pi\omega_o^2}\right] \qquad (3.13)$$

For c = 10 m, a = 1.5 mm and λ = 10.6 μm it is found that d ~ 0.75 cm. This is the value at which perfect matching of wavefronts with the mirror can be achieved. Abrams (1972) produced graphs of coupling loss versus $(\frac{d\lambda}{\pi\omega_o^2})$ at different constant ratios of $(\frac{\lambda c}{\pi\omega_o^2})$. In the system designed in this thesis a grating was used at one end of the guide which will be treated as a flat mirror. According to Abrams' study, a loss of < 2% could be achieved for $\frac{d\lambda}{\pi\omega_o^2} < 0.11$ which gives d = 3 cm from the guide. In Case (II) matching is more efficient for large radius of curvature mirrors or small (α) since the phase front becomes more spherical as the far field is approached. Degnan et al. (1973) produced maps for Case II where a plot was made of EH_{11} losses versus ($\alpha = ka^2/c$) at constant mirror aperture ($\alpha\gamma = kab/c$). The values of ($\alpha\gamma$) are chosen in such a way that the mirrors in the far field capture the large central lobe of EH_{11} when $\alpha\gamma = 5.52$ and capture both central lobe and first outer ring when $\alpha\gamma = 8.65$, and central lobe plus the first two outer rings at $\alpha\gamma = 11.792$. Losses of EH_{12} mode were also included for comparison (see Fig. 3.8a). For Case (III) coupling losses were also drawn versus mirror apertures. A minimum loss of 1.29% was achieved at $\alpha\gamma = 6.25$, for the EH_{11} mode, whereas EH_{12} losses reach a value of 77.98% (see Fig. 3.8b). The effect of the index of refraction (n) or type of waveguide material on the three types of mode can be obtained from the attenuation constant (Marcatili et al. 1964):

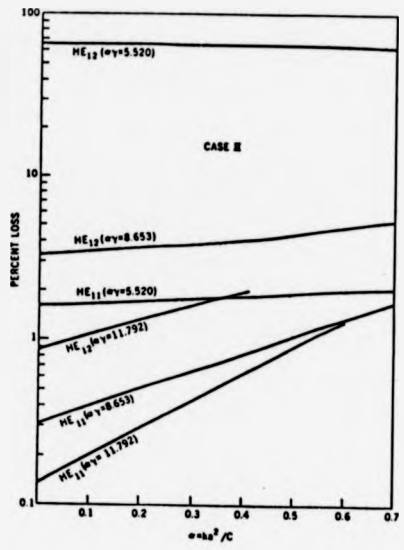

(a)

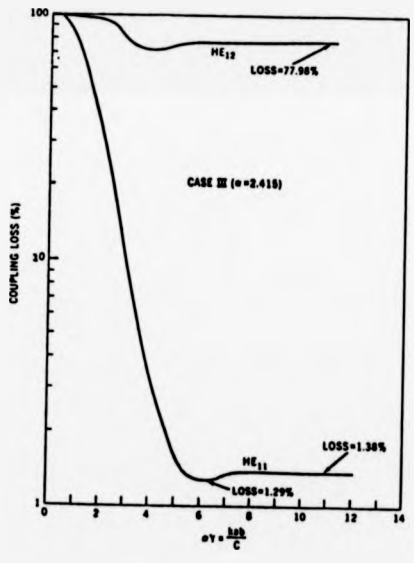

(b)

Fig. 3.8 : Losses of different hybrid modes as a function of mirror curvature and aperture in (a) and as a function of mirror aperture in (b). Reproduced from Degnan et al. (1973). HE_{11} in Snitzer's (1962) notation is equivalent to that of Marcatili (1964), or EH_{11}.

$$\alpha_{nm} = \left(\frac{U_{nm}}{2\pi}\right)^2 \left(\frac{\lambda^2}{a^3}\right) \times \begin{cases} \dfrac{1}{\sqrt{n^2-1}} & \text{for } TE_{0m} \quad (n=0) \\ \dfrac{n^2}{\sqrt{n^2-1}} & \text{for } TM_{0m} \quad (n=0) \\ \dfrac{\frac{1}{2}(n+1)}{\sqrt{n^2-1}} & \text{for } EH_{nm} \quad (n\neq 0) \end{cases} \qquad (3.14)$$

where U_{nm} is the mth root of the equation $J_{n-1}(U_{nm}) = 0$.
A table of U_{nm} values is given in the work of Marcatili et al. (1964) from which $U_{11} = 2.405$, $U_{12} = 5.52$. From eqn. (3.14) it is obvious that the attenuation constant is proportional to (λ^2/a^3) which means that losses can be reduced by making $a >> \lambda$. For an index of refraction $n < 2.02$ which is the case for most glasses the mode EH_{11} dominates. As an example, for a hollow waveguide mode from glass $n \sim 1.5$ and using eqn. (3.14) it is found that $\alpha_{11} = 0.886 \times 10^{-3}$ dB/m and $\alpha_{12} = 4.66 \times 10^{-3}$ dB/m which means that the mode EH_{12} is about five times more lossy than the mode EH_{11}. If $n > 2.02$ then TE_{01} is the mode with the lowest attenuation (Degnan 1976). There is also a special case when n is close to unity where the TE_{0m} mode becomes degenerate with the $EH_{n+2,m}$ mode (i.e. both have the same propagation constant). When these combine together with the same amplitudes and the appropriate phase they form a set of non-circulatory symmetric linearly polarized modes. When combined with the EH_{1m} modes the result is a TEM_{pL} mode similar to that obtained in a conventional laser resonator (Degnan 1976).

3.4 Laser tube:

3.4.1 Conventional laser tube:

For a given output power, Sections 3.2.1 and 3.3.1 offer a basis to take a decision about the laser tube design. Three important parameters need to be optimized as far as the laser tube is concerned. These are

tube length, diameter and material. The effect of length and diameter is far more important and effective in CO_2 laser operation than tube material. Length is one of the most crucial parameters for laser output power but it must not be chosen independently of other factors such as rate of gas flow in the tube, since the type of flow is also related to the amount of laser power expected. In the slow flow rate situation a temperature gradient is set up between tube centre and walls (Sasnet 1984). The predictor equation for the output power is given by eqn. (3.1). In contrast for fast gas flow the situation is different since a temperature gradient is set between input and output of the laser tube. The power output is given by eqn. (3.2) as $P_{out} = 120 \frac{dM}{dt} = 120 \rho v A$. Here $\frac{dM}{dt}$ is the gas flow rate, ρ is the gas density, v the gas velocity and A is the tube cross-section. It can be said that length is most important for slow flow while tube diameter is of special importance for the case of fast flow systems. A rigorous way to determine the active tube length (Fahlen 1973) is to make use of the small signal gain (g_o) (see section 3.2.1). Goldsborough (1972) suggested the selection of the tube length (L) and diameter (D_T) in one process by assuming the bore to be equal to ($KL^{\frac{1}{2}}$). In doing so the mode size is kept constant since the mode width is proportional to ($L^{\frac{1}{2}}$). Typical values of k (Goldsborough 1972) for CO_2 lasers is ~ 1.4×10^{-2} and $g_o L_A$ ~ 3 dB/m. Using $g_o L_A = \frac{2k}{D_T}$, it is possible to optimize the length of the laser tube for the best small gain signal. Of course it should not be forgotten when choosing D_T, its importance for single mode operation, as discussed in Section 3.3.1. It was found that for diameters larger than four times the beam waist a doughnut mode will be excited (Goldsborough 1972). For bores that are too small mode distortion occurs in a form of rings at the outer edge of the beam. Generally speaking a doughnut mode is set up for tubes with internal diameters $\geq$9 mm. This is due to the fact that the gas at the tube centre becomes

hotter than at the walls (Woods 1976). For a certain diameter there is a threshold value of discharge current, pressure and tube length. The relations are as follows: pressure and voltage/length is inversely proportional to diameter while current is proportional to the diameter. When the right proportions of these parameters are not selected, fluctuation (noise) might occur in laser power or frequency due to acoustic oscillations (Goldsborough 1972). Suzuki (1970) has managed to reduce this type of noise by dividing the plasma tube into short parts. As far as design is concerned some typical values for different laser parameters were given by Goldsborough for different laser types. For CO_2 lasers the relations take the following forms:

$$PD_T = 50 \tag{3.15}$$

where P is the CO_2 partial pressure in torr and D_T is the inner tube diameter in mm.

$$(\text{Discharge voltage/cm}) \times D_T = 2000 \ (\text{V cm}^{-1}\text{mm}) \tag{3.16}$$

with D_T in mm also, and

$$I/D_T = 2.5 \text{ mA mm}^{-1} \tag{3.17}$$

These relations will be used and applied in the following sections. The last parameter concerning the laser is the actual tube material. The first requirement for a suitable material is to be capable of maintaining low pressure and does not outgas (Goldsborough 1972). In general CO_2 laser tubes are fabricated from glass. Fused silica was found (Witteman 1966) to be better than pyrex as the latter is found to outgas as the discharge is struck. Thick wall capillaries are not desirable as a temperature gradient will build across the capillary wall (Goldsborough 1972). The capillary should be surrounded with a cooling water jacket

with enough volume to allow proper cooling of the laser. In the system described in this thesis a commercial pyrex tube of active discharge length ~150 cm and 10 mm diameter was used for the conventional 30 watt laser. The length as calculated in Section 3.2.1 is 135 cm to give 30 watts output power. Outgassing from the pyrex material was noticed and a warming up period of 10 min was allowed before introducing the gas mix into the tube.

3.4.2 Waveguide laser tube:

As has been seen in Section 3.3.2 the attenuation constant (α_{11}) of the lowest order hybrid mode (EH_{11}) depends on the internal bore of the dielectric guide, index of refraction and radiation wavelength. The waveguide diameter has to be chosen for an optimum coupling efficiency, alongside other parameters and mirror arrangements (see Sections 3.2.2 and 3.3.2). In this section other factors such as thermal expansion and conductivity, smoothness, straightness and ease of construction are taken into consideration. Hall, Gorton and Jenkins (1977) have performed a study on the variation of attenuation constant (α_{11}) of the lowest order mode (EH_{11}) for the three different dielectric materials: pyrex, alumina and beryllia. Their results are given in Fig. 3.9 which shows a discrepancy between the theoretical and measured curves for both pyrex and alumina. This is thought to be as a result of additional losses due to roughness, lack of straightness or minute contamination on the guide's wall. It is advisable to clean the guide wall before fitting it into the laser system. Three materials have been checked for transmittance (pyrex n = 1.474, quartz n = 1.458 and soda lime n = 1.512). No significant difference was found between the different materials (Sawartani and Kapany 1970). The most promising material for waveguide lasers is boron nitride (BN) which is considered to be safe, easily and precisely machineable to a

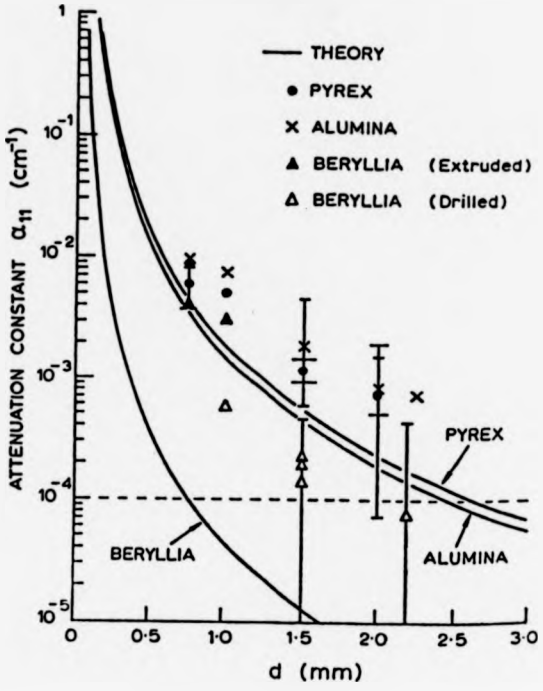

Fig. 3.9 : Attenuation constant (α_{11}) vs. tube diameter (after Hall et al. 1977). The dashed line sets a limit on the measurements imposed by laser stability and power measurement accuracy.

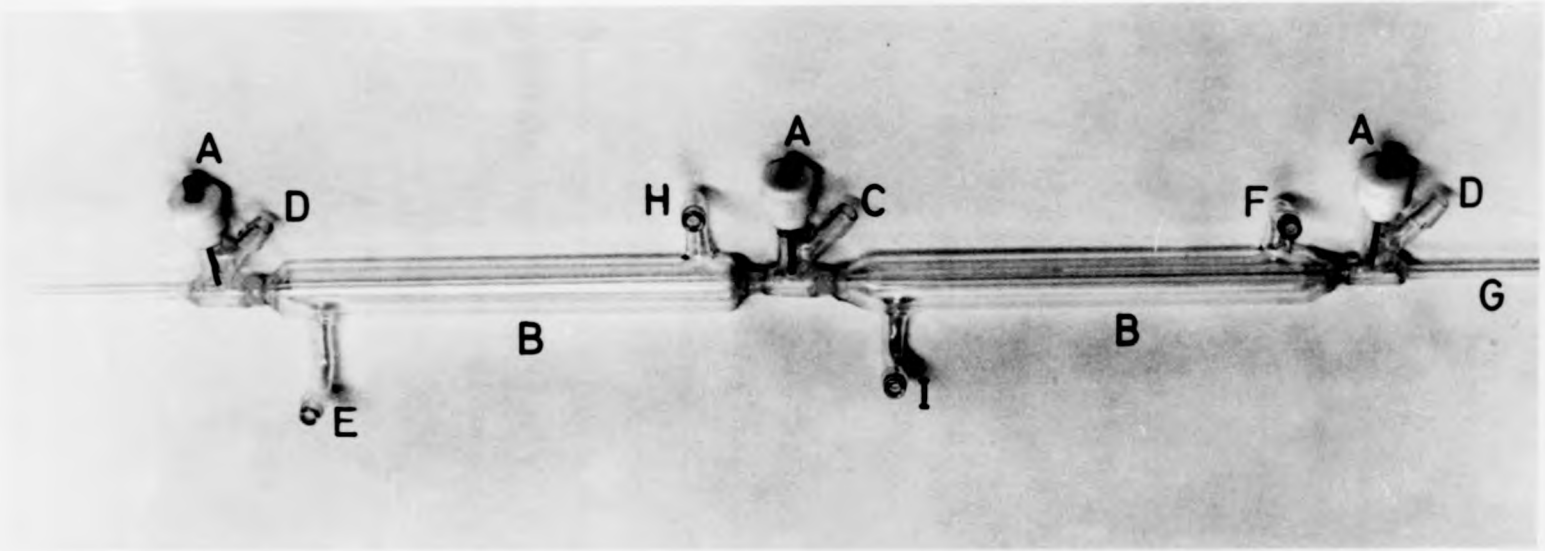

Fig 3.10 The constructed waveguide laser tube : material : Pyrex.
The joints are sealed with silicone rubber glue.

(A) Laser electrode (B) Water cooling jacket

(C) , (D) Gas inlet and outlet respectively

(E) , (F) Water in and out respectively

(G) Pyrex guide tube

(H) and (I) are joined together by rubber tubing

smooth surface (Papayoanou 1977). Moreover it has a good thermal conductivity which is important for proper cooling. Its thermal expansion is lower than all other materials. The author claims that no frequency stabilizer is needed if boron nitride is used as a waveguide material. In the present work a pyrex waveguide 3 mm i.d. and 5 mm o.d. has been used for the waveguide laser. Pyrex is an inexpensive and readily available material and proves to be satisfactory. Three 1 mm diameter holes were drilled at points along the tube. These holes drilled from the same side are 21 cm from a central hole, giving an active discharge length of 42 cm. The holes were made using an ultrasonic drill. It is found that placing a nylon insert of the same diameter as the tube bore into the waveguide permits round holes to be made and prevents chipping of the pyrex. After drilling, the nylon was removed and the guide carefully cleaned. Hall et al. (1977) found that four holes of 1 mm diameter had a negligible effect on transmission. The guide was then inserted within its water jacket and the electrode-gas feedthroughs were vacuum sealed using a silicone based rubber glue. This was found to be very satisfactory and gives the necessary flexibility to avoid strain in the waveguide. The constructed laser tube is shown in Fig. 3.10. The total length of the guide is 57.5 cm. Waveguide laser tube lengths range from 10.8 cm (Willetts and Hartwright 1978) to ~60 cm (Ioli et al. 1980). It is not advised to construct long waveguides because of the possibility of being bent. Losses are expected to increase with length (Hall et al. 1977).

3.5 Laser electrodes:

Electrode materials should satisfy certain properties for successful laser operation. Intuitively, electrode materials should be inert to the gaseous components involved in the gas mixture. Other properties (Hochuli and Sciacca 1974) such as very low sputtering rate, having a minimum of

negative ions in the sputtered products and consuming no oxygen, are of great importance for a problem-free laser. The parameters involved can be categorized as follows: gas composition, current density, temperature and composition of cathode surface involved. Depending on the situation of the above mentioned parameters, certain processes will occur in the laser tube both good or bad. Some of these can be easily controlled such as gas composition. The current density depends on the geometry of the cathode and temperature of the electrodes can be controlled by thermal isolation or cooling depending on what is best for laser performance. The composition of the cathode surface is a complex matter. The most serious problem created by laser electrodes is sputtering of the cathode material (Smith, Shield and Webb 1983; and Hochuli et al. 1974). Sputtering results in the deposition of a non-desirable conducting film near the cathode. If gaseous compositions of the cathode materials are formed they will travel down the tube colliding and condensing upon the laser tube walls and optical components. Condensation usually results in power degradation (Smith et al. 1983). From the experience of Smith and Browne (1974) cathodes act as an active catalyst to the reaction:

$$CO_2 \rightleftarrows CO + O$$

For example platinum (Pt) was found to create a density gradient across the tube. Their result showed 54% dissociation away from the cathode and 10% near the cathode. In the following a brief account will be presented of laser electrode performance based on the experimental studies of Hochuli et al. (1974) and Smith et al. (1983). The results were obtained in a sealed CO_2 laser using CO_2, He, N_2 and Xe mixtures unless otherwise specified.

(1) **Gold:** gold sputters very badly with lifetimes surprisingly short in comparison with other materials.

(2) **Silver:** this material was found to behave badly in He-CO_2-N_2-Xe mixtures; but its behaviour was completely different when N_2 was replaced by CO whereupon a visually dark spot was formed at the cathode. Eventually it becomes very dark corresponding to complete oxidation. The spot then moved to a new position and so on. When the temperature was about 200 - 300^{o}C it was found that the first spot clears as a result of dissociation of the oxidization layer. A silver cathode has a long lifetime and is sputter free. The only snag is the moving spot which introduces electrical instability. Other silver components such as Ag-CuO were found to work well; but with the moving spot problem.

(3) **Copper cathodes:** copper cathodes perform very well in He-CO_2-CO-Xe mixtures. A moving spot was formed at high current densities. Sputtering occurs at low current densities and is confined to the cathode region only. Surprisingly, copper performs well only with the exclusion of N_2 from the mixture. This fact was noticed by Smith et al. (1983) and Hochuli et al. (1974). The reason for this behaviour is not clear. Pure copper produces moderate sputtering, copper-zirconium produces light metallic deposits, and copper-nickel produces brown deposits.

(4) **Nickel, Molybdenum and Tungsten:** these materials sputter lightly and form deposits along the capillary as a result of carbonyl (i.e. $Ni(CO)_4$, $Mo(CO)_6$ and $W(CO)_6$ formed in the gaseous state at ~180^{o}C which travel along the tube to condense on the tube walls and optical

components. This results in a loss of CO molecules from the gas mixture. As a result more CO_2 dissociation follows hence a net CO_2 gas loss.

(5) **Zirconium, Aluminium and Tantalum:** these metals oxidize due to the availability of oxygen from CO_2 dissociation. Al has the highest oxidation rate. This also results in the removal of CO_2 from the discharge. The sputtering rate for these metals is low and no traces of cathode metals are found in the tube. But the large oxidation rate makes these metals unacceptable as electrodes for long life laser operation.

(6) **Platinum and Platinum-Rhodium (90-10):** both metals showed low loss of CO_2 molecules although sputtering was heavy for both materials.

(7) **Stainless steel:** CO_2 loss was low and comparable to that of platinum. There was no sputtering. Smith et al. (1983) concluded that stainless steel, especially Type 304 which contains {Cr 18%, Ni 10%, 0.5-1% Si, 1-2% Mn and the balance Fe} will make the best electrode for CO_2 lasers. The use of copper is considered to be undesirable.

The problem of CO_2 loss and deposition of cathode material on the tube walls can be reduced by pumping out the gas near the cathode and having the gas flow direction from anode to cathode. This sort of arrangement is adopted in the present work. In the conventional laser described in this thesis nickel electrodes are used. For the waveguide laser thoriated-tungsten electrodes were used such as are used in argon arc welding (as recommended by the University of Nijmegen, Holland).

3.6 Optical components:

Optical components such as mirrors, gratings and Brewster windows determine the laser output power and final laser beam shape. Great care must consequently be taken when choosing them. Ideal properties of window material (Duley 1976) are: lower absorption coefficient at the laser operating wavelength, high thermal conductvity and low thermal expansion, high heat capacity, excellent polishing properties, suitable for dielectric coating, and its refractive index is independent of temperature. It is difficult to find a material that satisfies all these properties perfectly, but it is possible to find a material that can satisfy many of them.

3.6.1 Mirrors:

Mirrors are the most important of optical components as their transmission determines the power from the laser. Care must be taken to select the right coating for the relevant laser wavelength. Beam shape is mostly determined by the mirror radius of curvature (R) and mirror separation (L_c) (Fahlen 1973). When larger radius of curvatures are used frequency fluctuations occur due to mechanical perturbations (Sanderson and Streifer 1969). As far as mirror separation is concerned, a correction is needed if an object such as a Brewster window is placed in the way of the beam (Fahlen 1973). Cavity length correction will be more important for short cavities. For a cavity of length L_c and an object of width L_n and index of refraction (n) placed perpendicularly to the beam, the effective length is given by (Fahlen 1973):

$$L_{eff} = L_c - L_n(1-\frac{1}{n}) \qquad (3.18)$$

In the system described in this thesis a Brewster window placed at an angle (i) with respect to the laser beam has a width of L_n and the

effective length will be given in the following form:

$$L_{eff} = L_c - L_n\left(1 - \frac{n}{\sqrt{n^2-\sin^2 i}}\right) \tag{3.19}$$

which will give for a cavity length of 200 cm an effective length of 200.04 cm which is a negligible difference as mentioned before for long cavities. The most important issue of mirror selection will now be considered. Depending on the type of laser and cavity length it is necessary to be able to choose a mirror with a certain radius of curvature value. The starting point for the determination of mirror radius is to calculate the mode sizes on both laser mirrors using the following formula (Boyd and Kogelink 1962):

$$\omega_1^4 = \left(\frac{\lambda}{\pi}\right)\left(\frac{R_1^2 L_c}{R_1R_2-L_c}\right)\left(\frac{R_2L_c}{R_1-L_c}\right) \tag{3.20}$$

where ω_1 is the mode radius on mirror 1, R_1 and R_2 are the radii of curvature for mirrors m_1 and m_2 respectively, L_c is the cavity length and λ is the laser wavelength. For ω_2 calculations the subscript 1 is replaced by 2. Then these values need to be compared with the laser tube diameter and should be three times less than any apertures used in the laser system. The above situation is for two curved mirrors; but if a curved and a plane mirror are to be used, mode radii can be obtained from the following formula (Bridges and Chester 1965A):

$$\omega_c = \left(\frac{\lambda}{\pi}\right)^2\left(\frac{R^2L_c}{R^2-L_c}\right) \tag{3.21}$$

$$\omega_p = \left(\frac{\lambda}{\pi}\right)^2 L_c(R-L_c) \tag{3.22}$$

where ω_c and ω_p are the mode radii on the curved and plane mirror respectively. It is worth mentioning here that the best arrangement for the plane mirror, or in the system to be described the grating, is to

be at a distance $L_c < R$ of the curved mirror. A disadvantage of this arrangement is that the light cone might not fill the laser tube all the way down (Goldsborough 1972). Again the g-factor given by eqn. (3.10) can play an important role in selection of a suitable mirror radius. So by choosing the best value of g which will give a reasonable diffraction loss leading to single mode operation, R can be evaluated. Then all values of ω_c, ω_p and bore can be compared. The two mirrors used in the work to be described are of 10 m radius of curvature and give a beam radius of $\omega_c = 2.14$ mm and $\omega_p = 3.60$ mm. The 5 m mirror will give $\omega_c = 2.17$ mm and $\omega_p = 2.85$ mm. These values go quite well with the tube of diameter 10 mm, as the tube diameter is not larger than 3.5 times the spot size. As far as the waveguide laser is concerned there is a special mirror arrangement as discussed in Section 3.3.2 according to which the radius of curvature will be selected. For the work described here a 10 m radius of curvature was used successfully for the waveguide laser. A gap of ~0.75 between mirror and guide tube is maintained as calculated in Section 3.3.2. Germanium mirrors 4 mm thick, 25 mm diameter and 80% reflectivity have been used in both conventional and waveguide lasers.

3.6.2 Grating:

Taking into consideration the different types of isotopes of CO_2, the carbon-dioxide laser can oscillate on a large number of vibrational-rotational transitions amounting to as many as 400 lines (Duley 1976). As a consequence of the high gain of the laser many lines may oscillate simultaneously. So a line selection component is a necessity in the laser although some of the laser power will be lost by the dispersive element (Degnan 1976). Gratings can be used more successfully in CO_2 lasers than any other type of laser because of their high gain (Goldsborough 1972). Properties such as low loss at the selected line wavelength, a high degree

of wavelength selectivity and adequate spectral range must be maintained in the wave selector employed (Hard 1970). The grating equation can be written in the form

$$m\lambda = d(\sin i + \sin r) \tag{3.23}$$

where m is the diffraction order, λ wavelength, i angle of incidence, r angle of reflection and d is the grating line separation. An interesting situation is when r = i then,

$$m_L \lambda_L = 2d \sin i \tag{3.24}$$

where L stands for the Lithrow configuration. Low losses and high selectivity at the desired wavelength λ can be achieved by making d small (Hard 1970). The groove profile (blaze angle of the groove) will determine the intensity distribution of the reflected light in different directions. It was found in the visible region that grating efficiency (Hard 1970) is high when the incident light polarization is perpendicular to the grating grooves. Generally it follows that the best efficiency of the grating occurs for radiation at an incident angle greater than the blaze angle. For the 30 watt conventional laser a replica grating on a copper substrate was used with 100 lines/mm and blazed for 10.6 μm. For the 3 watt waveguide laser a replica grating on a quartz substrate with 150 lines/mm blazed for 10.6 μm was used. Gratings should be handled with care and their surfaces must not be touched under any circumstances. Cooling of the grating to prevent damage from excessive heating was found unnecessary although a small air fan was included in the conventional laser design.

3.6.3 Brewster window:

Brewster windows are used to obtain low transmission loss. The windows are placed at an angle such that $\tan \theta = n$ where n is the index of

refraction of the material from which the windows are manufactured. Insoluble materials are preferred although windows made of different salts (e.g. NaCl) have been used by Woods et al. (1976). It is possible to use two windows, one at each end of the laser tube (Crocker et al. 1981). But one Brewster window is preferred for two reasons: firstly, absorption and scattering is kept to a minimum, and, secondly, any misalignment in one of the Brewster windows can cause frequency instabilities. 10^{-6} radians of window tilt can cause 0.5 MHz frequency shift (Woods et al. 1976). As far as diffraction losses are concerned Brewster angle tolerances up to $\sim 1^{o}$ are acceptable without causing significant losses (Goldsborough 1972). Other properties of the windows are also relevant such as their thermal expansion and flatness. Even a very small sphericity in the window can produce a lens effect. This is also caused when the window absorbs power even at the level of milliwatts. The effect appears in the form of mode distortion (Goldsborough 1972). Brewster windows must not be stressed since this can cause birefringence. In this case the easiest way is to glue the window to the quartz tube suitably cut at the Brewster angle, but the window might be wasted if the fragile waveguide is accidentally broken. A special adapter was designed for housing the Brewster window. To reduce the stressing effect a very soft "O" ring was made from silicone based rubber glue by filling a mould engraved in a nylon block then flattening it with a steel blade and then leaving it to form for about 6-8 hours. This procedure was found to make a very flexible "O" ring for Brewster windows. It was found that silicone based rubber can be used safely to glue Brewster windows and it can be peeled easily off glass and other window materials. Brewster windows can be located (to advantage) very close to the waveguide where the wave curvature is weak, thereby reducing astigmatism (Lyszyk 1977). For both lasers a ZnSe window was used. Windows made from this material have the following properties

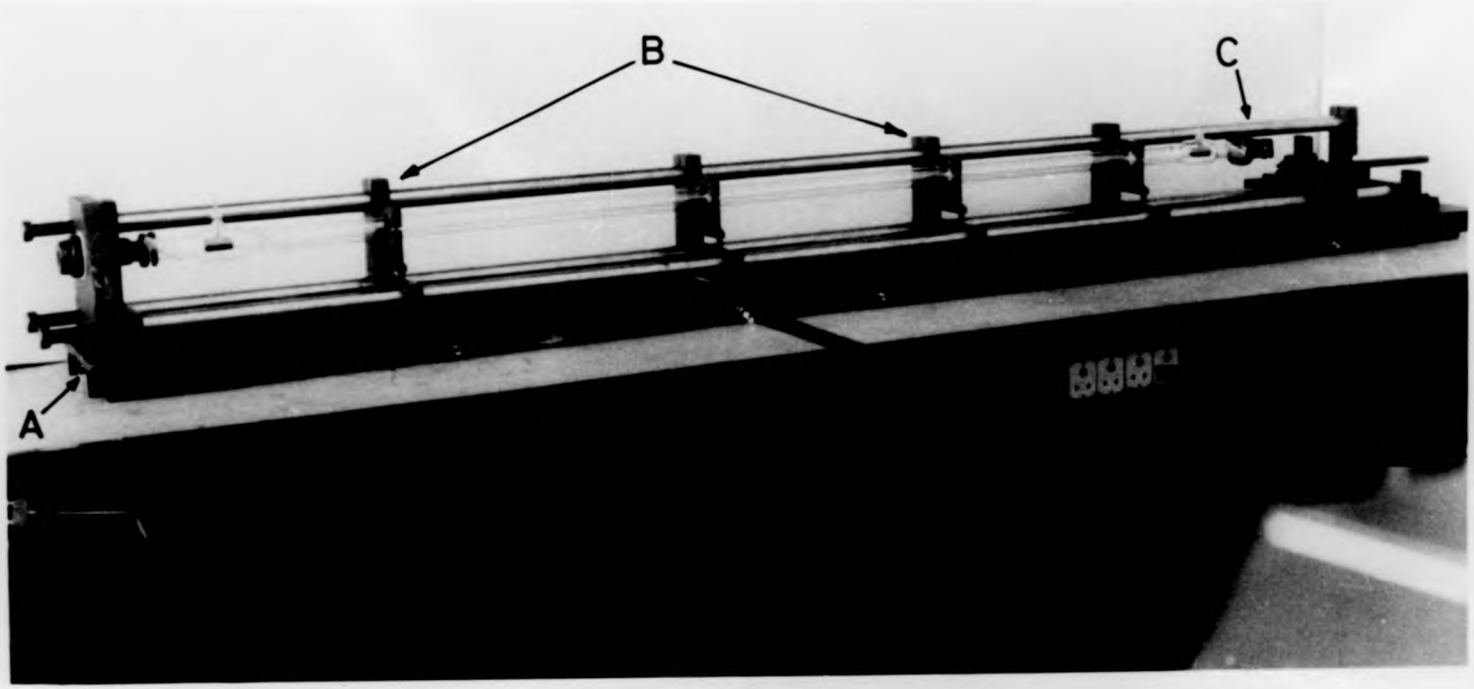

Fig 3.11 Structural backbone of the conventional laser.

(A) Baseplate

(B) L-shaped holders

(C) Invar rod

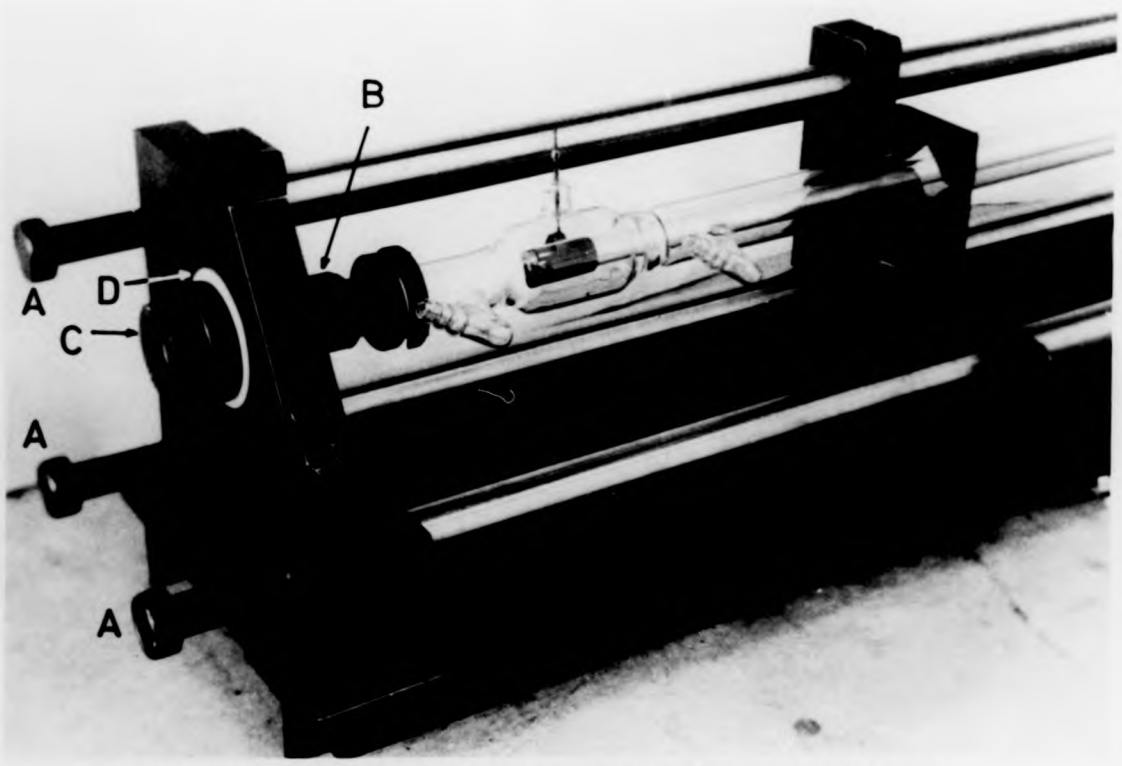

Fig 3.12 Front view of the conventional laser showing :
(A) Adjusting screws of the output coupler holder
(B) The flexible bellows (C) Output coupler holder
(D) Isolation ring

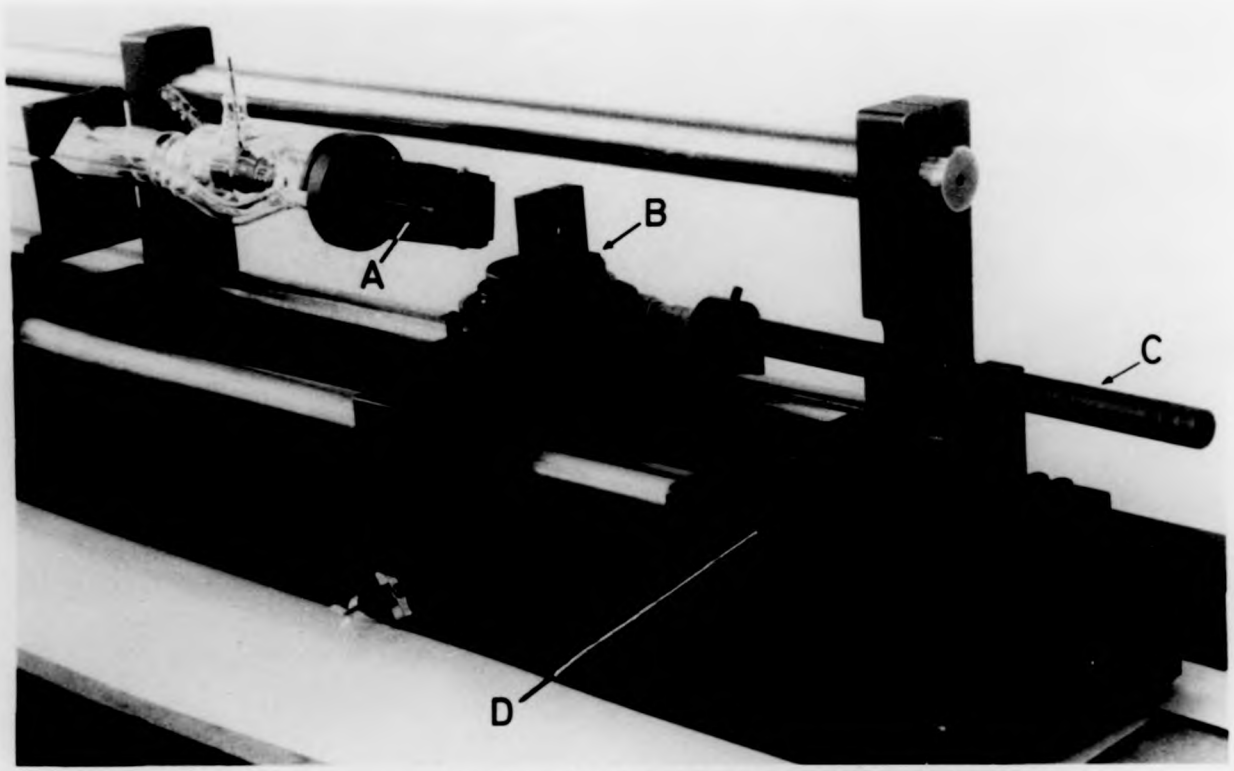

Fig 3.13 Tuning arrangements of the conventional laser showing :
(A) Brewster angle window (B) Grating mount
(C) Grating angle-adjusting micrometer rod
(D) Suspension mechanism

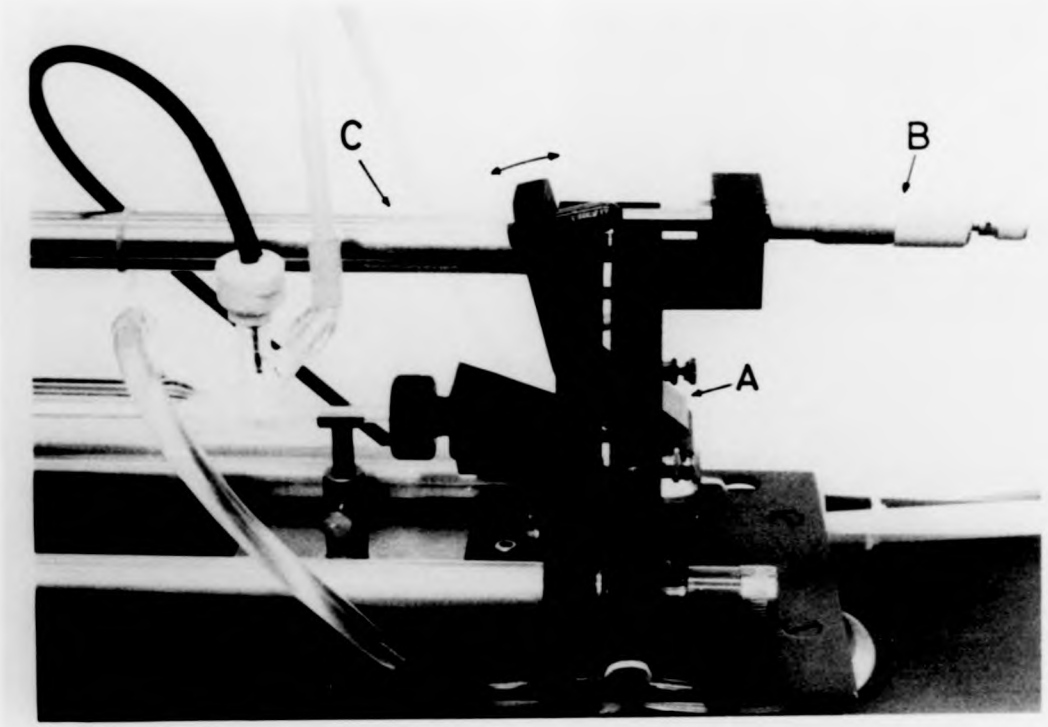

Fig. 3.14 Photograph showing the mechanism used for adjusting the grating in the waveguide laser.

(A) Grating (B) Micrometer

(C) Aluminium tube encasing the quartz tube.

(Duley 1976):

thermal expansion	$7.7 \times 10^{-6}/^{o}C$
thermal conductivity	13×10^{-2} W/cm ^{o}C
heat capacity	2.646 J/cm^3

and an absorption coefficient $\sim 6 \times 10^{-3}$ cm^{-1} at 10.6 μm.

ZnSe is chemically stable. Windows must be kept clean to avoid both scattering and absorption of laser radiation. ZnSe windows can be cleaned with acetone-wetted lens tissue papers. ZnSe is a toxic material and so must not be touched nor its vapour inhaled.

3.7 Mechanical Structure:

When all dimensions of the laser components are decided, the mechanical structure can be designed. Its importance is to hold all the components together and allow for easy access and optical alignment (see Fig. 3.11). It must maintain the condition of low thermal expansion. For both laser systems aluminium has been used to form the backbone base. A simple rule for choosing the material for the laser structure is the ratio of the thermal conductivity to that of thermal expansion (Goldsborough 1972). Large values of this ratio means that the metal can dissipate heat rather than expanding by absorbing it. For aluminium this ratio is $\sim 10^7$ watt/m at room temperature. However in the present design the length used imposes a limit on the distance of the output coupling plate which accommodates the mirror and the grating at the far end. The output coupling plate can be positioned by three adjusting screws thereby adjusting the mirror (see Fig. 3.12). The laser tube was held by spring loaded tufnol holders (see Fig. 3.11). A rotating table, Oriel Type 1641, was adapted for grating rotation in conjunction with a fine motion motor for the micrometer rotation. The motor, not shown in Fig. 3.13, was capable of rotating the grating clockwise or anti-clockwise. In Fig. 3.13

only the rotation axle is shown. The rotor was fitted to sit on the two bottom invar rods (see Fig. 3.13). The L-holder near to the output coupling plate was fastened to the base of the laser and at the other end the invar rods were suspended using flexible phosphor bronze sheets (a stack of five sheets each 0.5 mm thick) and short aluminium posts as shown in Fig. 3.13. The grating was held in a specially constructed grating housing sitting on three spring loaded pins for proper alignment in an xyz plane. The laser tube was closed at one end by an adapter housing a ZnSe Brewster window and at the other end with a bellows welded to the mirror holder. The mechanical structure of the waveguide laser is very similar except for the grating. In this case the normal to the grating can be rotated around an axis perpendicular to the laser beam in the plane of incidence (see Fig. 3.14). Mirror and grating separation was limited using three quartz tubes enclosed by aluminium tubes which act as a guard as well as provide a measure of thermal isolation. The quartz tubes were closed with stainless steel cups with vee circular or conical cuts to allow for easy mirror-grating alignment.

3.8 Discharge and d.c. supply:

The amount of current (I) required to sustain the laser gas discharge depends on the value of the laser tube bore since I is linearly proportional to diameter (Goldsborough 1972). The predictor equation can be written in the form of $(I/D_T) = 2.5$ mA mm^{-1} where D_T is the bore in mm. The optimum current was found to be independent of the gas pressure and the cooling liquid temperature (Bridges and Patel 1965B). On the other hand there is a linear dependence between population inversion and current density up to 10^{11} cm^{-3} where electron excited helium becomes a loss mechanism (White and Gordon 1963). Usually a d.c. supply is used to excite the discharge, but a rectified but unfiltered voltage proved

(Patel, Tien and Mcfee 1965) to increase the laser power. Voltage-current plots (Goldsborough 1972) of the gas glow discharge showed that the laser tube has a negative resistance and in order to maintain a discharge in the tube a larger positive resistance, called the ballast resistance, must be connected in series with the anode. As (I) is increased the tube resistance decreases gradually and a smaller value of ballast resistor is required. The opposite is true as I is decreased. A point is reached when a ballast resistance is not enough and instabilities are expected in the discharge. The discharge colour is normally blue-red with a redder colour near the anode. Formation of CO in the discharge is checked by the appearance of a blue tint (Smith 1969). Blue striations appear clearly at a pressure of ~0.1 torr indicating CO_2 dissociation through the equation

$$2CO_2 \longrightarrow 2CO + O_2.$$

A loss of CO_2 can reach 30% under these circumstances. The CO_2 dissociation rate increases with current and decreases with gas pressure. At a pressure of 15 torr and current of 40 mA it is of the order of 15% and larger than 65% for 4 torr pressure and 10 mA (Smith 1969). The existence of H_2O in the discharge can be checked for by looking out for a redder discharge; when P_{H_2O} is increased the colour becomes faint and normally the discharge dies at about 1 torr. An approximate value of the required discharge voltage (V) and current (I) can be obtained from the following formula (see eqn. 3.16):

$$(V \text{ volts/cm}) \times D_T(\text{mm}) = 2000$$

The supply used in the system reported here gives an open circuit voltage of 38 kV and has an internal ballast resistance of 300 kΩ. The supply incorporates a potentiometer for current adjustment. When the supply current is increased, the voltage across the laser tube was found to drop

i.e. constant current generator. The supply contains a facility for a piezo-electric tube voltage supply and an optogalvanic sensor for frequency stabilization. Early trials of the discharge in the waveguide laser was achieved using a 15 kV, 8mA supply. The middle electrode (see Fig. 3.10) was connected to the high tension (negative polarity) of the supply and each of the side electrodes were connected through a 1 M ballast resistance to the earth line. Other arrangements such as connecting the ballast resistance with the cathode line or connecting both the side electrodes to the same ballast resistance failed to give a stable discharge. At pressures larger than 30 torr discharge instabilities set in. These instabilities can be checked by increasing the ballast resistance, but at the expense of the necessary discharge current. The alternative solution is to use a higher voltage power supply.

3.9 Gas pressure and flow rate:

Gas mixtures used in conventional lasers are CO_2, N_2, He and Xe. The role of each of these gases was discussed in Chapter 2. The best ratios (Smith 1969) are 6% CO_2, 12% N_2 and 82% He. Other ratios can also be used. In the system studied a ratio of 6% CO_2, 24% N_2 and 70% He proved very successful. The optimum pressure depended on the threshold value determined by the diameter of the plasma tube. This follows from the fact that the current is affected by the value of bore diameter. A simple rule as mentioned before is Pd = 50 torr mm, where P refers to the partial pressure of CO_2 (Goldsborough 1972). The right pressure value must be maintained in order to avoid CO_2 dissociation which can be as large as 50%. It was found that dissociation decreased with an increasing flow rate of the gas. This results in the removal of hot gas and other gaseous products even before they dissociate. Increasing the flow rate with pressures up to 10 torr can increase the power output but no further

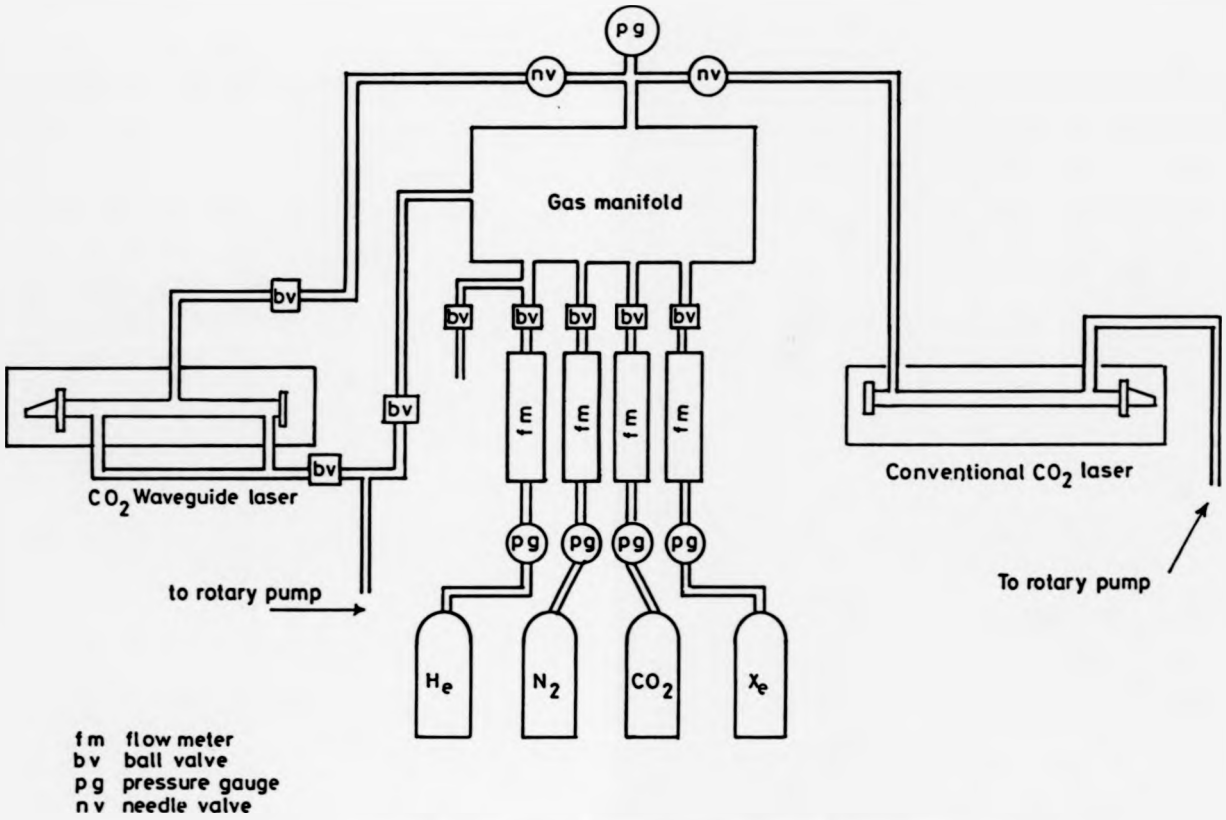

Fig. 3.15 : Gas mixing system for a CO_2 laser.

advantage is obtained at higher pressure (Smith 1969). To get rid of chemical reactions in the tube (Goldsborough 1972) the gas must pass through the laser tube in not more than 0.2 s. By taking a flow of about 100 l/h, calculations were carried out using a normal calculation procedure explained in Brooks Corporation Catalogue (1984 copy). Four flow meters were selected to suit the flow of CO_2, N_2, He and Xe. The flow meters are connected to a mixing chamber which supplied the laser through a needle valve, with a pressure gauge positioned as shown in Fig. 3.15. Early tests of the laser in operation were performed using a pre-mixed gas of 70% He, 24% N_2 and 6% CO_2. The mixing system was used for both lasers and the flow rate to each laser could be adjusted independently through the needle valve connecting the laser tube to the mixing chamber. The gas manifold was pumped prior to refilling using the same rotary pump as used to pump the waveguide laser. The flow rate was such that the gas was changed 120-150 times/min when the laser was operated at a pressure of 20 torr. Separate gas cylinders were not used, rather only the premixed gas for reasons of low cost.

3.10 Cooling the laser tube:

Experiments by many authors, for example Thomas et al. (1969), showed that a temperature gradient exists between laser tube centre and its walls. This can be as high as 300^{o}C. The gain of the laser is proportional to $T^{-3/2}$. Bridges and Patel (1965B) managed to increase the gain by 1.5 times when cooling the laser tube from +40^{o}C to -60^{o}C. This shows the importance of cooling for effective laser operation. The decrease in the gain is due to the filling of the lower laser level thereby decreasing the population inversion (Sasnet 1984). Thomas et al. (1969) managed by proper cooling and pumping to obtain a power of 140 watts from a laser tube only 10 cm long and 1.35 cm diameter.

According to their calorimetric calculation 8% of the input energy was transferred to the cooling water. Frequency tunability can be increased by cooling (Lyszyk et al. 1977). The two laser systems described in this thesis were cooled using tap water. As an extra safety precaution the water was made to pass through a pressure trip switch which cuts the power off the power supply in case of water failure.

3.11 Alignment of the resonator:

Proper alignment of the laser resonator is critical for laser operation. The first target of laser operation is to achieve what is called a near-alignment and once the laser is oscillating further alignment can be carried out for optimum power output and single mode operation. Depending on the type of resonator being used the alignment operation can be described as simple or difficult. As a simple rule in mirror alignment the oscillating mode axis must lie on the line joining the centre of the two mirrors if both concave, or the perpendicular to the surface of the plane mirror and the centre of the concave mirror (Bloom 1968). The optimum condition of course for optimum laser power output is that the line joining the mirrors lies in the centre of the tube (Sinclair 1964). Assuming two concave mirrors of radius of curvature R_1 and R_2 at a distance L_c apart, then if one of the mirrors is tilted by an angle θ, assuming small angle approximations, the mode will be displaced a distance "X" on this mirror (Bloom 1968), given by:

$$X = \frac{R_1(R_2-L_c)\theta}{R_1 + R_2 - L_c} \qquad (3.25)$$

On the other mirror the mode displacement is given by:

$$Y = \frac{R_1R_2\theta}{R_1 + R_2 - L_c} \qquad (3.26)$$

From these relations it is easily seen that the confocal assembly is the easiest to align as $X = 0$ and $Y = R\theta$. In this case the two mirrors can be moved independently for achievement of optimum power. For long radius mirrors a method called a "walking procedure" is advisable. One mirror is adjusted until power is reduced by 3 dB of the peak value, then the other mirror is adjusted along the same axis until the power is at a maximum. If the power is larger than the one adjusted at the commencement, then the process can be repeated in the same way. If the power is reduced then the process is reversed along the other direction. Alignment of the laser systems in this work follows the alignment procedure necessary for a hemispherical cavity although in this case a grating was used instead of a plane mirror. The following steps were followed for optical cavity alignment:

(1) A He-Ne laser beam was passed through a pin-hole drilled in a plastic disc closing one end of the laser tube and through a pinhole in a second disc made with the dimensions of the mirror and temporarily placed in the mirror holder. The light spot had to look sharp, clear and free of any scattering.

(2) The laser tube was then removed and if the laser beam passed through the centre of the tube, the beam was then found to pass through the hole in the plastic disc in the mirror holder. If it did not, then the beam was guided by the tube and the light spot seen was the result of internal reflection. In that case steps 1 and 2 had to be repeated until the aim was achieved.

(3) The laser mirror was then placed in the mirror holder instead of the disc with a centre hole. Screws were then adjusted until the smallest diameter spot was achieved and made to coincide with the

incident beam. This procedure guaranteed that the mirror reflected radiation along the laser tube centre.

(4) The grating was placed in its holder and rotated to face the laser beam to make an angle of 90^{0} with the incident He-Ne beam. The three adjusting screws on the grating mount base were then adjusted until a situation was reached where all the fringes from the rotatable grating passed over the pin hole position. The He-Ne laser beam that emerged then illuminated a white screen with a pinhole in front of the He-Ne laser. This step was easily and quickly achieved by using a small T shaped spirit level to align the grating. In the case of the waveguide laser this step was taken before setting the mirror in place since the grating rotates around an axis perpendicular to the place of incidence. The grating is then removed and the output mirror is placed in its holder and the best focusing situation is located as mentioned earlier.

(5) Final adjustments of grating and mirror were carried out with the laser in operation, checked to be operating at optimum power and in single mode.

3.12 Laser performance:

The two lasers constructed were optimized for their best performance. The conventional laser oscillated at pressures from 10 torr and up to $\leq$25 torr. It oscillated on all four branches of the spectrum $(00^{0}1\text{-}10^{0}0)$ and $(00^{0}1\text{-}02^{0}0)$ giving the following results:

Branch	Pressure (torr)	No. of oscillating lines
P(001-100)	12	17
R(001-100)	12	16
P(001-100)	16	19
R(001-100)	16	19
P(001-02^{0}0)	12	14
R(001-02^{0}0)	12	9
P(001-02^{0}0)	16	16
R(001-02^{0}0)	16	9

The best stable and spark-free pressure was found to be in the range 10 to 25 torr. When the grating was used as a mirror (i.e. perpendicular to laser beam) the line P(20) of the (001-100) transition dominated which gave a power of about 8 watts. When the grating was rotated to the corresponding angle of P(20) the power was about 24 watts. Reducing the pressure gave discrete and well separated lines since many lines stopped oscillating. Single mode operation was easier to obtain with a mirror of 80% transmission and 10 m radius of curvature in contrast to a 90% mirror of 5 m radius of curvature. The power supply used for the conventional laser was a constant current generator. Hence maximum power was obtained at the lowest current which gave the maximum voltage drop along the laser tube. For example, at a gas pressure of 12 torr the laser oscillated on the line P(20) with a current of 12 m, a voltage V = 11.4 kV and gave 10 W output power. When the current was increased to 28 mA, the voltage dropped to 9.4 kV and the power was reduced to about 1.2 watts. In another experiment the laser was operated at a gas pressure of 16 torr, again using the line P(20): I = 12 mA, V = 15.5 kV and the power output was approximately 20 watts. When I = 28 mA, V = 12.8 kV, the power output dropped to about 10 watts. In the initial work with the conventional

laser a problem was encountered when the electric field of the radiation was parallel to the ruling of the grating. It was found that with P_{out} = 18 watts, about 14 watts was delivered in the zero order diffraction pattern of the grating. When the Brewster window was rotated 90^{o} in such a way that the electric field of the radiation is perpendicular to grating rulings, the side power was reduced to less than 1 watt and the output power increased from 18 to ~24 watts. This is due to the enhanced efficiency of the grating. The reason is not obvious; this was also noticed by Hard (1970) in the visible region of the spetrum (see Section 3.6.2).

The waveguide laser was operated using a simple power supply without smoothing. With careful alignment, a power of 2.8 watts was delivered with 3.5 kV applied across both branches of the discharge. The tube current was 5.4 mA. The capability of the available supply was 12 kV and 8 mA. The optimum pressure for the waveguide laser was 50 torr. The efficiency and hence the power of the laser would be raised by using a better supply and operating at a higher pressure. It is concluded that both lasers operated satisfactorily in terms of oscillation on the laser lines intended and in respect of their power output.

Chapter 4

The optogalvanic effect

4.1 Introduction:

The optogalvanic (OG) effect is simple, inexpensive, sensitive and has found many useful applications. It has been used successfully in spectroscopy (Goldsmith and Lawler 1981; King and Schenck 1978; Zalewski, Keller and Apel 1981; Webster and Rettner 1983B). In fact OG spectroscopy has proved to be a good alternative to other spectroscopic methods and indeed has successfully overcome a number of the experimental problems (Goldsmith et al. 1981). For example OG spectroscopy is important in studies of noble gases when direct absorptive transitions from the ground state require vacuum ultraviolet spectroscopy. It is also a good alternative to absorption spectroscopy where intensity fluctuations of the order ~1% cannot be avoided. In fluorescence spectroscopy where the fluorescent signal is weak, OG spectroscopy is a useful alternative method. However the optogalvanic effect (OGE) has limitations of its own, in particular discharge noise (Moffatt and Smith 1981). OGE spectroscopy can also be used to avoid the need for special experimental equipment such as low noise detectors, interferometric-quality optics or high quality polarizers (Lawler, Ferguson, Goldsmith, Jackson and Schawlow 1979). To get an idea of the sensitivity of OGE spectroscopy, some comparative examples will be given. Firstly the OGE has been used in analytical flame spectroscopy (Turk, Travis and Devoe 1978) with a detection sensitivity less than one part per billion (1 ppb). Concentrations of sodium as small as 1 ngr/ml have been detected in flame absorption spectroscopy by Zalewski et al. (1981). Secondly, in an isotope ratio-analysis experiment, Keller, Engleman and Zalewski (1979) measured concentrations of ^{235}U as small as

10^8 atoms/cm^3. Thirdly, the OGE has also been used in RF discharges (Vasudev and Zare 1982), fourthly, in two-photon spectroscopy (Goldsmith, Ferguson, Lawler and Schawlow 1979) and fifthly in Zeeman spectroscopy (Beverini, Galli, Inguscio, Strumia and Bionducci 1983). In this chapter the use of the OGE is described for the purpose of CO_2 laser frequency stabilization. Such an application of the OGE has been very successful (Kavaya, Menzies and Oppenheim 1982; Moffatt and Smith 1979; Moffatt and Smith 1981; Skolnic 1970 and Walsh 1985). In the rest of this chapter the theory of the OGE associated particularly with CO_2 laser discharges will be discussed. The method of OG signal detection together with the OG sensing circuit is given in Section 5.3. Simultaneous detection of laser oscillations using OG and OA techniques will be presented in Chapter 6.

4.2 The optogalvanic effect:

The OGE was first discovered by Penning (1928) when one discharge tube was irradiated by another. It was observed subsequently in a CO_2 laser discharge by Rigden and Moeller (1966) who noticed a variation in the colour of the plasma accompanied by a change in the discharge current. The OGE shows itself as a change in the laser tube impedance resulting in a voltage change across the tube upon irradiation with a strong optical radiation field (Smith and Moffatt 1979B; Goldsmith and Lawler 1981; Webster and Menzies 1983A; and Doughty and Lawler 1983). Laser tube impedance can be thought of as composed of two parts (Carswell and Wood 1967). The first part is current dependent z(i) and the other intensity dependent (z'). By changing the laser intensity the laser impedance (z') will change by say (Δz') bringing about a change in the total laser impedance. In discharge tubes containing atomic vapours when a radiation field illuminates the discharge at a frequency that is coincident with an atomic transition, a change in the equilibrium condition of the discharge

occurs, hence the discharge electrical properties change. Several ionization reactions can play a role in producing the effect. These frequently involve collisions between metastable atoms (Goldsmith et al. 1981). The increase of the discharge current can be seen as a result of atoms being excited from levels of small ionization probability to levels of higher ionization probability from which they are more easily ionized. The opposite effect can also occur. Many models had been formulated to give a phenomenological account of the OGE (Pepper 1971; Erez, Lavi and Miron 1979; Lawler 1980; Doughty and Lawler 1983; and Moffatt and Smith 1984). In this thesis the model that has been suggested by Moffatt et al. (1984) which is mostly concerned with the OGE in CO_2 lasers will be discussed. Three mechanisms are thought to be responsible for the OGE (Smith and Brooks 1979A). These are as follows: gas temperature change, momentum exchange and two step ionization of N_2. The gas temperature model will be discussed in some detail and the other two mechanisms will be discussed only briefly. The gas temperature model is sometimes called the temperature perturbation or discharge cooling model. It was first established by Smith et al. (1979A) as follows. The $CO_2(00^01)$ level is usually pumped by electron collisions or V-V collisions with N_2 gas molecules in the multi-gas laser medium. This level then relaxes through the vibration-vibration-translation (V-V-T) and stimulated emission. But when the medium is coupled to the laser field giving rise to laser oscillations as a result of stimulated emission, the energy which could have been coupled to the discharge is now lost from the system as the laser output. This of course results in a gas cooling effect, which leads to an increase in the number density of laser gas in the plasma region and consequently there is an increase in electron-molecule collisions. In this case either a larger voltage is required to maintain the same current resulting from the impedance increase, or a constant potential drop across

the tube forces the current to decrease. In the following a brief account of the theory of Moffatt et al. (1984) will be given. In a molecular gas laser it can be said that any change in the energy gained by the discharge is equal to that lost by the electron stream. Assuming that all colliding partners have a density n it can easily be shown that:

$$\frac{\Delta P_{coll.}}{P_{coll.}} = \frac{\Delta n}{n} \tag{4.1}$$

where $P_{coll.}$ is the energy gained per second by the laser gas as a result of electron molecule collision. This means that the fractional energy change gained by the discharge is equal to that of the fractional density change in the colliding partners. On the other hand the fractional change in the discharge input power ($\Delta P/P$) is equal to that lost to the stream of electrons so it follows that:

$$\frac{\Delta P}{P} = \frac{\Delta P_{coll.}}{P_{coll.}} = \frac{\Delta n}{n} \tag{4.2}$$

Assuming an ideal gas behaviour at constant pressure, then:

$$\frac{\Delta n}{n} = -\frac{\Delta T}{T} \tag{4.3}$$

where T is the translational temperature of the laser gas given as:

$$T = t_w + t_{dis} = t_w + m(P/L) \tag{4.4}$$

Here t_w is the wall temperature of the laser tube, t_{dis} is the temperature of the discharge, P/L is the input electrical power per unit laser length and m is a coefficient dependent on pressure and gas composition. Suppose Q watts are removed from the asymmetric stretch mode of CO_2 molecules when the laser oscillates, then the change in the translational temperature can be expressed as follows:

$$\frac{\Delta T}{T} = \frac{-mQ}{Lt_w + mP} \tag{4.5}$$

By substituting $Q = I(\gamma/2)A$ and using eqns. (4.2) and (4.3), eqn. (4.5) becomes:

$$\frac{-\Delta T}{T} = \frac{\Delta P}{P} = \frac{A\gamma I}{2(\frac{Lt_w}{m} + P)} \tag{4.6}$$

where I is the laser intensity

γ is the laser loss

A is the laser tube cross-sectional area.

By taking the coefficient X to be equal to:

$$X = P/2\ (Lt_w/m + P) \tag{4.7}$$
$$= 1/2(t_w/t_{dis} + 1)$$

X can be called the OGE coefficient, and the discharge power fluctuation can be written in terms of X as:

$$\Delta P = A\gamma IX \tag{4.8}$$

or in terms of the output coupler reflectivity

$$\Delta P = [(1+R)/(1-R)]\ P_{out}\ \gamma\ X \tag{4.9}$$

where P_{out} is the laser output power and R is the laser output coupler reflectivity. If now both sides of eqn. (4.9) are divided by the input electrical power P, then

$$(\frac{\Delta z}{z}) = (\frac{\Delta P}{P}) = \left[(\frac{1+R}{1-R})\right]\gamma X(\frac{P_{out}}{P}) \tag{4.10}$$

where (P_{out}/P) is the laser efficiency. Experimental results of Moffatt et al. (1984) showed that $(\Delta z/z)$ can be ~0.5 for high (P_{out}/P) or well

aligned cavities and can reach ~1.0 for badly aligned cavities. From eqn.(4.7) it is concluded that the OGE coefficient is dependent on t_w and t_{dis} and its value is determined on the level of excitation described by (P/L), gas composition and total pressure. Experimental results of Moffatt et al. (1984) (see Fig. 4.1) revealed that the OGE coefficient increases as the pressure rises with the constant current generator mode of excitation. As the electrical power (P) increases so does (P/L). From eqn. (4.9) it is evident that as the mirror reflectivity is increased, the factor $(\frac{R+1}{1-R})$ is increased but γ is expected to decrease. So $(\Delta P/P_{out})$ will increase as R is increased (see Fig. 4.2). This seems logical because when R is increased more of the radiation field is retained in the cavity hence P_{out} is less. The OGE signals usually disappear at modulation frequencies in the range 2-3 kHz; but it is possible to detect OG signals at modulation frequencies up to 100 kHz (Moffatt and Smith 1981). Stabilization at these frequencies is expected to be much better than those established at low frequencies, since this will improve the signal to noise ratio (S/N), the noise level from supply harmonics is less and stabilization can be achieved in a shorter time. A full account of the processes involved for both high and low frequency regimes is given, (Moffatt et al. 1981) (see Fig. 4.3). The upper part of the figure shows that there is a competition between stimulated emission and other processes represented by the reaction

$$CO_2(00^0 1) + M \longrightarrow CO_2\ (n,m,0) + M + T_u$$

where M is all possible collision partners, and T_u the translational energy resulting from the upper laser level collision with the M molecule. Usually the $CO_2(n,m,0)$ end up in the (010) state according to the following reaction (Patel 1968):

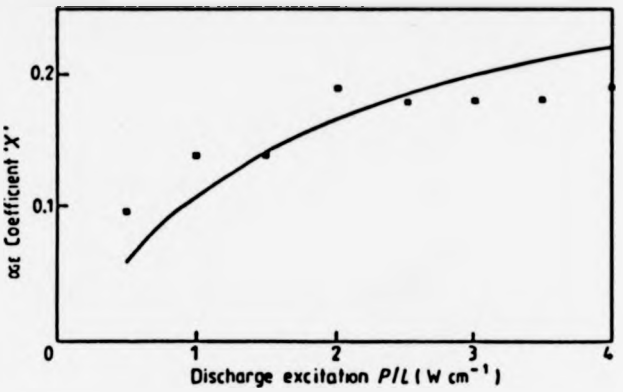

Fig. 4.1 : Change of the OGE coefficient "X" versus discharge power per unit length of laser tube. (After Moffatt et al. 1984.)

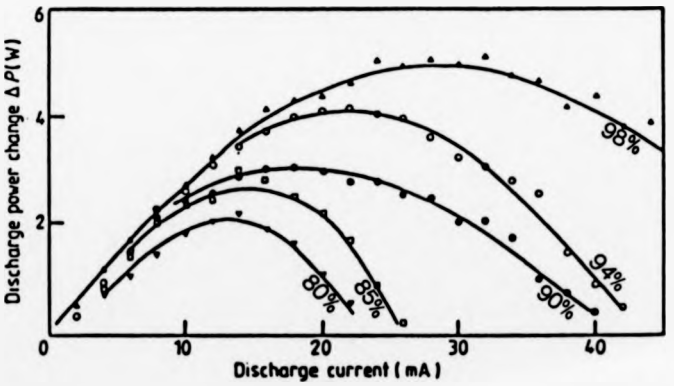

Fig. 4.2 : Electrical power change versus supply current at different mirror reflectivities for 3 torr Xe, 3 torr N_2, 16 torr He and 4 torr CO_2. (After Moffatt et al. 1984.)

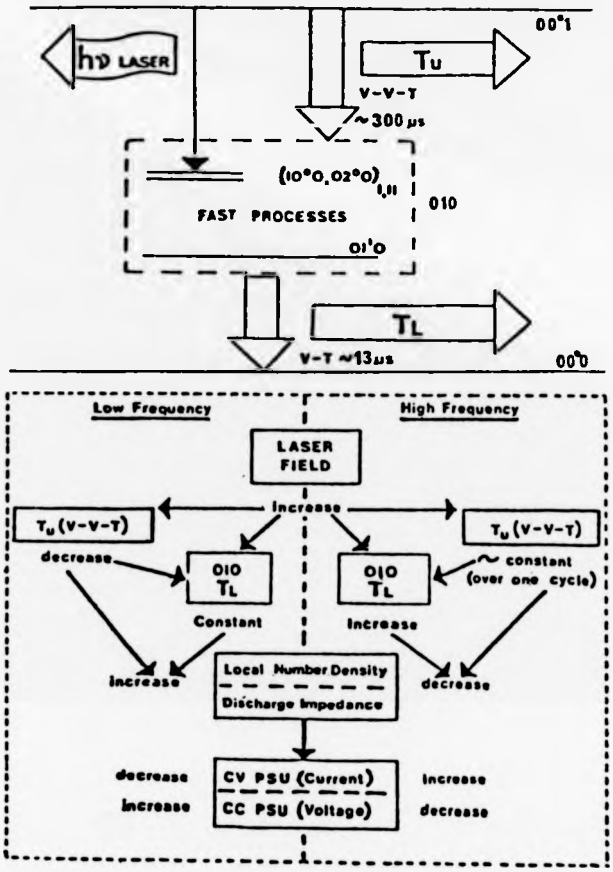

Fig. 4.3 : The OGE process in CO_2 lasers for high and low frequency regimes.
Reproduced from Moffatt et al. (1981).

$$CO_2(10^00) + CO_2(000) \longrightarrow CO_2(01^10) + CO_2(01^10)$$

When the (01^10) level relaxes to the ground state (000) level all energy will be released as translational energy (T_L) represented by the reaction:

$$CO_2(01^10) + M \longrightarrow CO_2(000) + M + T_L.$$

If the laser field is increased by driving the laser oscillation towards the line centre, then T_u is expected to decrease since the majority of (001) levels are removed by the stimulated emission. T_L is expected to stay the same as all the population still flows through the (010) level and the pump rate of (001) is constant for both halves of the cycle. So there is a net decrease in the energy transferred to the gas following the decrease of T_u. This results in gas cooling and hence an increase in the local number density resulting in impedance increase. Hence the current is modulated at the modulation frequency. When the modulation frequency is slow the pumping and relaxation processes come into equilibrium over the period of a small cycle. The OG signal will approach zero when the modulation frequency is of the order $\sim 1/2\ \tau_{001}$, where τ_{001} is the relaxation time of the upper laser level of the order ~300 μs (Moffatt et al. 1981). When the modulation frequency is increased further then T_L will acquire a modulated component. Moffatt et al. (1981) expected the crossover frequency to be about 40 kHz corresponding to the lower laser level lifetime of ~13 μs. In summary, the voltage for the constant current generator mode should increase when the modulation frequency is low and will decrease at a high frequency modulation (see Fig. 4.3). Moffatt et al. (1981, 1984) performed their OG studies in a conventional type of laser at working pressures of 15 to 25 torr, composed of He, CO_2, N_2 and Xe. OGE studies at higher pressures in waveguide lasers in the range 15 to 60 torr were carried out by Walsh (1985).

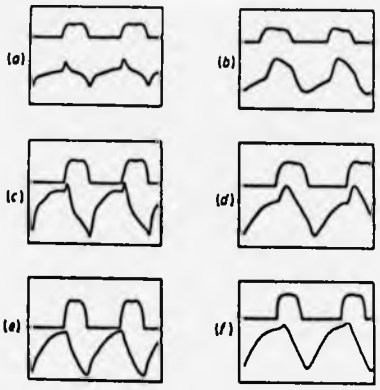

Fig. 4.4 : Oscilloscope traces of the OG signal (lower trace). The top trace is the chopped laser power. Operational conditions are: (a),(b) 16 torr, 4 mA; (c),(d) 25 torr, 6.5 mA; (e),(f) 54 torr, 8 mA. The chopping frequency was 500 Hz for (a),(c) and (e) and 2.5 kHz for (b),(d) and (f). Reproduced from Walsh (1985).

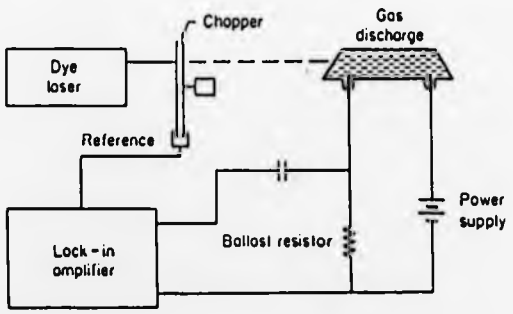

Fig. 4.5 : Schematic to show the most common way of OG signal detection. (After Goldsmith et al. 1981).

His gas mixture was He:CO_2:N_2 in the ratio of 75:15:10 respectively. The OG signals obtained by chopping the beam are shown in Fig. 4.4. The signals are composed of two components. An in-phase short-lived component was accompanied by an out-of-phase long-lived component. The latter was noticed to be of larger amplitude at high gas pressure and current. The OG response was found to cease at a certain frequency called the crossover frequency. This particular frequency is very dependent on pressure and current (Walsh 1985).

The second mechanism which has been suggested as being responsible for the OGE is called "momentum exchange". This has been suggested by Lobov, Shtykov, Bogatkin and Drugov (1972). The essence of this approach assumes a change in the rate of energy exchanged between molecules and electrons in elastic collisions which will affect the electron mobility and hence the discharge current. In Lobov et al. (1972) electron mobility was derived on the basis that there is no change in electron density or mean free path. But Smith et al. (1979A) in their study measured pressure changes, rejecting the idea of constant mean free path. The third mechanism was suggested by Nowiki and Pienkowski (1982) who assumed that a two step ionization of N_2 was responsible for the effect. They found that when radiation was coupled to the laser gas discharge there was a change in the ionization rates of N_2 which results in a current change. This model was checked by Smith and Moffatt (1984) and was dismissed as being responsible for the OGE in CO_2 laser discharges for the following reasons. The model was not considered to be complete as it does not account for the OGE amplitude response with frequency, gas composition and pressure. When N_2 was replaced by CO in the same mixture it was found from the i-v characteristics that the mixture with CO has a lower impedance, contrary to the fact that two step ionization predicts a lower impedance when N_2 is used. Finally Smith and Moffatt (1984) used the experimental results of

Smith et al. (1979A) which showed that there is a large OG signal in gas discharges of pure CO_2 as well as in CO_2-N_2-He mixtures. This showed that signals could be obtained with or without the existence of N_2. It can be concluded that the gas temperature model offers a satisfactory explanation to the different aspects of the OGE as has been proven by the experimental results of Moffatt et al. (1981, 1984). Their results will be used to explain the OA compared with the OG results (see Chapter 6).

4.3 OG signal detection:

Any optogalvanic sensing circuit should overcome the problem of high voltage isolation. One of the most common techniques of OG detection is to couple out the a.c. signal through a blocking capacitor used for d.c. isolation (King, Schenck, Smyth and Travis 1977; Green et al. 1976; Lawler et al. 1979; Goldsmith et al. 1981; Rettner et al. 1981; and Zalewski et al. 1981). As an example the circuit used by Goldsmith et al. (1981) is shown in Fig. 4.5. Alternatively Thomson and Elbers (1975) detected the OG signal by connecting a parallel R-C combination in series with the ballast resistors. One advantage of this arrangement is to dampen high frequency oscillation of the supply (see Fig. 7.3). Other pick-off techniques have been reported in the literature by Suzuki (1981). He detected the OG signals by winding a coil of inductance 10 nH around the laser tube. This method is simple and provides a solution to high voltage isolation (see Fig. 4.6). In the present work the OG signal was picked up using an optogalvanic sensing circuit built into the supply (Edinburgh Instrument Type PS4R) as shown in Fig. 4.7. The back to back diodes act as a safety clamp to the circuit preventing the voltage applied to the 100 kΩ resistor from rising above 6.9 volts. The inclusion of the capacitor-resistor combination acts as a low frequency filter discriminating against noise pulses below 300 Hz.

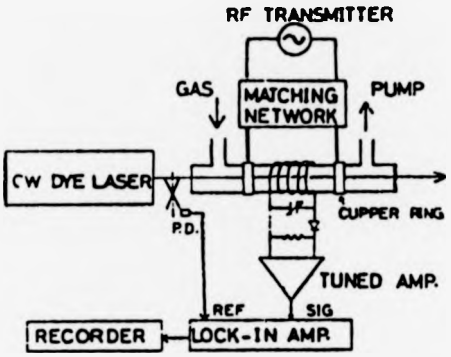

Fig. 4.6 : Schematic to show OG signal detection employing the coil method.
(After Suzuki 1981).

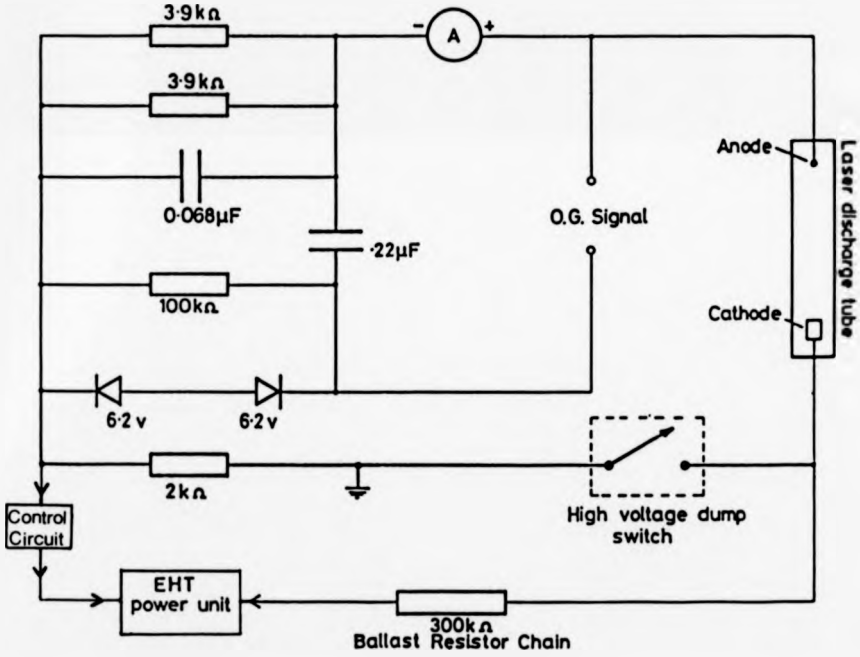

Fig. 4.7 : The built in supply OG sensing circuit used in the present study.

Chapter 5

The optoacoustic technique

5.1 Introduction:

The optoacoustic (OA) technique was discovered by Bell as early as 1880. For many years the optoacoustic phenomenon lay dormant; but interest in it was renewed following the discovery of the laser and its applications, as first demonstrated by Kerr and Atwood (1968). Subsequent work has shown the versatility of optoacoustics for studies of a wide range of phenomena. An example is that of trace gas analysis which when performed in an intra-cavity optoacoustic cell showed that absorption coefficient as low as 3×10^{-10} cm^{-1} could be measured (Shtrikman and Slatkin 1977). The method has as a consequence found an important application in air pollution studies (Dewey, Kam and Hackett 1973; Rosengren, Max and Eng 1974; Goldan and Goto 1974). For wider applications of the optoacoustic technique in physics, chemistry, biology, microelectronics and medicine the reader is referred to the book by Rosencwaig (1980).

In this thesis the optoacoustic effect has been detected for the first time in a laser cavity within the plasma tube envelope and used for laser stabilization at any chosen laser line frequency in an analogous way to the optogalvanic method. In the sections that follow the OA technique is discussed and two cells used for internal and external detection of OA signal are described, together with a suggested cell for OA detection in a waveguide laser.

5.2 The optoacoustic technique - theoretical background:

5.2.1 Optoacoustic theory in an acoustic cell:

The optoacoustic technique is simple, inexpensive and sensitive. The principle of the method (Dewey et al. 1973) is simply to allow a modulated laser beam to pass through a cell containing a gas sample with an absorption transition coincident with the laser wavelength. This will result in a modulated pressure which can be detected very sensitively using a microphone. The first step in generation of optoacoustic signals (OAS) is efficient absorption of light which in turn produces a varying source of heat, thus gas expansion which is detected as a sound (Kreuzer 1977). Assuming no other absorption mechanism is responsible the OAS is proportional to the density of the absorbing molecules (Goldan et al. 1974). If a laser beam of intensity $I(\vec{r},t)$ is passed through an OA cell the heat $H(\vec{r},t)$ produced as a result of light absorption is given by (Kruezer 1977):

$$H = \alpha I \tag{5.1}$$

$\vec{r}$ describes the position and t the time, and α is a proportionality constant. The above equation is true if two conditions are satisfied. Firstly (I) should be small so that saturation does not occur. If this condition is not satisfied a nonlinear term should be added to eqn. (5.1). The second condition is that any time variation of (I) should be small compared with the rate of transfer of absorbed energy from the absorbing transition into heat. If the first condition is satisfied but not the second then the variation of (H) with time lags behind that of I and α in this case is frequency dependent and eqn. (5.1) becomes:

$$H(\vec{r},\omega) = \alpha(\omega)I(\vec{r},\omega) \tag{5.2}$$

If both conditions are not satisfied at the same time the situation is complex. For the condition of small I, for a given density of upper state population (n_1), the generated heat will take the following form:

$$H = (n_1/\tau_c)\, h\nu \tag{5.3}$$

$$\alpha = \frac{NS\,\tau}{\pi\Delta\nu\tau_c} \tag{5.4}$$

where N is the density of the absorbing molecules, $h\nu$ is the energy of the transition, $\Delta\nu$ is the linewidth of the transition, S is the line strength and τ_c is the collisional lifetime and τ_r is the radiative lifetime of the upper state such that $\tau^{-1} = \tau_r^{-1} + \tau_c^{-1}$. This last quantity τ is called the total relaxation lifetime of the upper state. This source of heat described by eqn. (5.3) will cause a varying gas pressure which is detected by a microphone. This pressure is given by the following expression (Rosencwaig 1980):

$$P = \frac{kE_1N^2}{C_v\omega}\left[\frac{2\,\tau_c^{-2}BI_o\,\delta}{(2BI_o+\tau^{-1})\,[(2BI_o+\tau^{-1})^2+\omega^2]^{\frac{1}{2}}}\right] e^{i(\omega t-\gamma'-\pi/2)} \tag{5.5}$$

The measured optoacoustic pressure by the microphone is q = -P. In the above equation k is Boltzmann's constant, N the number of molecules cm^{-3}, C_v the specific heat/cm^3 at constant volume, ω the modulating angular frequency and $\gamma' = \omega\tau$. Here γ' is of physical importance as $\gamma' = \tan\Phi$ where Φ is the phase angle between the OAS and the chopped laser power (Kaiser 1959 and Claspy 1977). $B = B_{10}\, h\nu/c$ where B_{10} is the Einstein coefficient for stimulated emission from level 1 → 0. δ is a factor arising from the assumption that the modulated intensity at frequency ω is given by $I = I_o(1 + \delta\exp(i\omega t))$ and E_1 is the energy of excitation of the upper state.

As far as the microphone signal is concerned two situations can be considered. If I_o is small then $2BI_o << \tau^{-1}$ and the microphone signal is given by

$$q = \frac{kEN^2}{C_v \omega} \left(\frac{\tau}{\tau_c}\right)^2 \left| \frac{2BI_o \delta}{(1+\omega^2\tau^2)^{\frac{1}{2}}} \right| e^{i(\omega t - \gamma' - \pi/2)} \qquad (5.6)$$

It is obvious that the OAS is linearly proportional to N^2 and I_o. The proportionality of the signal to $(\frac{\tau}{\tau_c})^2$ should also be noted. The value of τ_c usually decreases with a rise of temperature, hence the signal is expected to increase as the cell temperature is increased. For high intensities $2BI_o >> \tau^{-1}$ and eqn. (5.5) becomes:

$$q = \frac{kE_1N^2}{C_v \omega} \tau_c^2 \frac{1}{BI_o} \delta \, e^{i(\omega t - \gamma' + \pi/2)} \qquad (5.7)$$

This is the case for saturation absorption and the signal is proportional to I_o^{-1}.

The next important step in understanding the origin of the magnitude of OA signals is to probe the relation to the cell in which the sample is kept. Assuming the sample cell is a cylinder of radius (a) and length (L) then the normal mode solution (P_j) of the acoustic pressure can be written as:

$$\frac{1}{r}\frac{\partial}{\partial r}\left(r \frac{\partial P_j}{\partial r}\right) + \frac{1}{r^2}\frac{\partial^2 P_j}{\partial \theta^2} + \frac{\partial^2 P_j}{\partial z^2} + k_j P_j = 0 \qquad (5.8)$$

A full account of the origin of the solution (Morse 1948) for eqn. (5.8) is given by Kruezer (1977) and Rosencwaig (1980). The normal mode solution is equal to:

$$P_j = \begin{matrix}\cos \\ \sin\end{matrix}(m\phi)\,[A\, J_m(k_r r) + B\, N_m(k_r r)]\,[C \sin(k_z z) + D \cos(k_z z)] \qquad (5.9)$$

J_m is Bessel function of the first kind

N_m is Bessel function of the second kind

Since $N_m(0) = \infty$ then B = 0. To satisfy the boundary conditions then the gradient of P perpendicular to the walls must be equal to zero since the cell walls are rigid. Thus

$$\left(\frac{\partial P_j}{\partial z}\right)_{z=0,L} = 0 \quad \text{and} \quad \left(\frac{\partial P_j}{\partial r}\right)_{r=a} = 0.$$

This sets $C = 0$ and $k_z = \left(\frac{\pi}{L}\right) n_z$, $n_z = 1,2,3$ (5.10)

$$k_r = \left(\frac{\pi \alpha_{mn}}{a}\right) \tag{5.11}$$

n_z, n, m are the eigenvalues related to longitudinal, azimuthal and radial modes respectively. α_{mn} is the nth root of the equation involving the mth order Bessel function so the final solution for P_j will take the following form:

$$P_j = \begin{matrix}\cos \\ \sin\end{matrix} (m\phi) \, [A \, J_m(k_r r)] \, [D \cos(k_z z)] \tag{5.12}$$

Substituting this solution in the cylindrical wave eqn. (5.8) and using $k_j = \omega_j / C_o$, the resonant frequencies of the optoacoustic cell can be found from the following formula (West 1983):

$$f_{res} = \frac{C_o}{2} \sqrt{\left(\frac{n_z}{L}\right)^2 + \left(\frac{\alpha_{mn}}{a}\right)^2} \tag{5.13}$$

where C_o is the sound speed of the sample. An example of f_{res} calculation will be carried out in Section 5.2.2. The acoustic pressure produced in the cell can be expressed as a summation over all modes:

$$P(r,\omega) = \sum_j A_j(\omega) \, P_j(r) \tag{5.14}$$

where $A_j(\omega)$ is the mode amplitude and equal to

$$A_j(\omega) = -\frac{i\omega}{\omega_j^2} \frac{[(\gamma-1)/V_c \int P_j^* H dV]}{(1-\omega^2/\omega_j^2)} \qquad (5.15)$$

γ is the specific heat capacity ratio at constant pressure to that of constant volume. It is clear that $A_j(\omega) = \infty$ as $\omega_j = \omega$ or when the modulating frequency ω is equal to the cell's natural resonance frequency. In practice this is not true because no loss has been included. Usually losses in the OA cell (Kruezer 1977) arise from viscosity and heat conduction. It can be said that gas in the cell is composed of two layers. The gas near the cell wall has a constant temperature because the wall is a better conductor than the gas. The gas in this region expands and contracts in an isothermal manner. Far from the wall the gas expands and contracts in an adiabatic process. Acoustic losses from heat conduction will take place in the region where the gas expansion is both partially isothermal and adiabatic. For analysis of the different types of losses in the OA cell the reader is referred to Kruezer (1977). The quality factor (Q_j) of the cell is defined as

$$Q_j = \omega_j \frac{\text{energy stored in mode j}}{\text{rate of loss of energy from the mode}}$$

To see the effect of Q_j it is interesting to look at the noise equivalent power (NEP) which is the amount of power that is to be absorbed to create a signal equivalent to the noise amplitude.

$$(NEP)^2 = 8\pi\rho\, T\, C_o^2 k\, V_c\, \omega^2/\omega_j Q_j (\gamma-1)^2 \qquad (5.16)$$

where ρ is the gas density, k the thermal conductivity, and V_c is the cell volume. As Q_j is increased the value of $(NEP)^2$ will decrease. Introducing the quality factor Q_j in eqn. (5.15) and using eqn. (5.1), the mode amplitude will take the following form:

$$A_j(\omega) = \frac{-i\omega\alpha[(\gamma-1)/V_c] \int P_j^* \, IdV}{\omega_j^2[1 - \omega^2/\omega_j^2 - i\omega/\omega_j Q_j]} \tag{5.17}$$

If (I) is constant then the integral in the numerator is zero for $j \neq 0$. Hence the lowest order mode P_o has a resonant frequency $\omega_o = 0$ and represents a constant pressure change in the cell independent of position with a mode amplitude equivalent to:

$$A_o(\omega) = \frac{i\alpha(\gamma-1)\, I}{\omega(1 + (i/\omega\tau_T))} \tag{5.18}$$

where τ_T is the damping time of P_o as a result of heat conduction. For a cell of volume V_c and length L the intensity can be written as $I = WL/V_c$, where W is the laser power in watts. Eqn. (5.18) then becomes

$$A_o(\omega) = \frac{i\alpha(\gamma-1)\, WL}{\omega(1 + i/\omega\tau_T)\, V_c} \tag{5.19}$$

If the first mode is excited then inserting the above mentioned values of V_c, L and I in eqn. (5.17) then $A_1(\omega)$ is given by the following formula:

$$A_1(\omega) = \frac{i\omega}{\omega_1^2} \frac{\alpha(\gamma-1)\, WL}{V_c[1-(\omega^2/\omega_1^2)-i(\omega/\omega_1 Q_1)]} \tag{5.20}$$

The last two equations can be used to estimate the preferred mode to be detected. For example at low frequencies $\omega\tau_T \ll 1$ and $A_o(\omega) = \alpha(\gamma-1) \times WL\ \tau_T/V_c$ and is independent of frequency. At high frequency $\omega\tau_T \gg 1$, and $A_o(\omega)$ decreases as ω^{-1}. The first order mode is a maximum only at $\omega = \omega_1$. The ratio of the maximum amplitude of $A_1(\omega_1)$ to that of $A_o(0)$ is given by

$$A_1(\omega_1)/A_o(0) = Q_1/\omega_1\tau_1 \tag{5.21}$$

Since this ratio is larger than unity, then the first mode amplitude can be made larger than that of the zero mode.

5.2.2 Optoacoustic effect in discharge plasmas:

The optoacoustic effect in an acoustic cell is extensively studied and is very well known as has been seen in Section 5.2.1. Detection of optoacoustic signals in discharge plasmas has been reported (see, for example, Arimondo, Vito, Ernst and Inguscio 1984, and Hameu, Arimondo, Wascat and Clorieux 1985). The only theoretical model to account for OA signals in plasma discharges and known at the time of this study is by Sofonea and Popescu (1986). They extended a model that accounts for the OGE in a discharge to include that of an OA effect. The idea that OG and OA signals are related in a discharge was supported by the experimental work of Muenchausen et al. (1984). An OA model in neon gas discharges developed by Sofonea et al. (1986) makes two assumptions. Firstly, following laser radiation absorption, the change in population of the excited levels (n_i) gives rise to a change in the multiplication factor (K), i.e. the number of electrons generated in the discharge through collisions by a single electron leaving the cathode. When K increases then $(\partial K/\partial n_i) = a_i > 0$; hence there will be a current increase that can be expressed by the change in the number of electrons per unit volume (Δn_e). Secondly, due to changes in the population of the excited levels the total amount of ionization energy is changed and this will be followed by a change in the electron gas temperature (ΔT_e). The partial pressure of the electron gas is given by:

$$P_e = n_e k T_e \tag{5.22}$$

where k is the Boltzman constant. The change in the electron density (n_e) and temperature (T_e) gives rise to a pressure change given as follows

$$\Delta P_e = k T_e \Delta n_e + n_e k \Delta T_e \tag{5.23}$$

Assuming transitions occur between level 1 with density n_1 and level 2 with density n_2, Δn_e can be calculated and ΔT_e can be obtained from the energy balance. Substituting in eqn. (5.23) and integrating, the electron gas pressure is then given by:

$$P_e = I\, n_e\, a_1\, \Delta n^o\, [i\, A[(\alpha-1)\, k\, T_e + \alpha E_2 - E_1 - (\alpha-1)E_0] - B(k\, T_e + E_1 - E_0)\,]\,/Ai(Ai+B) \qquad (5.24)$$

where I is the beam intensity, Δn^o the change in the ground state population, and i the current. A is defined from $\tau_1^{-1} = Ai$; τ_1 is the relaxation time of level 1, $\tau_2^{-1} = Ai + B$ is the relaxation time of level 2 and B accounts for radiative decay of the relaxation time. α is constant equal to (a_2/a_1). E_0, E_1, E_2 are the energies of the ground state, levels 1 and 2 respectively. From the last equation it is easily seen that the OA signal vanishes at a critical current (i_o) given as follows:

$$i_o = \frac{B(k\, T_e + E_1 - E_0)}{A\,[(\alpha-1)\, kT_e + \alpha E_2 - E_1 - (\alpha-1)E_0]} \qquad (5.25)$$

Applying eqn. (5.25) to neon discharges, it was found that for currents $i > i_o$ the signal is positive and negative for currents $i < i_o$. This is supported by the experimental work of Arimondo et al. (1984) who assigned positive OA signals for high currents and negative OA signals for low currents.

5.3 Optoacoustic detection:

Microphones are the most widely used method of detection in OA experiments. The condenser type is preferred (West 1983), as it is insensitive to mechanical vibration and has a flat frequency response up to 15 kHz. These condenser microphones employ air as a dielectric material between the electrodes. Sound signal detection is achieved when the OA wave creates a capacitance change of the microphone which is then

transformed into voltage signal (V_s). This signal is proportional to the biasing voltage and microphone diaphragm area. In comparison, the electret microphone contains a solid material of high dielectric constant and can be manufactured to a very small size. Kruezer (1977) treated the problem of detection using the condenser microphone by considering two models. In the following, a brief account of both the mechanical and electrical models will be presented. The average position of the microphone diaphragm can be written as $X = \frac{1}{2}X(0)$, where $X(0)$ is the full displacement of the diaphragm centre. The force exerted on the diaphragm is of two kinds: one resulting from the sound pressure and the other is a result of biasing the microphone which causes a displacement of the diaphragm by an amount given by:

$$X_o = \frac{C_m V_B^2}{d\, k_m} \tag{5.26}$$

where $k_m = 8\pi T_m$ is called the microphone restoring force, C_m is the unbiased microphone capacitance, d is the displacement between the microphone plates, V_B is the biasing voltage and T_m is the microphone diaphragm stiffness and should be sufficient to stop the bias voltage from bringing the diaphragm into contact with the back plate of the microphone. It is useful to define a quantity called the 'microphone equivalent volume' V_m which is the volume of air that when compressed will produce the same restoring force on the diaphragm as that of T_m.

$$V_m = \frac{\gamma P_o A_m^2}{8\pi T_m} \tag{5.27}$$

where A_m is the microphone diaphragm area, and P_o the average pressure over the diaphragm. V_m is very important in understanding the coupling between the microphone and the gas as will be explained later. The microphone is connected to a bias voltage through a ballast resistor in

one of two possible ways: (i) The electric charge on the diaphragm is kept constant and the signal is detected as a voltage using a high impedance amplifier. (ii) The voltage remains constant and the signal is detected as a current using a low impedance amplifier. In the work reported in this thesis scheme (i) was used.

For this system Kruezer (1977) gave the following relation for the signal (V_s) which in fact was originally given by Olson (1947) as follows:

$$V_s = P_m \frac{V_B A_m}{d\, k_m} \left[1 - \frac{\omega^2}{\omega_m^2} \frac{i\omega}{\omega_m Q_m} \right]^{-1} \qquad (5.28)$$

where ω_m is the ith microphone resonance frequency defined as $\omega_m \equiv \sqrt{\frac{k_m}{m}}$, m is the diaphragm mass, and Q_m is the quality factor of the microphone given as $Q_m = \sqrt{\frac{m k_m}{\sigma}}$ where σ is the damping. Eqn. (5.28) gives the electrical signal produced, but the pressure exerted on the microphone (P_m) should be corrected since the boundary conditions have changed as a result of implanting the microphone in the cell as the walls near the microphone are no longer rigid. In this case the velocity of sound waves normal to the walls at the diaphragm is not zero. If the container is small and the modulation frequency made less than the first resonance frequency of the container and the microphone, then pressure will be constant and independent of position. Under this assumption the microphone can be treated as an additional volume (V_m) given before in eqn. (5.27). The amplitude of the zero mode can then take the following form:

$$A_0(\omega) = \frac{i\alpha(\gamma-1)\ WL}{\omega(1+i/\omega\tau_T)(V_c+V_m)} \qquad (5.29)$$

and accordingly the signal produced voltage can take the new formula as follows:

$$V_s = \frac{i(\gamma-1)}{\omega\gamma P_o A_m} \frac{V_B}{d} \left[\frac{V_m}{V_c+V_m} \right] (\alpha\, WL) \qquad (5.30)$$

This equation is useful in determining the effect of cell design changes on the signal amplitude. Another thing which is expected to be modified by addition of the microphone to the cell is the microphone resonance frequency (ω_m). As a result the spring constant changes from K_m to $K'_m = K_m(1 + V_m/V_c)$ and the modified effective volume becomes $(V'_m)^{-1} = V_m^{-1} + V_c^{-1}$ and accordingly the resonant frequency becomes:

$$\omega_1 = \omega_m \sqrt{1 + \frac{V_m}{V_c}} \tag{5.31}$$

The noise signal is of the following form:

$$|V_{sn}(\omega)|^2 = \frac{4\,k\,T\,\rho\,c^2}{\omega_m\,Q_m\,V_m(1+V_m/V_c)^2}\;S_m^2 \tag{5.32}$$

where $S_m = \dfrac{V_B V_m}{d\gamma P_o A_m}$ is called the open circuit sensitivity.

A second model is now examined based on an electrical equivalent circuit. This is shown in Fig. 5.1 which comprises a series R-L-C resonant current shunted by a capacitor. The acoustic pressure generates a signal which appears as a voltage source (V_G) in series with the RL'C' circuit:

$$V_G = \frac{A_m d}{V_B C_m} P_m \quad , \quad C_m = \varepsilon_o A_m/d \tag{5.33}$$

$$C' = \left(\frac{X_o}{d}\right) C_m = C_m^2\, V_B^2\, /d^2\, k_m \tag{5.34}$$

$$L' = (\omega_m^2\, C')^{-1} \tag{5.35}$$

and

$$R = (Q_m\, C'\, \omega_m)^{-1} \tag{5.36}$$

It can be said that the Johnson noise at the output terminals is of exactly the same amplitude as the thermal fluctuation noise. To calculate the electrical noise it is important to consider the microphone-gas

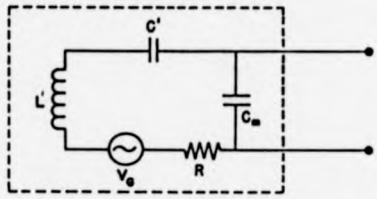

Fig. 5.1 : Equivalent circuit for the microphone.
Reproduced from Kruezer (1977).

TABLE I. Characteristic values α_{mn} for the cylindrical cavity.

n \ m	0	1	2	3	4
0	0.0000	1.2197	2.2331	3.2383	4.2411
1	0.5861	1.6970	2.7140	3.7261	4.7312
2	0.9722	2.1346	3.1734	4.1923	5.2036
3	1.3373	2.5513	3.6115	4.6428	5.2036
4	1.6926	2.9547	4.0368	5.0815	6.1103

Table 5.1 : Values of α_{mn} useful for the calculation of resonance frequencies.
Reproduced from Goldan et al. (1974).

container coupling which increases the effective spring constant of the diaphragm. In the electrical model this results in reduction of C' by a factor $(1 + V_m/V_c)^{-1}$. Hence the voltage at the output terminals generated by Johnson noise in R is given by:

$$|V_n|^2 = \frac{4\ kT\ R}{\omega^2 C_m^2} \left| R^2 + \left(\omega L' - \frac{(1 + V_m/V_c)}{\omega\ C'}\right)^2 \right|^{-\frac{1}{2}} \qquad (5.37)$$

In the low frequency limit this reduces to:

$$|V_n|^2 = \frac{4\ kT\rho c^2}{\omega_m Q_m V_m (1+V_m/V_c)^2}\ S_m^2 \qquad (5.38)$$

which is identical to eqn. (5.32). This means that both models yield the same results for the noise voltage.

5.4 Cell design:

5.4.1 General considerations:

Optoacoustic cell design is aimed towards the maximum possible signal to noise ratio. Cells have been constructed of different sizes and shapes (Rosencwaig 1980). Cells have been designed with a length as small as 5 mm (Klimcak and Gelbachs 1985) and 18 cm (Lehmann, Scherer and William 1982), and with quality factors ranging from 10 (Lehmann et al. 1982) to 164 (Dewey et al. 1973) and as high as 766 (Goldan et al. 1974). When designing an optoacoustic cell the resonance frequencies should be kept small compared with the reciprocal of the vibrational relaxation time of the gas involved otherwise severe reduction of Q value will result.

There are two types of operation for OA detection (West 1983) either to operate at low frequency or at the natural resonance frequency of the cell. The resonance frequencies can be calculated using eqn. (5.13). An example concerning the cell used in this work will be given in the next section. For an optimum cell design it is relevant to consider the signal

to noise ratio obtained by dividing eqn. (5.30) by eqn. (5.32) to give the following formula (Kruezer 1977):

$$(S/N)^2 = \frac{(\gamma-1)^2}{4kT\omega^2} \left(\frac{LA_m}{V_c}\right)^2 \left(\frac{\omega_m Q_m}{K_m}\right) \Delta f^{-1} \alpha^2 W^2 \qquad (5.39)$$

The factor $(\gamma-1)$ can be increased using monoatomic gases such as He or Ar for dilution of the sample. Luckily, in a CO_2 laser gas mixture, He is used with the highest partial pressure percentage ~ 70%. Δf depends on the choice of modulation frequency and the microphone resonance frequency. The factor $(L\ A_m/V_c)$ can be written as $(\frac{A_m}{A_c})$. This can be maximized by increasing the diaphragm area and reducing the cell cross-sectional area. This can be done to only a certain extent as it is difficult to fit large microphones in small bore cells.

One major problem encountered in optoacoustics is window heating (West 1983). This is a difficult problem to solve as it occurs at the modulation frequency hence interferes with the weak OA signals. Many solutions to this problem have been suggested in order to eliminate it. Acoustic baffles have been used within the cell by Bruce, Sojika, Hurd, Watkins, White and Derzko (1976) (see Fig. 5.2). A simple and straightforward solution has been employed by Shtrikman and Slatkin (1977) which involves an open optoacoustic cell placed in a larger container. They concluded that the background signal was reduced to a signal equivalent to 20 ppb (parts per billion) of ethylene in N_2. A similar idea has been used by Lehmann et al. (1982) where a waveguide 2.2 mm x 5 mm x 18 cm long was used in a larger container (see Fig. 5.3). Deaton, Depatie and Walker (1975) tried a more complicated method by using two cells in series. The idea is to fill both cells with non-absorbing gas. In this case the background signal will appear. When one of the chambers filled with the absorbing gas is mixed with the non-absorbing gas, the differential signal between the two chambers represents the gas absorption.

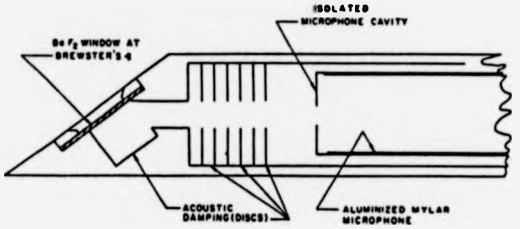

Fig. 5.2 : Schematic of an optoacoustic cell that employs acoustic baffles. (After Bruce et al. 1976).

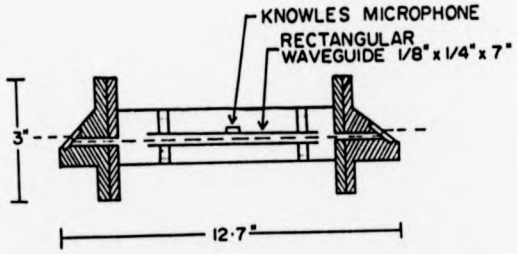

Fig. 5.3 : A resonant optoacoustic cell placed in larger container to reduce window heating. Reproduced from Lehmann et al. (1982).

5.4.2 Internal and external optoacoustic cells:

In the work presented in this thesis two different types of opto-acoustic cells have been designed. One was used which formed an extension of the laser tube at its anode end, and the other cell was used outside the laser cavity in the conventional way of OA spectroscopy.

In designing the intra-cavity cell, operation at the resonant acoustic frequency is not considered useful on the grounds that unwanted signals may be amplified, especially in an environment like that of the laser cavity in which plasma perturbations, pressure fluctuations, thermal variations and many other undesirable effects can easily arise. Another important reason is that the calculated speed of sound in the gas mixture of the CO_2 laser with an abundance of He ~ 70% is expected to be high ~ 460 m/sec at 20 torr. This leads to very high radial mode resonance frequencies at practical cell diameters. In addition the cell is not only open but also closely coupled to the plasma tube which makes precise calculation of the resonance frequencies impossible. The longitudinal mode resonances are lower in frequency and the cell can be designed to excite these modes, but because the effective cell length is going to increase when the cell is coupled to the laser tube, exact theoretical calculations of resonance frequencies are again precluded. Although resonance operation of the gas cell is not recommended as mentioned previously, it is advisable in the cell design to assume resonance frequency of a convenient value in the range (200 - 800 Hz) for the sake of successful optoacoustic cell design. The cell is then experimentally studied for the conditions of best operation.

The intra-cavity cell is shown in Fig. 5.4b and takes the form of a simple tube made from stainless steel 6 cm in length and 2 cm in diameter. The length is the maximum permissible for the cell because of the limited space between the laser mirror and grating. A microphone is fitted in the

middle of the cell wall. Assuming the cell is far enough from the plasma region (~ 12 cm) and that the laser is operated with continuous gas flow and with the gas introduced between the cell and plasma, it can be reasonably assumed that the cell is at room temperature. At a total pressure of 12 - 20 torr the laser gas mix (70% He, 24% N_2 and 6% CO_2), theoretical calculation shows that the speed of sound is in the range (4.3 to 4.6) x 10^4 cm/sec respectively. Using eqn. (5.13) and relevant values of α_{nm} from Table 5.1, the resonance frequencies for the lowest radial mode (n_z = n = 0, m = 1) is found to be 26 - 28 kHz for operating pressures 12 - 20 torr respectively. For longitudinal modes the cell length is assumed to be 27 cm (and not 6 cm) since the part of the laser tube beyond the plasma that has almost the same diameter as that of the acoustic cell, is 21 cm. This gives for the lowest order longitudinal mode (n_z = 1, n = m = 0) a resonance frequency of (790 - 850) Hz for the same range of pressures mentioned earlier.

The external cavity is manufactured from a brass tube 15 cm long and 5 cm diameter. It is closed with two Ge windows at its ends and the microphone is fitted in the middle of the cell wall. The cell is provided with a cross (four port) branch which left three ports for pumping, pressure gauge and gas filling (see Fig. 5.4a). In this work the cell is used for comparative studies of OA signals from internal and external cells. Assuming the same gas mix filling, the longitudinal mode resonance frequencies lie in the range (1.4 - 1.5) kHz and the radial resonances are (10 - 11) kHz for pressures (12 - 20) torr respectively. In the comparison of both signals from the two cells (see Fig. 6.8), the resonance frequencies are found to be very much less than calculated, amply illustrating the difference between the actual experimental conditions to those assumed theoretically.

In conclusion the OA signals are detected very successfully from the laser cavity by simply introducing a short tube fitted with a microphone in its wall. The signals are obtained with very good signal to noise ratio (see Fig. 6.10) and without the complications of additional optical windows.

For optoacoustic detection in the waveguide laser an adapter is used. It consists of a volume (V) under the microphone, which is joined to the waveguide tube with volume (V_g) through a channel (ℓ_c) with cross-sectional area (A) (see Fig. 5.4(c)). This combination makes use of the so-called Helmholtz resonator (Rosencwaig 1980), the resonance frequencies of which are given by,

$$\omega_H = C_o \left(\frac{A}{\ell_c V_r}\right)^{\frac{1}{2}} \tag{5.40}$$

$$\text{where} \quad V_r = (V\ V_g/V+V_g) \tag{5.41}$$

In the present work the resonator constructed has a radius 4 mm and length 3 mm, giving a volume V of 0.15 cm^3. The channel ℓ_c is 1 cm long and has a 0.15 cm diameter so its cross-sectional area is 0.0175 cm^2. The waveguide tube is 0.3 cm diameter and 58 cm long giving $V_g \sim 4\ cm^3$. Substituting all the above values into eqn. (5.40) gives:

$$\omega_H = 2995 = 2\pi f_r$$

from which it follows that

$$f_r = \sim 475\ Hz$$

This is a practical value for laser stabilization. It should not be forgotten that in this case resonant operation arises as a consequence of the waveguide tube being used as part of the Helmholtz cell itself.

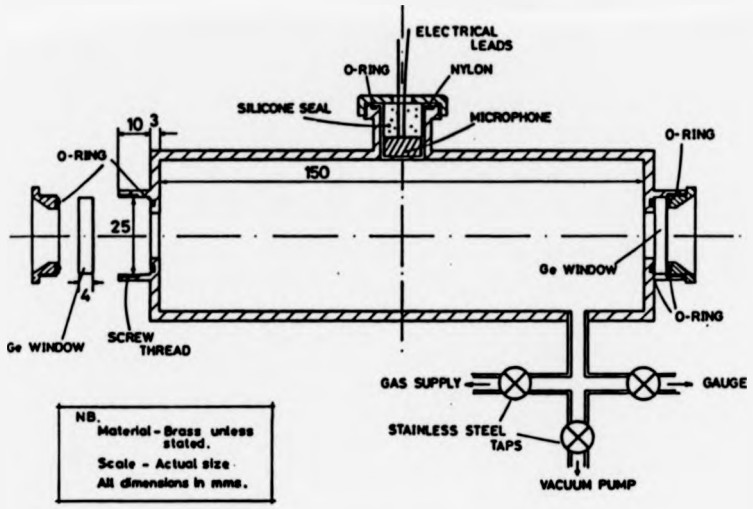

(a)

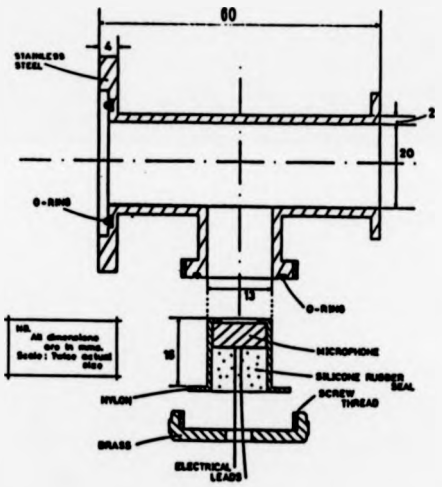

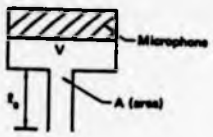

(b) (c)

Fig. 5.4 : Schematic to show (a) Ordinary OA cell (external cell), (b) Intracavity cell (self absorption cell), (c) Adapter and microphone used for optoacoustic detection in the waveguide laser cavity.

Chapter 6

Optoacoustic and optogalvanic signal detection: experimental results and discussion

6.1 Introduction:

It has been pointed out in the previous chapters that the optoacoustic (OA) and optogalvanic (OG) techniques can be used widely for different scientific purposes. Results taken simultaneously using both techniques are presented for the purpose of comparison of their characteristics. Discussion of the results will be presented in this chapter with the objective of gaining a thorough understanding of the newly detected OA signals in the light of what is known about the origin of OG signals. It is believed that the OA technique can be very useful as an aid to understanding of the different processes that occur inside the laser cavity; although this is not the main objective of this thesis.

In the next section, 6.2, a description of the experimental method and results will be given and in Section 6.3 a phenomenological explanation will be attempted and OG and OA methods compared.

6.2 Experimental methods and results:

In this section a description of the experimental results will be given. These have been taken in such a way that the signals are presented as a function of a variable parameter directly. Using a three pen recorder, simultaneous recordings of laser power (P), OG and OA signals are recorded against the variable parameter which is linearly swept using a preset speed motor. For example, if the signals are to be studied at different frequencies (over the range 120 - 3000 Hz), the motor is attached to the spindle of the frequency control of the intra-cavity

chopping unit. It is then allowed to rotate over the desired range, thereby changing the chopping frequency. The OG and OA signals are detected using two PSDs of the same type (EG and G, Model 5101), and fed into a three pen recorder. It is important to point out that the three pens are displaced from each other by a small distance of ~2 mm. The middle pen is used for OA signals and is set to start at the origin. The pen biased to the left in the traces to be shown in this chapter is used for OG signals and the one biased to the right for laser power. Accordingly the X-axis of the sketches can be referred to the start and finish of the OA curve, so the relative displacement of the three pens can be taken into account, i.e. added or subtracted according to the particular trace in question. The laser operates in a single mode with a power output of 8 - 10 watts.

In all the figures to come, curves are referred to as OA and OG for 'optoacoustic'and 'optogalvanic' respectively. The power curve is labelled (P). The phase $\phi_{OG} = 0^{o}$ and $\phi_{OA} = 90^{o}$, unless otherwise specified. The PSD time constant is 3 s for both OG and OA signals and will be specified if different. For the purpose of isolating the d.c. biasing voltage applied to the microphone, a 10 μF capacitor is used for a.c. signal coupling.

The first experimental results were to check any phase shift effect introduced by the coupling capacitor in the OA line. These results are shown in Fig. 6.1. Here, the coupling capacitor was increased from 10 - 30 μF in steps of 10 μF. No significant phase shift in the OA signal was found. Then a search for the optimum operating phase for each of the two signal channels was carried out (Fig. 6.2). At the beginning, the frequency was kept constant while the PSD setting changed from (-10^{o} to $+110^{o}$) for a succession of different pressures covering 14 to 20 torr in 2 torr steps. To study the effect of frequency chopping for a succession of

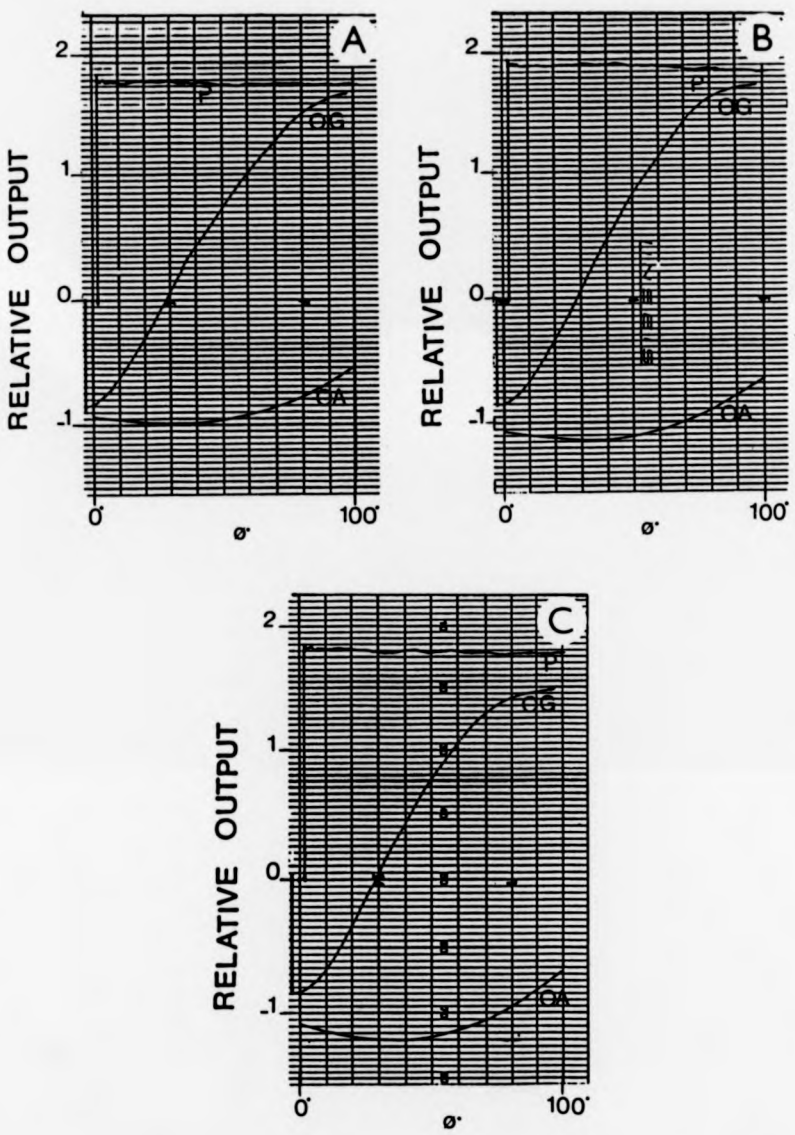

Fig. 6.1 : OG and OA signals versus phase (ϕ^0) for different isolating capacitors: (A) 10 μF, (B) 20 μF and (C) 30 μF. Chopping frequency is constant at 510 Hz.

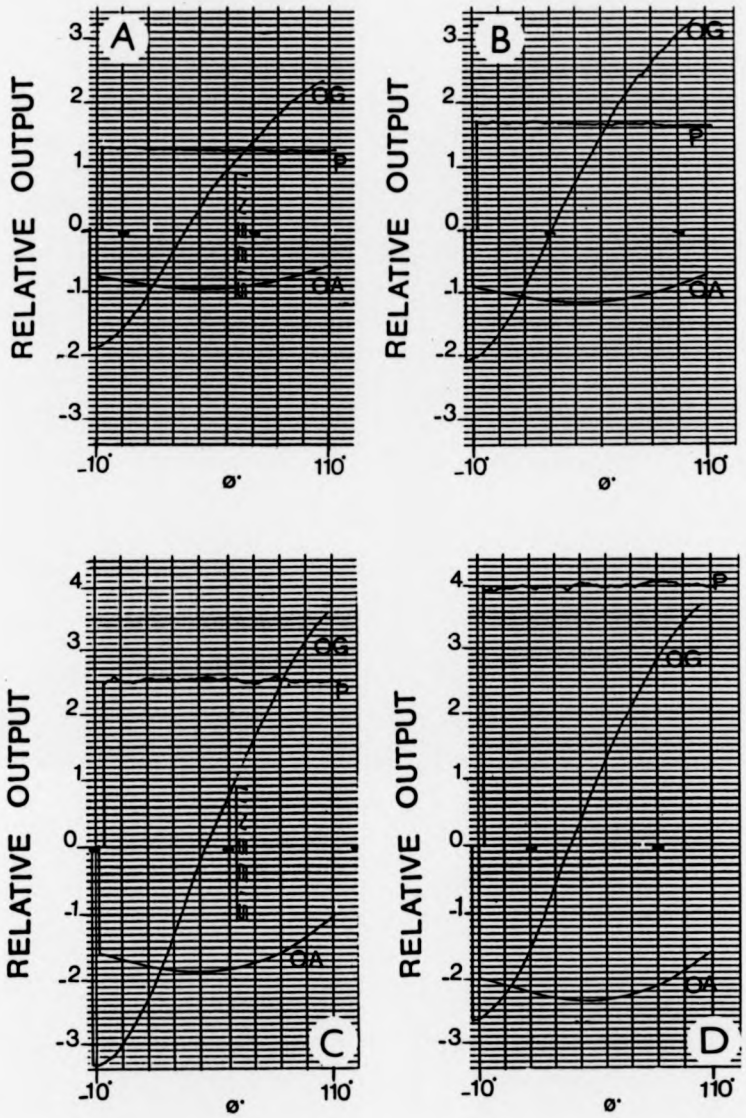

Fig. 6.2 : OG and OA signals versus phase (ϕ^{o}) obtained with constant chopping frequency (510 Hz) and the following pressures: (A) 14 torr, (B) 16 torr, (C) 18 torr and (D) 20 torr.

fixed values, the pressure was kept constant while the PSD phase was scanned and the resulting signals traced out. Results are shown in Fig. 6.3. The optimum operating frequency was then searched for by scanning the chopper frequency from 120 Hz to 3 kHz. This was carried out at pressures in the range 14 to 20 torr in 2 torr steps as shown in Fig. 6.4. The signal responses at different discharge currents at a constant pressure of 18 torr is also shown in Fig. 6.5. The effect of varying the current for different fixed chopping frequencies carried out at constant pressure is shown in Fig. 6.6. In this case the current was scanned from 12 to 30 mA at different fixed frequencies. The intention here was to study the effect of current on the OA and OG signals. Strong effects of discharge current on amplitude of both OG and OA signals were found. To see the effect of frequency in this respect, the experiment was repeated at a set of closely separated frequencies at 180, 195, 210 and 225 Hz as shown in Fig. 6.7.

To check that the detected OA signals occurred locally in the OA cell rather than from other effects within the plasma, simultaneous observations were made of OA signals from the existing internal cell together with those from an external cell. The results are shown in Fig. 6.8. Discharge current variations on the OA signals from internal and external cells were effected in a controlled way by scanning the supply current from 12 - 30 mA in a similar way to the method used for generating the results shown in Figs. 6.6 and 6.7. The results are shown in Fig. 6.9. Further results were then obtained with the internal cell for OA and OG signals from the plasma tube by using frequency modulation of the laser (such as used for CO_2 laser frequency stabilization) rather than by the method of beam chopping as used in the production of results for the above mentioned figures. Frequency modulation was effected by applying an a.c. voltage at an audio frequency to a piezo-electric tube mounted such that

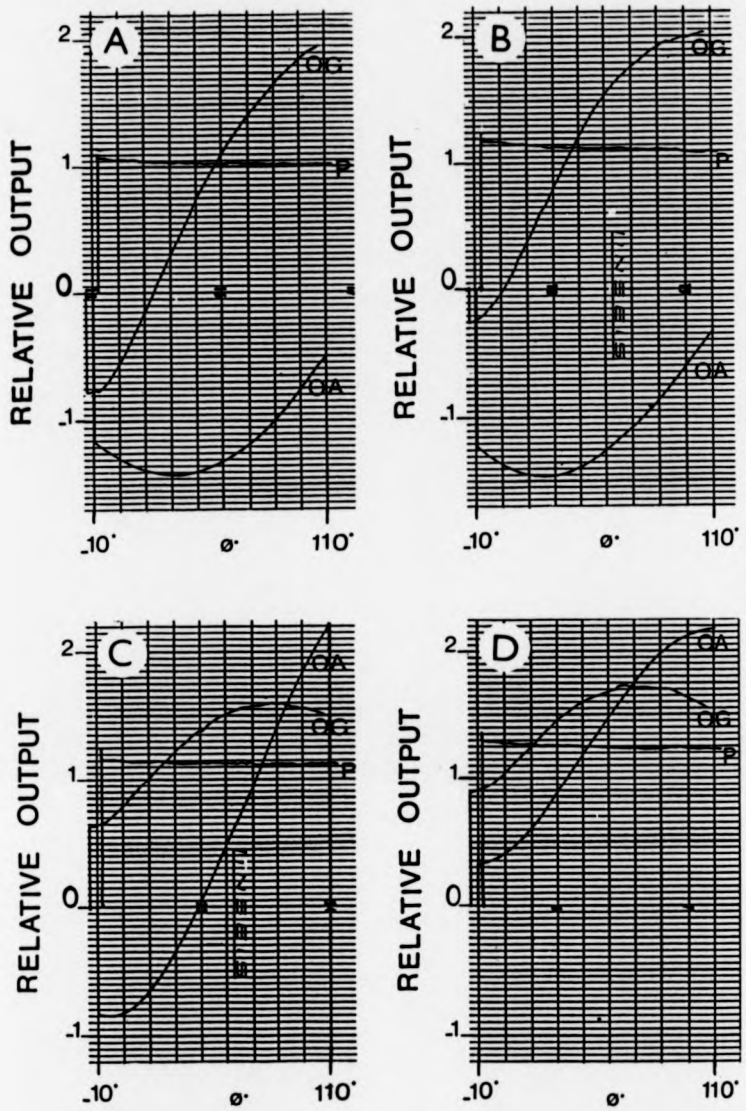

Fig. 6.3 : OG and OA signals versus phase (ϕ^{o}) at a pressure of 16 torr with the following chopping frequencies: (A) 560 Hz, (B) 615 Hz, (C) 745 Hz and (D) 790 Hz.

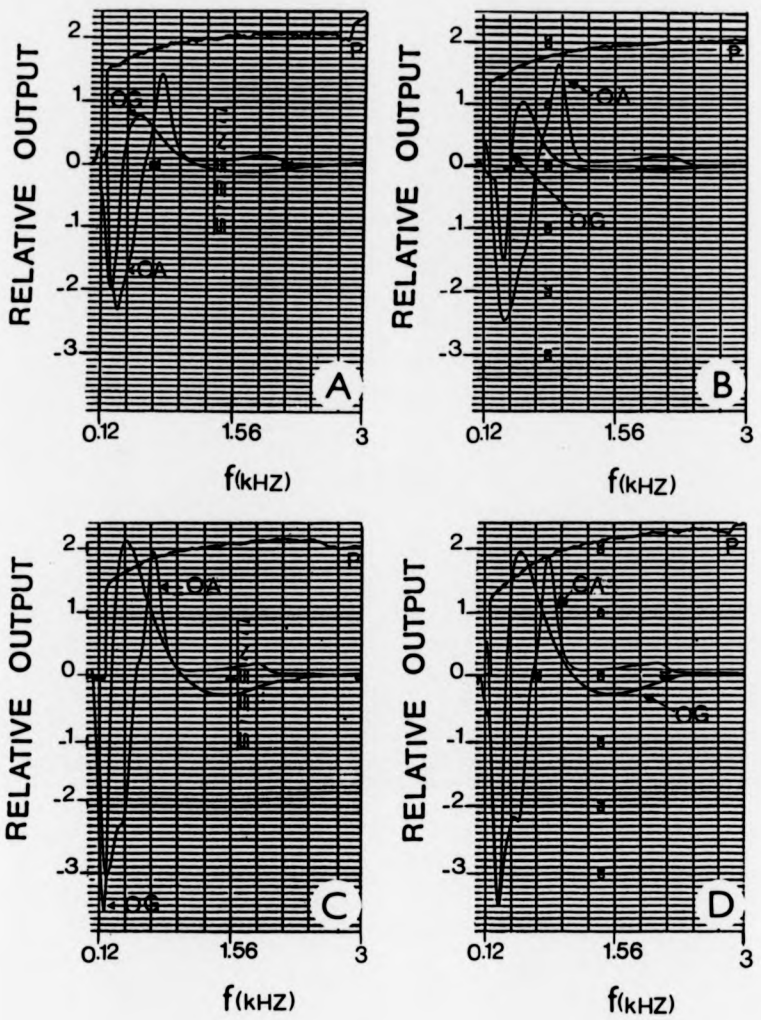

Fig. 6.4 : OG and OA signals versus chopping frequency (f) at the following pressures: (A) 14 torr, (B) 16 torr, (C) 18 torr and (D) 20 torr.
Phase angles are $\phi_{OG} = 0^{o}$ and $\phi_{OA} = 90^{o}$.

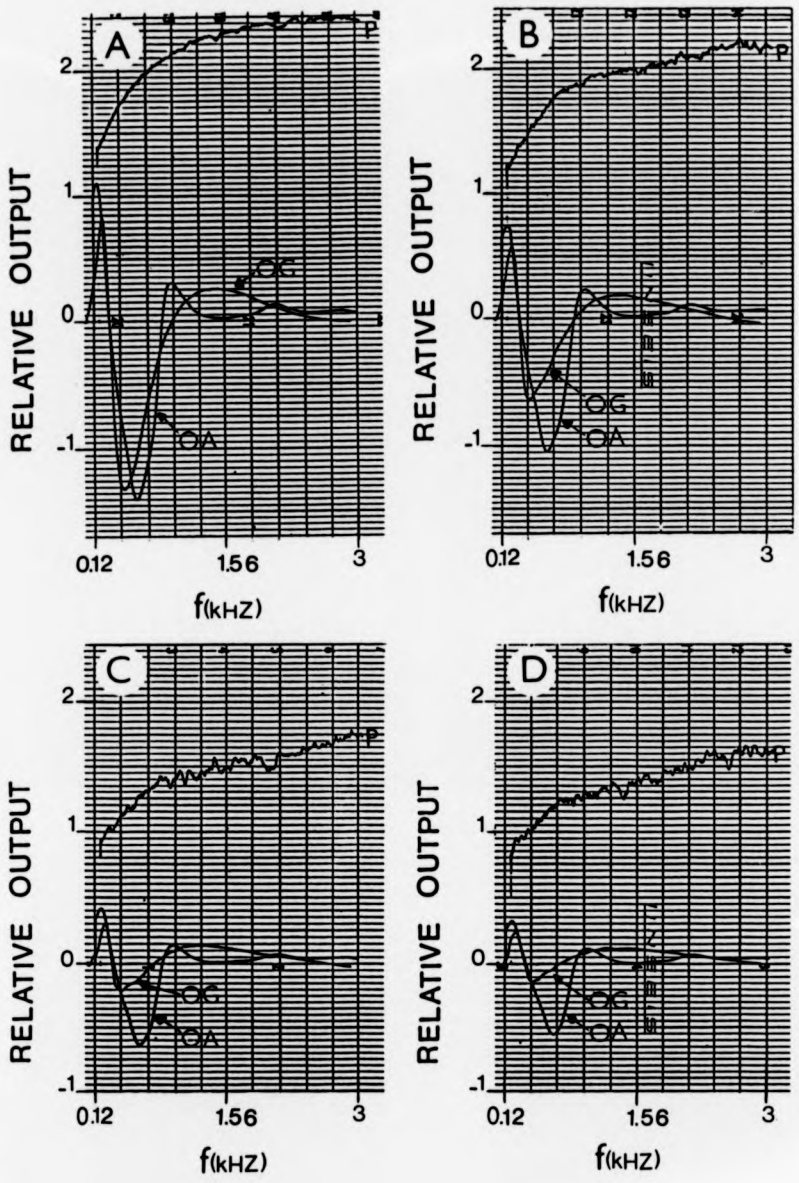

Fig. 6.5 : OG and OA signals versus chopping frequency (f) at constant pressure of 18 torr and the following discharge currents: (A) 12 mA, (B) 16 mA, (C) 20 mA and (D) at 24 mA.

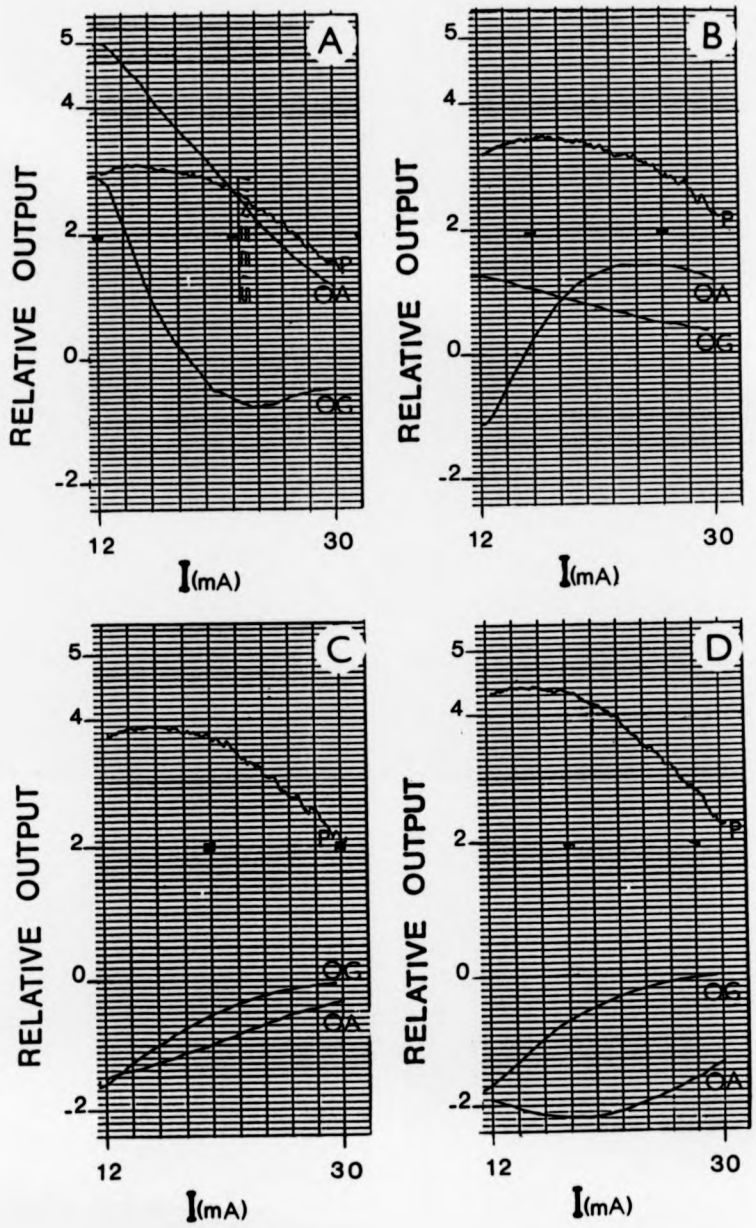

Fig. 6.6 : Effect of laser plasma discharge current (I) on the amplitude and polarity of the OG and OA signals at constant pressure (20 torr) and the following frequencies: (A) 120 Hz, (B) 210 Hz, (C) 420 Hz and (D) 720 Hz.

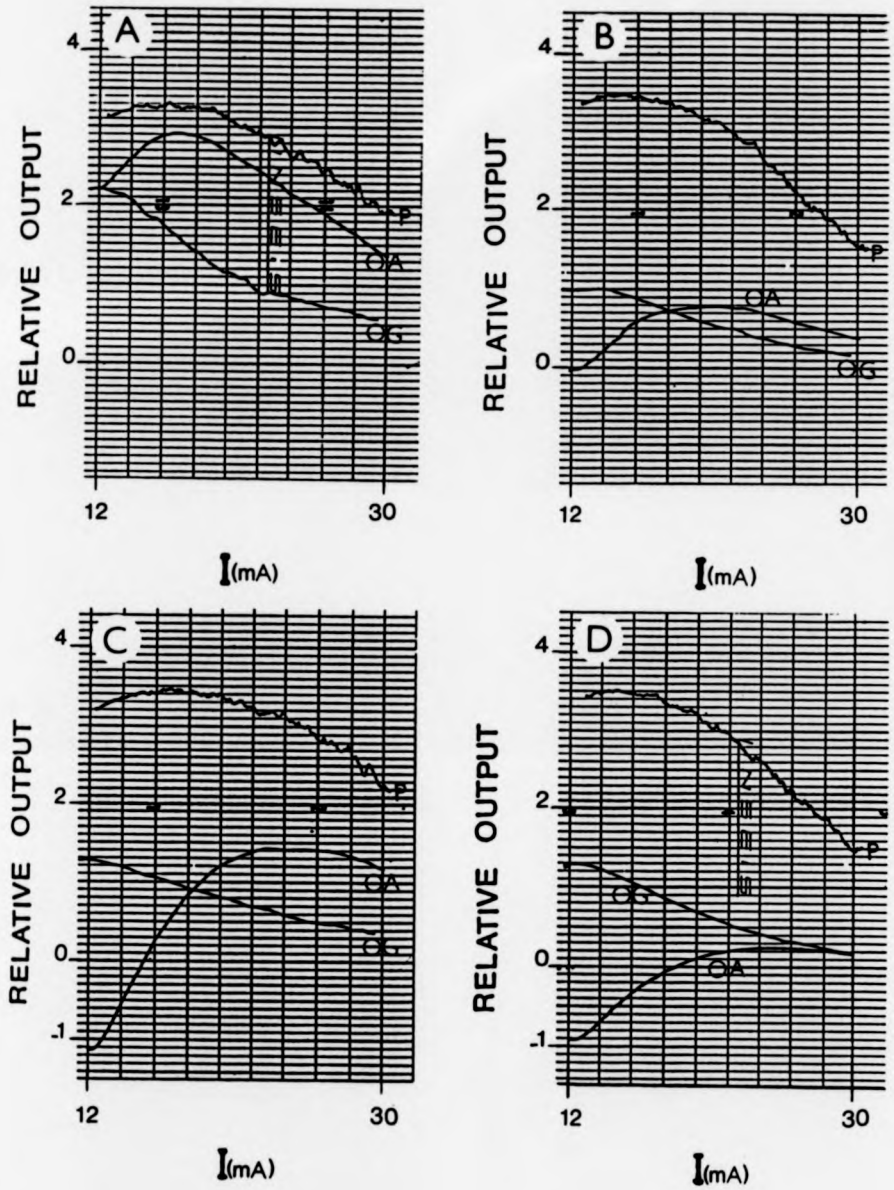

Fig. 6.7 : OG and OA signals versus current (I) at constant pressure (20 torr) and the closely spaced frequencies: (A) 180 Hz, (B) 195 Hz, (C) 210 Hz and (D) 225 Hz.

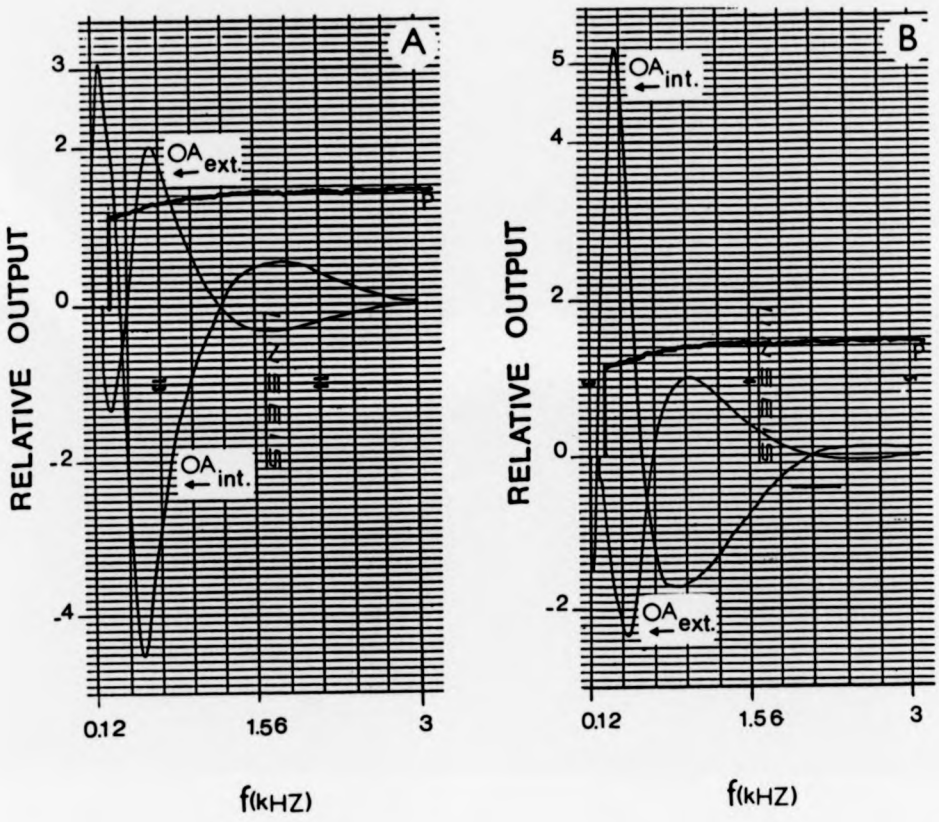

Fig. 6.8 : Comparison of OA signals derived from internal (OA_{int}) and external (OA_{ext}) cells with the same gas pressure (18 torr). (A) With PSD phase setting 0^{o} for both signals and (B) with PSD phase setting 90^{o} for both signals.

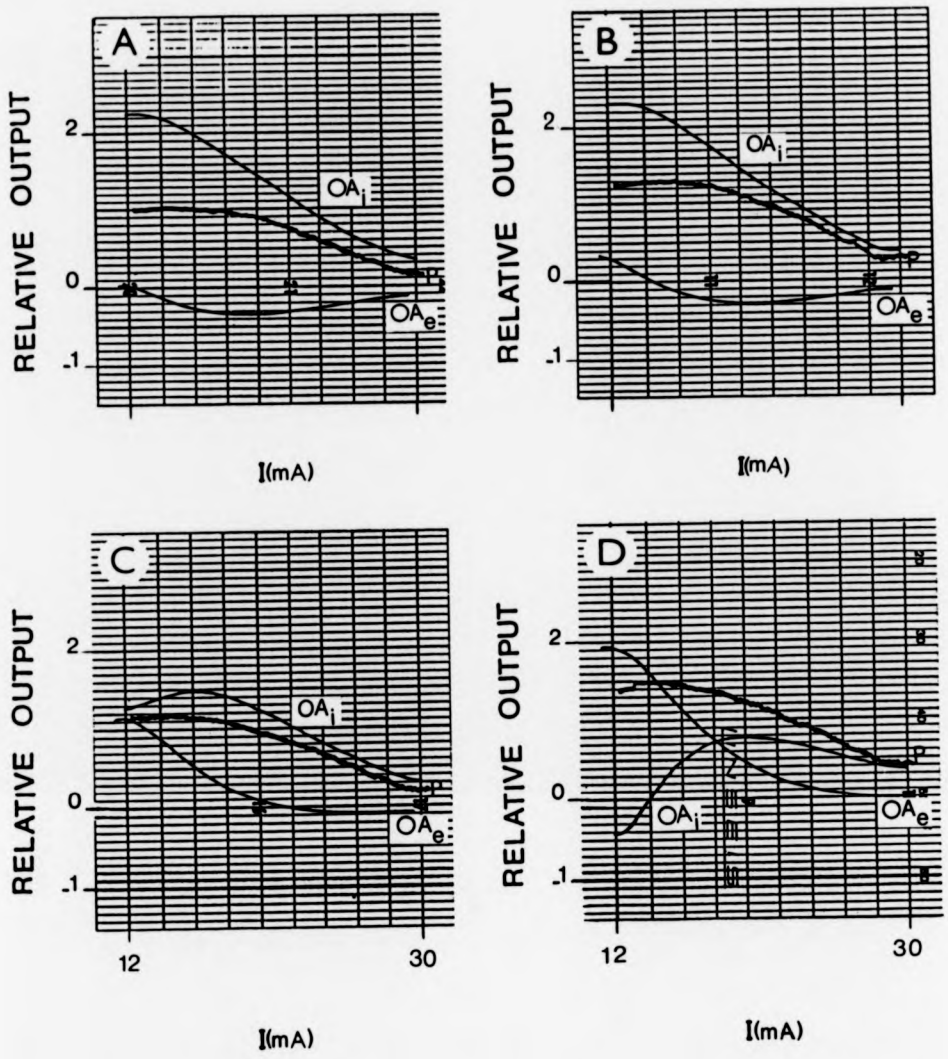

Fig. 6.9 : Optoacoustic signals from both the internal cell (OA_i) and from the external cell (OA_e) versus plasma discharge current (I) at frequencies (A) 125 Hz, (B) 135 Hz, (C) 165 Hz and (D) 195 Hz.

the grating was position modulated. In this case, signals in the form of a derivative were detected corresponding to a full scan of a laser line resulting from the rotation of the diffraction grating. Fig. 6.10 shows OA derivatives detected at a modulation voltage of 50 volts peak-to-peak corresponding to cavity length modulation of ~0.03 μm of the piezo transducer. Fig. 6.11 shows OG and OA derivatives detected at even smaller modulation voltages of 10 and 5 volts peak-to-peak respectively. Finally Fig. 6.12 gives an example of mode hopping encountered in this study.

6.3 Discussion

This discussion will be devoted to the explanation of the behaviour of both OA and OG signals and a comparison of the two methods. From Fig. 6.1 it is concluded that the isolation capacitor connected in series with the microphone does not have any effect on phase of the signal and hence any phase changes will be related to the experimental conditions rather than to the equipment used. The OG results will be interpreted using the theory of Moffatt and Smith (1981), as explained in Chapter 4. In brief, this theory assigns two types of translational energy T_u and T_L to the laser gas. Here, T_u is the translational energy transferred to the gas from the upper laser level as a result of collision between the (001) level and other molecules in the gas mixture following the reaction:

$$CO_2(001) + M \longrightarrow CO_2(n,m,0) + M + Tu$$

where M is any possible collision partner and can be CO_2, CO, O_2, N_2, He, Xe. When the lower laser levels relax to the ground state, then release translational energy T_L through the following reactions (Patel 1968):

$$CO_2(100) + CO_2(000) \longrightarrow CO_2(010) + CO_2(010)$$
$$CO_2(010) + M \longrightarrow CO_2(000) + M + T_L.$$

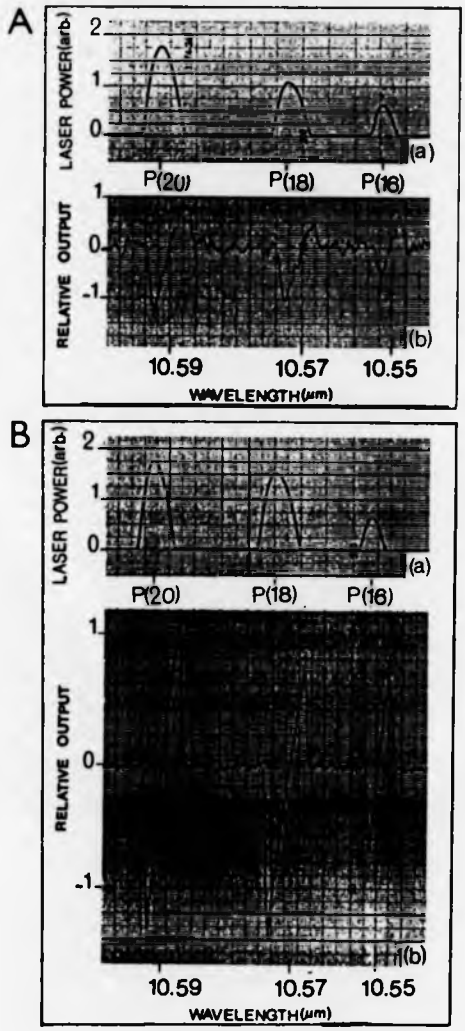

Fig. 6.10 : First derivatives of laser signature obtained by frequency modulation of the laser at 50 VP-P and laser gas pressure of 12 torr.
A(b) OG derivatives at 1005 Hz modulation frequency. PSD time constant : 1 s.
B(b) OA derivatives at 405 Hz modulation frequency. PSD time constant 0.1 s.
Traces A(a) and B(b) are for the corresponding laser output power.

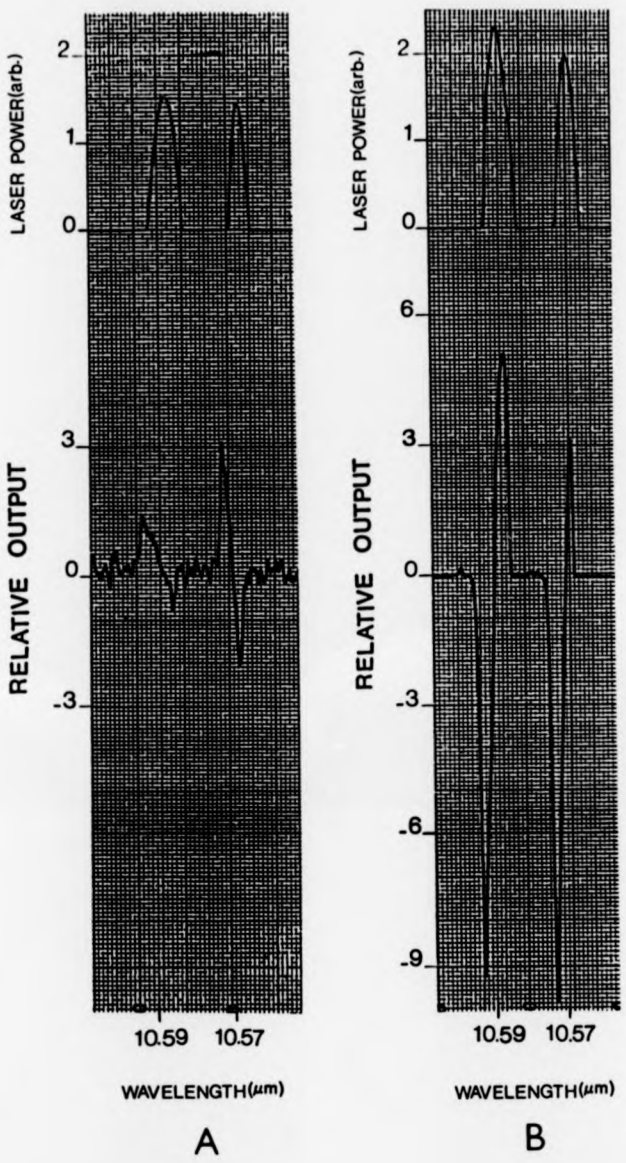

Fig. 6.11 : Derivatives of laser signature taken at a laser frequency modulation of 670 Hz.
(A) OG derivatives at 10 VP-P, PSD time constant 1 s.
(B) OA derivatives at 5 VP-P, PSD time constant 0.1 s, laser tube total gas pressure: 11 torr.

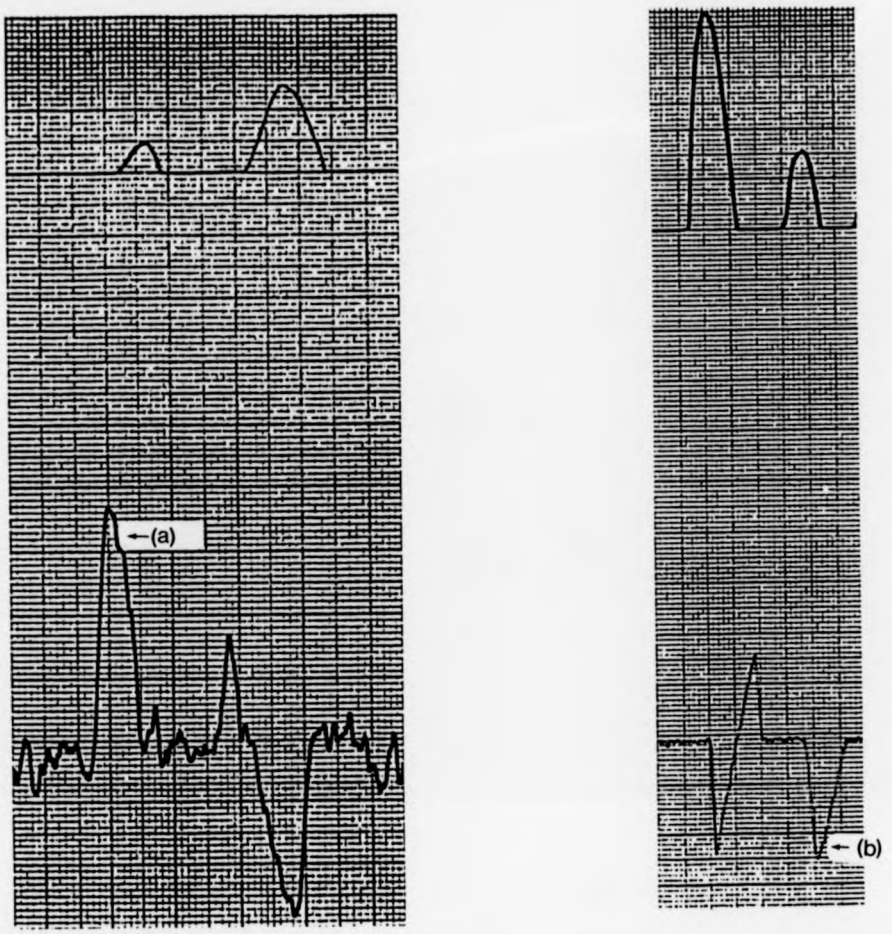

Fig. 6.12 : Examples of mode hopping which cause incomplete derivatives:
A(a) For OG derivative
B(b) For OA derivative.

Moffatt et al. (1981) discuss two regimes. The first is the low frequency regime (0 - 5 kHz) in which T_u is modulated, and the second the high frequency regime (>5 kHz) in which T_L is modulated. In view of the experiment of Muenchausen et al. (1984) in which they proved that a generated OA signal results in an induced OG signal , the OA signals in this work will be interpreted by means of a comparison with the OG signals. From Fig. 6.2 it was noticed that the OA signal amplitude is a maximum at $\phi \sim 45^{o}$ whereas the OG signal is zero at this phase angle. Over the pressure range 14 - 20 torr, the phase shift ranges from 42^{o} - 48^{o} which for four measurements averages to 45^{o}. This small range is insufficient to establish the direction of the phase shift with respect to gas pressure to make a direct comparison with the study of Louis, Lepoutre and Monchalin (1986). Their results for a CO_2-Ne gas mix showed an induced phase lag by the microphone dependent on the pressure and the mix of the gas components. High operating pressures >20 torr could not be achieved in the laser studied in this thesis. Instead, this phase shift study can be carried out in a laser-excited external optoacoustic cell using a CO_2-N_2-He gas mix with the same ratios as used in laser operation. Starting with 560 Hz (see Fig. 6.3A) the OG signal became zero at $\phi \sim 20^{o}$. This result is to be compared with Fig. 6.2B which was performed at the same pressure, but different frequency. Upon an increase in frequency, both OA and OG signals became positive and kept rising in strength with increasing phase angle, from -10^{o} to 110^{o} (see Fig. 6.3C). It is concluded that the PSD phase angle should be adjusted for the largest amplitude of signal output at different frequencies.

As far as the frequency response is concerned, two strong regions for both the OA and OG signals can be noticed over the pressure range 14 - 20 torr, experimental results are shown in Fig. 6.4. The first region lies between 120 and 450 Hz and gave negative polarity signal for

both OG and OA methods. The second range of positive polarity extends from ~450 Hz to 1.2 kHz. Both OA and OG signals have their maximum value at almost the same frequency in the first region. In the second region, the OA signal has its maximum at a frequency higher than that of the OG signal. The OG signals have two crossover frequencies in the range of 400 - 500 Hz and at ~1.1 kHz over the range of pressures used in the experiment, i.e. 14 - 20 torr. The OG signals then vanished at 2.4 kHz. The OA signals have only one crossover frequency in the range 600 - 700 Hz, in the same range of pressure as mentioned above. The OA signals then vanished at 2.4 kHz. The effect of pressure on the OA and OG crossover frequencies is not well pronounced over this range of pressure; so it is difficult to establish a definitive conclusion. The result reported here for the OG crossover frequencies is in total agreement with those of Walsh (1985) for frequencies <0.4 kHz and 1.4 kHz under discharge conditions of (5mA, 16 torr) and (6.5 mA, 25 torr) respectively. The only difference from Walsh's result in the present case is that two crossover frequencies of ~0.4 and 1.1 kHz were noticed to occur in a single trace with a laser tube current of 12 mA and gas pressure of 14 to 20 torr. The modulation frequency was not taken up to higher frequencies to compare with the highest value ~12 kHz obtained by Walsh (1985). Moffatt et al. (1981) talk about only one phase reversal in the range ~2 kHz, or when the modulation frequency is $1/2\tau_{001}$, where τ_{001} is the relaxation time of the upper laser level, of the order 300 μs (Moffatt et al. 1981 and Sobolev et al. 1967). Accordingly, the crossover frequency should be of the order of 1665 Hz. The difference in the crossover frequencies of OA and OG signals should be important in indicating the difference in the relaxation times inside and outside the plasma region. The relaxation time is longer for the colder OA cell, so crossover frequencies for the OA signals are expected to occur at a lower value than that of the OG signals. However,

the results do not substantiate this conclusion based on temperature difference. Another important factor that should be accounted for is the difference in the number density per unit volume which is larger in the OA cell, leading to shorter relaxation times. A more thorough investigation accompanied by accurate measurements of the temperature within and outside the plasma region is clearly needed. Concerning the quality factor of the OA cell, it was found that it lies in the range 4 to 8 when sound waves were generated in the cell mechanically by vibrating the mirror using a piezo-electric tube. Experimental measurements of the quality factor using Fig. 6.4, by calculating the ratio $(\nu_o/\Delta\nu)$, gave a Q value, ~ 2 in the low frequency range 120 - 500 Hz and ~ 6 for frequencies > 500 Hz. In the above ratio ν_o is the frequency at which maximum response occurs and $\Delta\nu$ is the peak width in frequency at $(\sqrt{2}/2)$ of the maximum relative output of the signal amplitude (Goldan et al. 1974), as the signal is measured in voltage.

The effect of plasma current on the crossover frequency was examined in Fig. 6.5. Here, the pressure was kept constant and the frequency swept over the range 0.12 - 3 kHz at different fixed values of plasma current. Apart from signal amplitude, the OG and OA signals retained the same form at different currents. Their maxima occur at almost the same frequency, whether positive or negative going, at all currents. As the current is increased there is a clear effect on the higher crossover frequency point for the OG signal, which was found to decrease with current. Intuitively when the current increases the discharge temperature is expected to rise and as a result the relaxation time should decrease, i.e. the crossover frequencies occur at a higher frequency. The result of Fig. 6.5 does not substantiate this however, and this point is left open for further study. The crossover frequencies of the OA signals and its shape were not affected by increasing plasma current and remained unchanged. This result

for OA signals contradicts the results of Arimondo et al. (1984) who reported the detection of an OA signal inside a discharge tube near an earthed anode. They associated a negative-going signal with low current and positive-going with high current, with which heating is associated. This effect has not been noticed in the present work where the signals retain the same polarity at all currents. The experimental findings of Arimondo et al. were supported by the theoretical study of Sofonea and Popescu (1986). Their model depends on electron gas pressure change following a temperature change (see Chapter 5). The critical current value at which the OA signals are expected to vanish was not noticed, probably for two reasons. Firstly, OA detection is carried out some distance (~ 10 cm) from the anode. Secondly, the signals are drawn showing amplitude versus frequency, rather than amplitude versus current as by Arimondo et al. (1984). To clarify this point, pressure and frequency were kept constant while the supply current was scanned from 12 - 30 mA. As Fig. 6.6 shows, as the current is increased, the power is expected to drop since the supply is constant current generator and the discharge voltage will decrease as the current is increased, with constant pressure. The effect of signal decrease (OA and OG) as the current is increased must be looked at carefully since some of the decrease is related to a drop in laser power. An interesting effect can be seen in Fig. 6.6A where the OG signal decreased to zero at ~ 20 mA and produced a negative going peak at ~ 24 mA. A similar effect is noticed in Fig. 6.6B for the OA signal. This agrees with the experimental study of Arimondo et al. (1984) and Sofonea et al. (1986). Since the effect does not appear in all scans shown in Fig. 6.6, it can be said that phase reversal of signals whether OA or OG, with current depends on both the modulation frequency and current and not on current alone. This idea is supported by Fig. 6.7 where traces have been taken at closely spaced frequency values. It is

concluded that when the modulation frequency is very close to the cross-over frequency of the OA signals there is a phase reversal. When the modulation frequency is far from the crossover frequency the signals only decreased in amplitude as a result of power drop when current is increased. An explanation can be offered at this stage. For the OG signal it can be said that as the current is increased the relaxation time is adjusted in such a way that when the modulation frequency is comparable to $1/2\tau_{001}$ the OG signal goes to zero. This explains why the signal does not go to zero at different modulation frequencies. The explanation offered before for the OG situation cannot be offered for the optoacoustic behaviour since the OA microphone is placed outside the plasma region. The OA signal behaviour can only be understood in the light of the model of Sofonea et al. (1968). In the model a change in the electron number density, gave rise to a pressure change leading to an OA signal that vanished at a critical current value at a particular frequency near the crossover frequency.

To clarify the possible influence of the internal cell on the behaviour of the OA signal a comparison was made of an OA signal detected from an external cell containing laser gas mix at the same pressure. Apart from the difference in magnitude in favour of the internal signal (see Fig. 6.8) both OA signals behaved similarly and have nearly the same value of crossover frequency. To confirm the idea that the OA signal detected from the intra-cavity cell is not affected by the plasma in the laser tube, the supply current was swept over the range 12 - 30 mA and both OA signals from the internal and external cells were detected simultaneously. Fig. 6.9 shows that the signal from the external and internal cells did in fact behave similarly. For example in Fig. 6.9 A, B and C the external OA signal reversed phase with current. No physical explanation can be offered and this point is left open for further clarifying

experiments. An important conclusion is that there is now some doubt about the validity of the experimental results of Arimondo et al. (1984) and the idea of the existence of the critical current derived by Sofonea et al. (1986). Finally the OA and OG derivative type signals detected showed very clearly that the OA method is at least five times better in terms of signal to noise ratio compared with OG signals (see Figs. 6.10 and 6.11). This of course will allow better control over frequency stabilization of the CO_2 laser. In Figs. 6.10 and 6.11 the OG signals have a larger absolute magnitude (although they appear smaller), but will look very noisy if the PSD sensitivity is increased to that of OA detection conditions. Another important point worth mentioning is the difference in PSD time constants for adequate signal to noise of detection, which is significant for the speed of response of laser frequency stablilization. Furthermore the OA derivatives are much easier to obtain than the corresponding ones for OG experiments on account of their superior signal to noise. It was noticed sometimes that incomplete derivatives were frequently obtained in which the signals go in one direction only. This has been observed in both OG and OA derivatives (see Fig. 6.12A(a) and B(b)). This effect was noted also by Walsh and Brown (1985) and was related to line hopping before reaching the centre point of the laser emission power versus frequency.

Chapter 7

Carbon dioxide laser frequency stabilization

7.1 Introduction:

Carbon dioxide lasers have been frequency stabilized in many different ways. Some examples have already been given in Chapter 1. In this chapter, which is dedicated to active frequency stabilization of a conventional carbon dioxide laser, it is shown that the OA method can be used in a similar fashion to that of the OG technique for laser frequency stabilization. In the following sections passive as well as active stabilization methods will be considered together with a discussion of the sources of frequency instabilities in the laser system. At the end of the chapter a review of the results will be presented.

7.2 Sources of instabilities in the laser system:

Drift of the laser frequency can occur as a result of changes of the environment in which the laser operates, to defects in laser construction and the laser medium itself. Many of these effects arise in connection with laser construction, as discussed in Chapter 3. In this section attention is given to the most troublesome sources of frequency drift and where possible a rough estimation of the expected drift will be given. A frequency instability of 1 part in 10^7 can be the direct result of simple constructional defects, which for example send part of the radiation back into the resonator as a result of unwanted reflection from surfaces within the laser cavity (Rowley and Wilson 1972). This can make the stabilization process difficult by giving rise to a signal in a different phase resulting in the control system having a tendency to pull the laser frequency out of lock. Proper mounting of the optical components usually

solves this problem. In the following, the relations used by Wallard (1973) will be used to calculate the ratio $\Delta\nu/\nu$, where $\Delta\nu$ is the change of frequency and ν the frequency of the line centre. This quantity gives a measure of frequency pulling of the CO_2 laser resulting from different effects. These can be categorized as follows:

(1) **Cavity length variation as a result of thermal effects.**

The resonance frequency of the cavity is given by

$$\nu_q = \frac{q_c}{2nL} \tag{7.1}$$

where c is the speed of light, q is an integer that represents the mode order, n is the refractive index of the medium and L is the cavity length. From the above relation it is easily seen that

$$\frac{\Delta\nu}{\nu} = \frac{\Delta L}{L} = \alpha\,\Delta T \tag{7.2}$$

where α is the linear thermal expansion of the material determining the length of the cavity and ΔT is the temperature change. Assuming a net length change of 0.1 μm in the laser cavity studied in this thesis, of length ~1.8 m, then $\Delta\nu/\nu = 5.5 \times 10^{-8}$. If the laser is oscillating on the CO_2 line $P_{(20)}$ of the $(00^01 - 10^00)$ branch, the laser frequency will be of the order 28,306,251 MHz (Schiffner 1972), so $\Delta\nu$ = 1.6 MHz. If a temperature change of 0.1^oC is assumed and taking $\alpha = 1.26 \times 10^{-6}\ {}^oC^{-1}$ for Invar, then $\Delta\nu \sim 3.6$ MHz.

(2) **Effects that occur in the gap between Brewster window and grating.**

In some lasers, as in the system studied here, a space is left between the grating and the Brewster window. As this is open to the atmosphere, it is subject to atmospheric change such as temperature (ΔT), pressure (ΔP) and humidity (Δh). In the case of temperature changes

$$\left(\frac{\Delta\nu}{\nu}\right)_T = (X)\, B_T\, \Delta T \qquad (7.3)$$

where X is the fraction of the length between window and grating to that of the cavity length, which for the system in question is ~ 0.06. The constant $B_T = 9.3 \times 10^{-7}\ {}^{o}C^{-1}$ so $\Delta\nu \sim 0.2$ MHz for $\Delta T \sim 0.1^{o}C$. Taking $B_p = -3.6 \times 10^{-7}\ \text{torr}^{-1}$ and assuming 0.5 torr change, substitution of these values in eqn. (7.3) and replacing ΔT by ΔP gives $\Delta\nu = -0.3$ MHz. The effect of the final parameter, humidity, can be calculated using

$$(\Delta\nu/\nu)_h = XB_h\, \Delta h \qquad (7.4)$$

$B_h = 5.7 \times 10^{-8}\ \text{torr}^{-1}$; in this case Δh, can be used in torr. Assuming a pressure change of 0.1 torr, then eqn. (7.4) gives $\Delta\nu = 9.6$ kHz. From the above it is concluded that draughts can cause frequency instabilities of several MHz. To overcome such a problem the laser is covered and in addition, the distance between window and grating is reduced to the minimum possible (see Fig. 7.1B which shows the effects of draughts).

(3) **Mechanical Vibrations.**

Mechanical vibrations can cause a severe perturbation of the laser frequency of a magnitude depending on their strength. Frequency fluctuations can be estimated using the following relation:

$$-\left(\frac{\Delta\nu}{\nu}\right) = \left(\frac{\Delta L}{L}\right) = \left(\frac{2kT}{yV}\right) \qquad (7.5)$$

where k is Boltzmann's constant, T the temperature, V the volume of the material determining the length of the laser cavity (e.g. Invar rods) and y is Young's modulus of that material, which is equal to $1.44 \times 10^{11}\ \text{Nm}^{-2}$ for Invar rods. This effect gives a very small frequency drift for temperature changes of $\pm 1^{o}C$. Vibrations can result from vibrations of the building, and laboratory equipment (e.g. pumps) also has some effect

in this respect (White 1965). Acoustic vibrations contribute to frequency drift to some extent, by a factor of 10 less than laboratory vibrations (Nagai 1972).

(4) **Variation in optical component position.**

Another source of frequency drift is the position of optical components. Rotation of plane mirrors around an axis perpendicular to the optical axis of the cavity produces a larger frequency shift than with rotation of spherical mirrors (Nagai 1972). The change that results from Brewster window angle change is given as follows (Wallard 1973):

$$\left(\frac{\Delta\nu}{\nu}\right) = -t/L \sin\theta \qquad (7.6)$$

where t is the Brewster window thickness and θ is the Brester window angle. Any change in the Brewster window angle can be disastrous. For example in the system studied here the window thickness is 4 mm, $\theta = 22.3^{o}$, L = 180 cm which gives $\Delta\nu$ = -7.5 MHz for a change of 0.001^{o}.

(5) **Miscellaneous.**

Current variations, plasma oscillations and change in the flow of the coolant liquid will also lead to frequency drifts. Pressure changes can cause power variations up to several percent of the total laser power.

In the system researched in this thesis, passive stabilization is achieved using massive invar rods 2.5 cm in diameter, 2 m long. Since the cavity is shorter in waveguide lasers, it is convenient to use a material with a smaller thermal expansion coefficient than invar. For the waveguide laser, quartz tubes with $\alpha = 0.5 \times 10^{-6}\ {}^{o}C^{-1}$ are used. Vibration is eliminated by a simple inexpensive method as suggested by White (1965) and Wallard (1973) in which inflated car tyre inner tubes are topped with a wooden platform upon which the laser rests. A simple test of the effectiveness of passive stabilization in the system investigated was

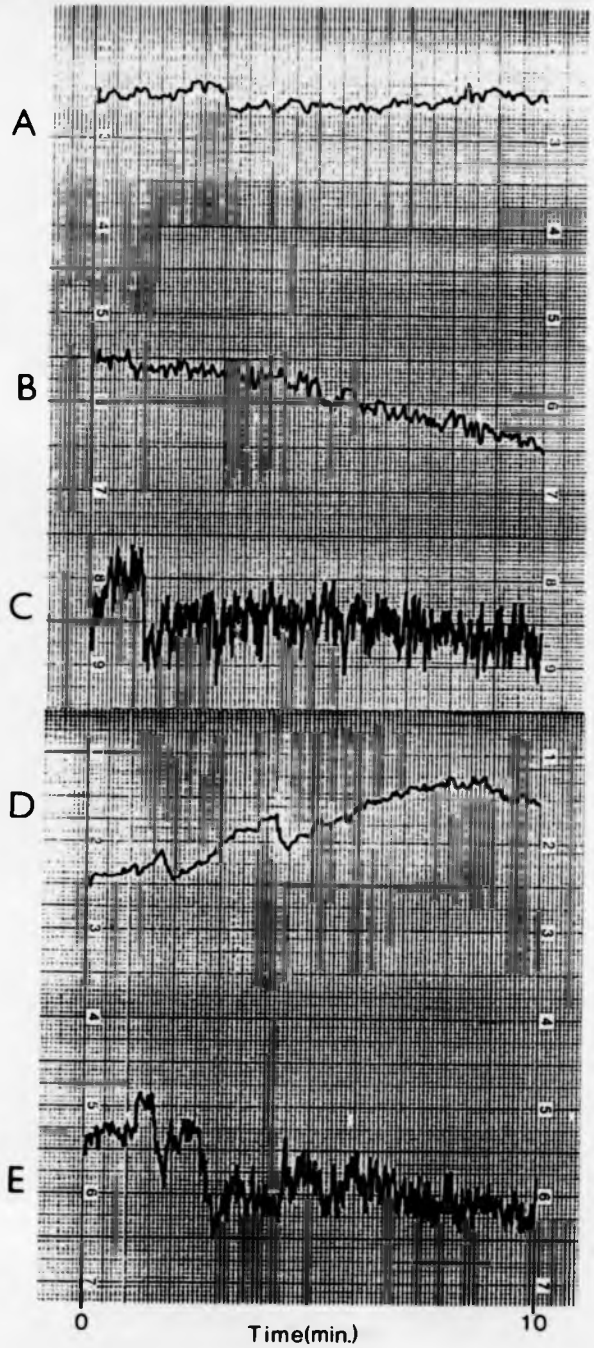

Fig. 7.1 : Investigation of sources of power instabilities under the following conditions: (A) Vibration and draught isolation; (B) Laboratory ventilator on; (C) Laser cover off; (D) Inflated tyres removed; (E) With all instability sources acting simultaneously.
Each cm represents ~11% of the total laser power.

carried out, and the results are shown in Fig. 7.1. After half an hour of warm up time, the laser power variation without stabilization was recorded with vibration isolation and laser cover on. Then a ventilator fan was operated to act as a source of vibration (but little draught as the laser cover was left on) and the frequency variations were found to be bigger. The cover then lifted off whereupon the level of frequency variation was found to increase still further. The level of frequency variation was estimated by the percentage change of the laser power from its peak value relative to its half power value on either side of the gaussian curve of width ~150 MHz at gas pressure of 20 torr. To inspect the effect of vibration, the inflated tyres were removed and trace 7.1D was obtained which showed up to 20% change as a result of frequency shift. Then the effect of all perturbations acting together was investigated (i.e. draught and vibrations) with long term drift caused amplitude fluctuations as large as 30%. The rapid vibrations caused by draughts showed itself clearly on the laser oscillation amplitude trace as shown in Fig. 7.1E. It is concluded that proper vibration and draught isolation can reduce the power variation enormously.

7.3 OG frequency stabilization - previous work:

The first step towards frequency stabilization is the attainment of single longitudinal and transverse mode operation. The laser design, discussed in Section 3.2, should take care of that. Single longitudinal mode operation can be achieved by choosing the length of the laser so that the mode separation is larger than the transition linewidth (Massig 1977). Higher order transverse modes can be discriminated against by proper selection of the laser tube diameter and introducing an iris into the laser cavity. What remains to be done to achieve single mode frequency stabilization then depends on the detection of a signal referenced to the

laser frequency. This signal, which arises through frequency modulation of the laser by applying an a.c. voltage to the piezo-electric tube placed against the laser mirror is synchronously detected and fed into a high voltage amplifier, which then amplifies it to a level of a few hundred volts. This d.c. voltage should be sufficient to derive the PZT tube carrying the laser mirror to compensate for any cavity length changes, thereby restoring the laser frequency to its original value through seeking the null signal.

Suppose the laser emission line centre frequency is (ν_c) and the laser oscillation frequency is shifted to ν'. The correction signal accordingly brings the laser frequency to ν'' which lies between ν' and ν_c, and very close to ν_c. This is where an integrator is important in applying a steady voltage proportional to the error signal. The ratio $(\nu'-\nu_c)/(\nu''-\nu_c)$ is a measure of the system effectiveness in correcting the frequency variations (Shotton and Rowley 1975). However any system to be suitable must be efficient in producing the laser frequency reference signal with the shortest possible response time (Wallard 1973). Many units have been constructed for CO_2 laser stabilization and will be presented here as examples, rather than as tested units in this work. A complete system including modulator and PSD has been designed by Shotton et al. (1975) (see Fig. 7.2). A special system for stabilization of Sylvania Model 948 CO_2 laser was developed by Thomson et al. (1975) and is shown in Fig. 7.3. This system has the disadvantage of low voltage amplification which makes it unsuitable for insensitive PZT tubes. Fig. 7.4 shows a very simple and inexpensive circuit as used by Lund et al. (1979).

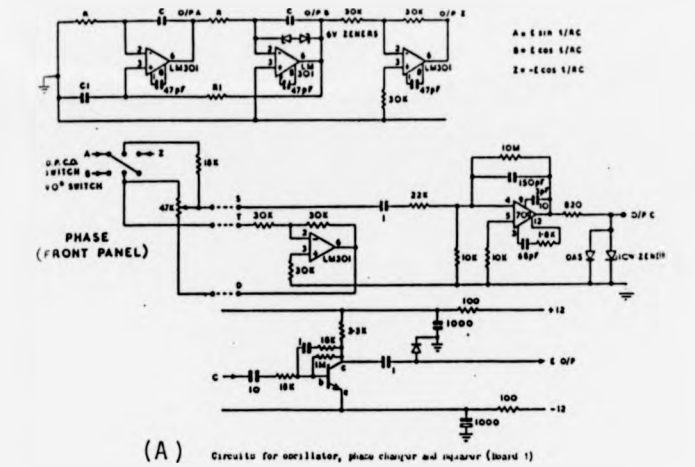

(A) Circuits for oscillator, phase changer and squarer (Board 1)

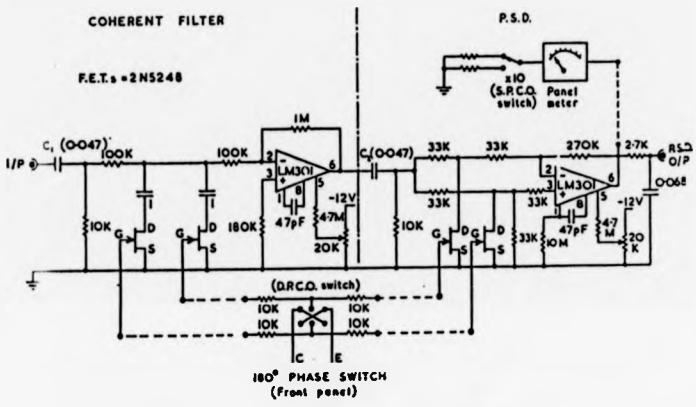

(B) Circuits for coherent filter and PSD (Board 2)

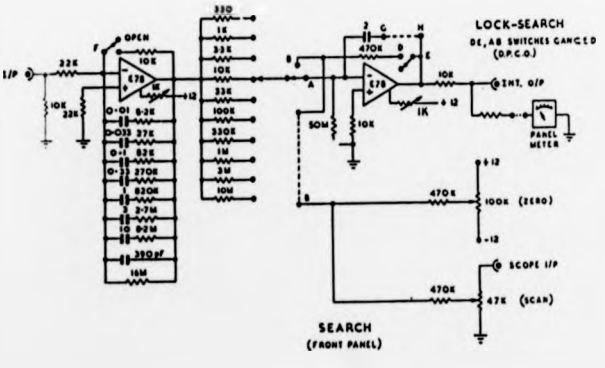

(C) Circuits for 3 dB per octave filter and integrator (Board 3)

Fig. 7.2 : The full stabilization system including (A) Oscillator phase changer and squarer; (B) Coherent filter and PSD; (C) 3 dB per octave filter and integrator. Reproduced from Shotton et al. (1975).

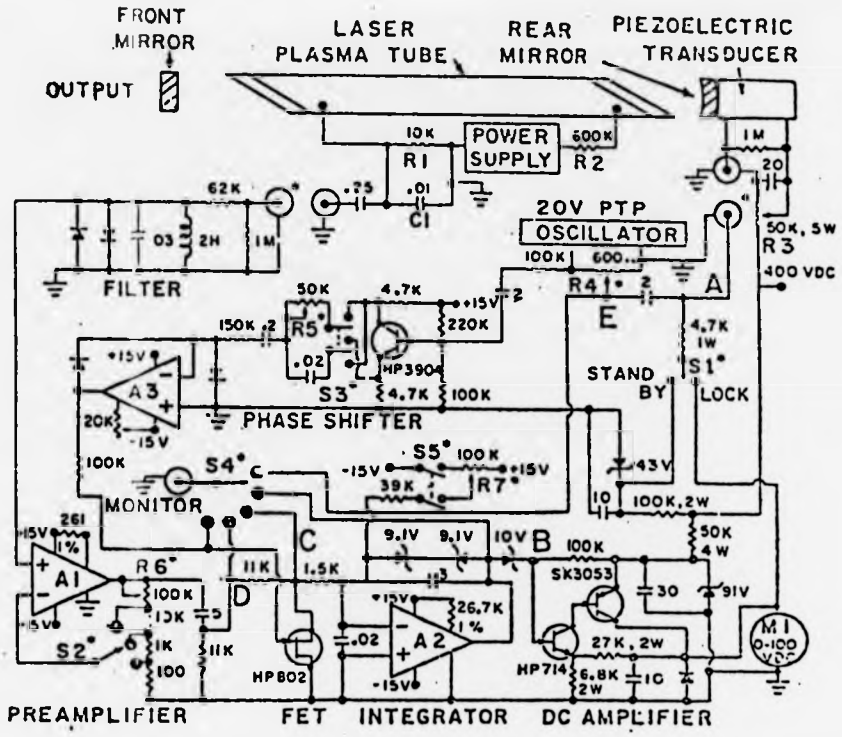

Fig. 7.3 : Full frequency stabilizing system used for Sylvania Model 948 CO_2 laser stabilization.
Reproduced from Thomson et al. (1975).

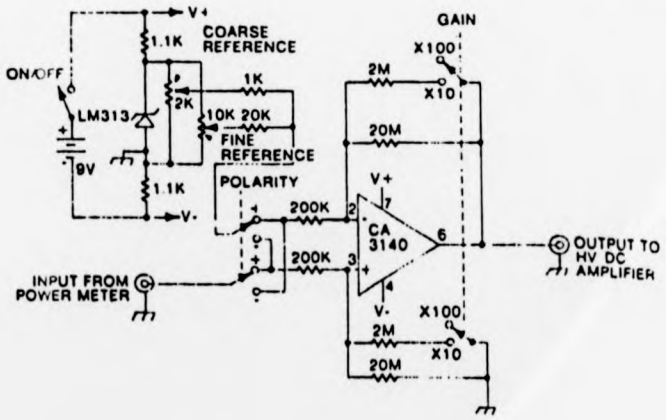

Fig. 7.4 : An interface circuit for CO_2 laser stabilization.
Reproduced from Lund et al. (1979).

7.4 The system of OA and OG stabilization

In the work described here a system has been designed for frequency stabilization with both OA and OG methods. The signal, whether OG or OA, is detected using a PSD unit and fed into an interface unit (see Fig. 7.5), constructed to act as an amplifier of the signals obtained from the PSD. The interface unit (circuit obtained from the Physics Department, University of Nijmegen, Holland, 1986) provides an output that is restricted to 10 volts which is the maximum input to the high voltage amplifier (Physik Instrumente, Model 265), and has an amplification factor of 100. It is also possible to get a constant d.c. voltage reference signal which is useful for frequency stabilization off line centre. The high voltage is then fed to the PZT tube to establish the necessary correction of the cavity length. The complete system of stabilization is shown in Fig. 7.6.

To stabilize the laser the following procedure is followed:

(1) An a.c. voltage is applied to the PZT tube, part of which (~ 0.5 V) is applied to the PSD reference signal input. The PSD gain is adjusted and a signal is obtained with a positive or negative polarity that depends upon which side of the central frequency the laser is oscillating. If the laser oscillates at the centre frequency of the emission line, the feedback signal is zero (see Figs. 6.10 and 6.11).

(2) The modulation frequency is then adjusted for the best detection conditions as discussed in Chapter 6.

(3) The PSD phase is then changed 0^{o} to 90^{o} to check that the signal can be swung positive-zero-negative. This ensures that the possibility of frequency correction on both sides of the central frequency can be achieved.

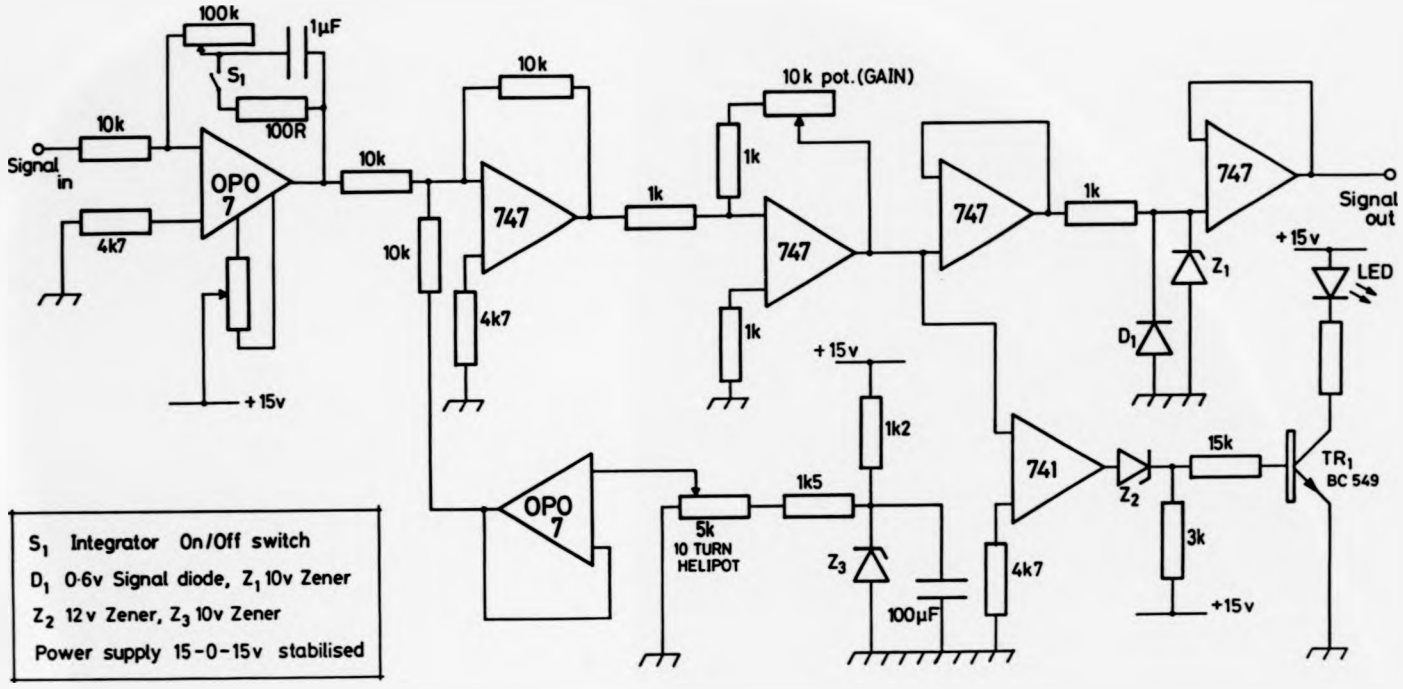

Fig. 7.5 : Interface unit circuit used in this work for CO_2 laser stabilization.

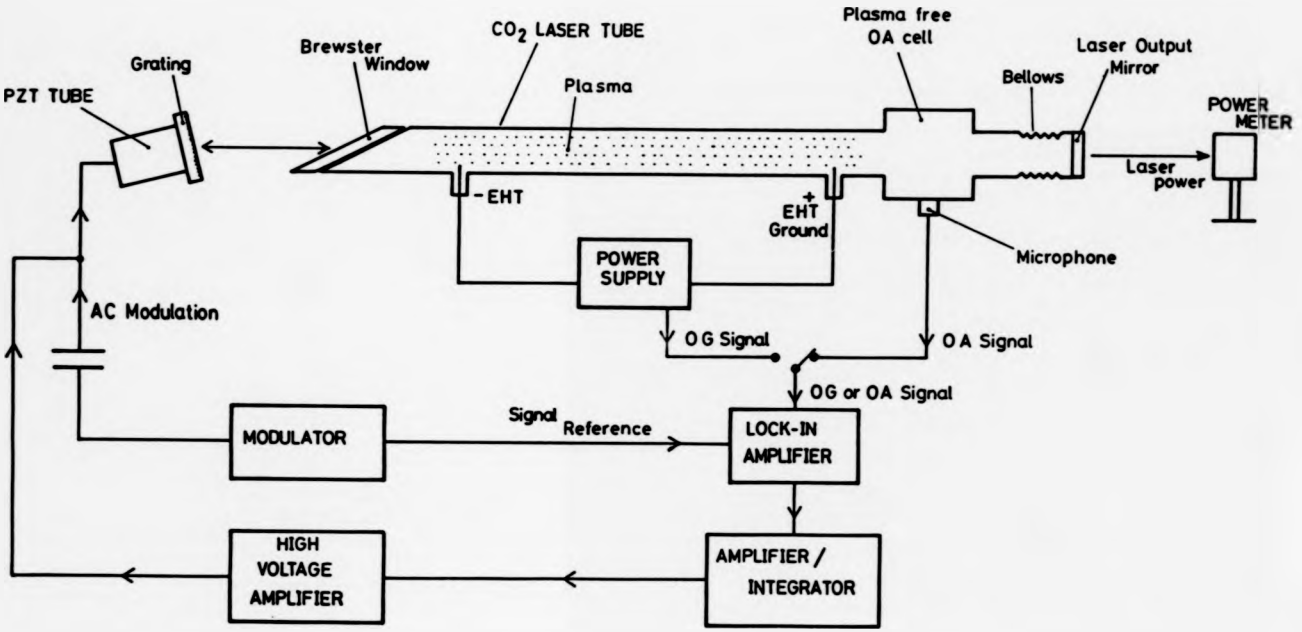

Fig. 7.6 : Scheme of frequency stabilization used for both OG and OA methods.

(4) The PSD output is then connected to the interface unit input. The high voltage amplifier output is also connected to the PZT tube.

(5) The feedback loop gain value is confirmed as being sufficient by slowly increasing or decreasing the high voltage correction signal applied to the PZT tube until a small signal is registered by the PSD meter. The PSD phase reference is reversed so as to check that the error signal correction is always towards zero. The phase finally chosen is the one that reduces the error signal. The interface unit output is then connected to the high voltage amplifier to increase or decrease the voltage applied to the PZT bringing the error signal back to zero. If this does not occur the gain should be increased until the condition is satisfied. If the pointer crosses to the opposite polarity when the loop is closed the gain should be reduced.

(6) To stabilize at the laser line centre frequency the high voltage amplifier is adjusted manually until the error signal is zero with the interface unit disconnected. The feedback loop is then closed by reconnection of the interface unit. To stabilize off-line centre, the high voltage amplifier is manually adjusted to shift the laser frequency to the required value and the loop is again closed. This can also be achieved by applying a constant reference d.c. voltage from the interface unit to the high voltage amplifier.

7.5 Experimental results:

The feedback loop was closed and frequency stabilization was achieved using either OA or OG. The laser power was monitored with a sensitive thermocouple power meter. When the laser oscillates at the peak frequency the power meter gives an output signal indicated by its meter and a pen recorder provides a visual trace which can be inspected at leisure. If the laser frequency is reduced the power reading should

follow the change by a drop in its value. It will similarly be reduced when the laser frequency increases to $(\nu_c + \Delta\nu)$. If CO_2 laser lines are assumed to be pressure broadened to ~70 MHz, then the percentage fluctuation in the power value can be used as an indication of frequency instability. For example, a fluctuation of ± 1.5% of the amplitude of laser power would mean a frequency instability of ± 1 MHz. This method of assessment is used in the present work. Other methods of stabilization assessment were not available at the time of the experiment. These can include mixing of two laser beams on metal-insulator-metal diode or on a fast pyro-electric detector with frequency sensitivity of few MHz. By tracking the beat frequency of the two adjacent beams from the two lasers it is possible to estimate the frequency drift of the stabilized laser under examination.

An example of both OG and OA stabilization methods is shown in Fig. 7.7. The frequency of the piezo modulation was 430 Hz with modulation voltages in the range 40 - 60 V peak-to-peak. This modulation corresponded to a length modulation of 0.026 - 0.039 μm respectively or a frequency modulation depth of 0.4 - 0.6 MHz. The PSD time constant could have been smaller in the case of OA stabilization as the signals were less noisy: 30 ms, 0.1 s were used for OA and OG stabilization methods respectively. Fig. 7.8 shows an example of stabilization performed with a piezo voltage modulation of 40 V peak-to-peak.

7.6 Discussion

It has been shown that the OA method of stabilization is, on the basis of results to date, superior to the well known OG method. A power stability of 0.2% - 1% had previously been achieved with the OG method (Smith et al. 1979). In the work described in this thesis a similar figure was obtained with both the OG and OA methods (see Fig. 7.7).

With the system studied here it is concluded that the OA stabilization has more control over the long term drift on account of its improved signal to noise over OG stabilization. Thus the use of OA stabilization permits the use of smaller time constants. From Fig. 7.8 where stabilization is performed at 40 VPP, it is noted that OG stabilization does not hold for very long periods of time before it starts drifting. Since the OA signal is highly dependent on laser power absorption at the frequency of the absorbing CO_2 gas, it can be said that the OA method is fully frequency sensitive. This is clearly advantageous for laser frequency stabilization. In contrast, the OG method derives its frequency sensitivity not only from the gas resonance but also from the variation of laser impedance which can be affected by many parameters, including the formation and neutralization of ions and laser tube wall temperature. Thus the OG method is much more subject to drift and diverse fluctuation in comparison with the OA approach. In conclusion, the OA frequency stabilization method as an alternative method for laser stabilization is most promising.

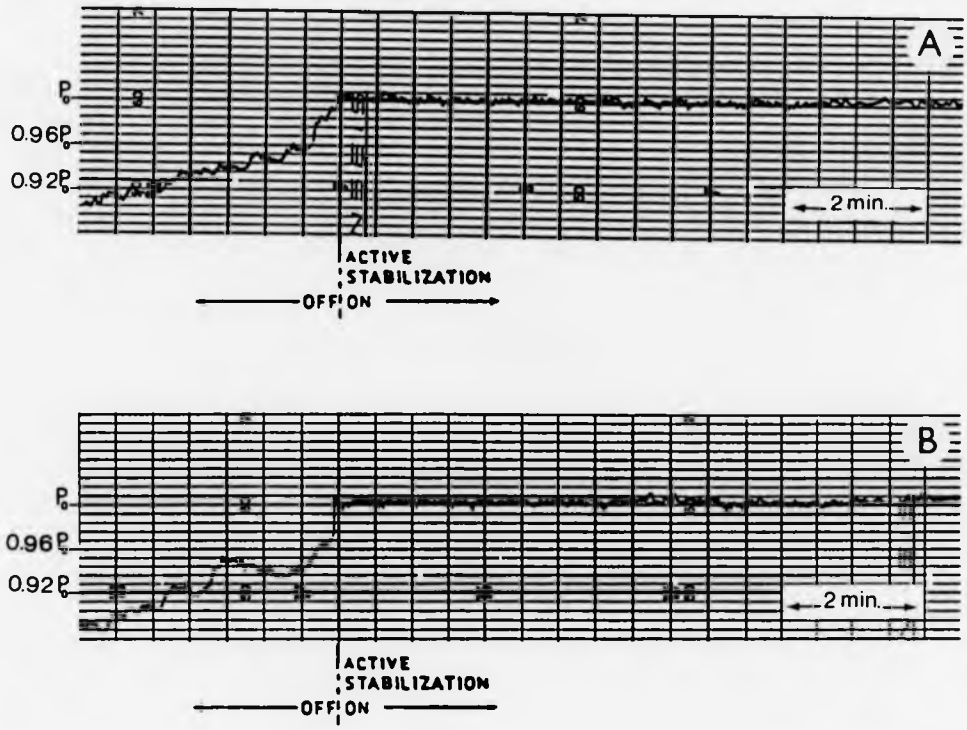

Fig. 7.7 : Examples of optoacoustic and optogalvanic stabilization taken at a modulation voltage ~60 VPP, modulation frequency ~420 Hz.

(A) OA stabilization with PSD time constant of 30 ms.

(B) OG stabilization with PSD time constant of 100 ms.

P_o is the maximum laser power at 8 W.

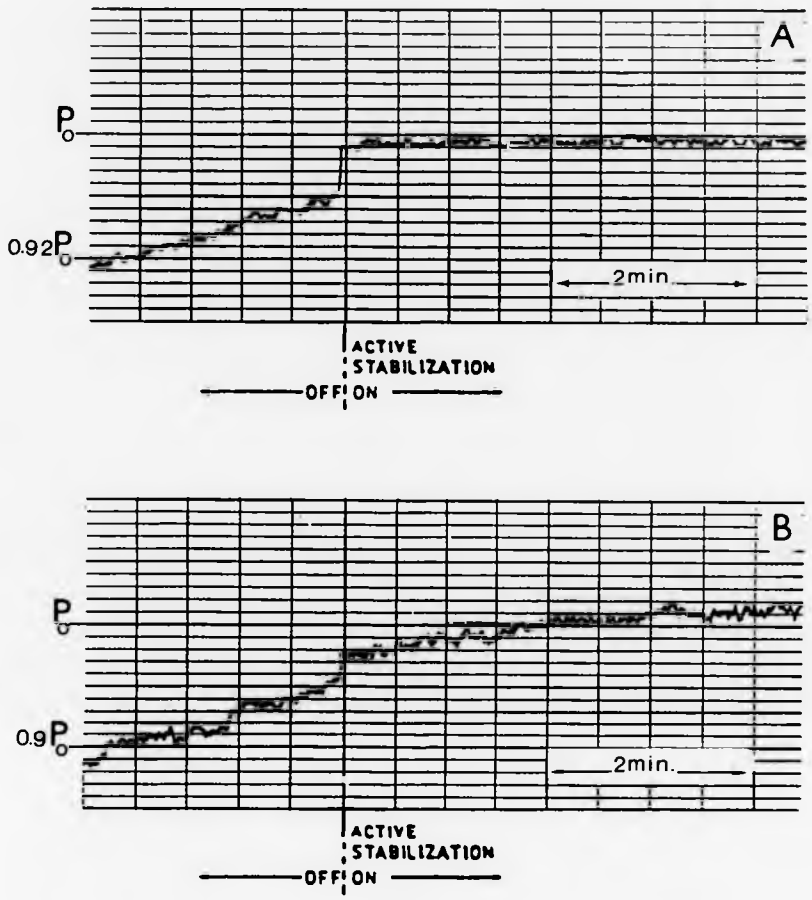

Fig. 7.8 : Examples of OA and OG stabilization taken with piezo modulation of 40 VPP at 420 Hz.
(A) OA stabilization with a PSD time constant of 30 ms.
(B) OG stabilization with a PSD time constant of 100 ms.
P_o is the maximum laser power at 8 W.

Chapter 8

Conclusions and further work

It was demonstrated in the previous chapter that the optoacoustic method for frequency stabilization of a CO_2 laser is at least as sensitive as and even superior to the optogalvanic technique. Both approaches share the properties of being simple, inexpensive, sensitive and compact with no added optical components and associated alignment problems. Since the gas discharge is run at high d.c. voltages, plasma fluctuations and electrical noise is expected to be picked up in the OG method. In addition, supply harmonics and mains transients add to low noise signal detection problems. The OG signals are even affected by the pressure fluctuations of the cooling water for the laser tube resulting in signals not directly related to laser frequency changes. These problems do not arise for the OA signal. Hence it is possible to detect the OA signals with a smaller time constant and low levels of cavity tuning piezo modulation voltage. This has the advantage of low noise and fast control over stabilization and avoids spectral broadening of the laser oscillation as a direct result of the small range of frequency modulation. However, the OA method does have some problems of its own. The first problem is concerned with the laser modulation process. It is difficult to modulate the longitudinal position of the mirror in contact with the gas without the mechanical generation of a sound wave which can be detected by the microphone. The solution is to modulate the position of the mechanically isolated grating by a piezo instead. The second problem is concerned with the microphone lifetime in a flow laser system such as used in the work reported in this thesis. It was found that the microphone sensitivity decayed due to pressure cycling

of a conventional laser tube, as a result of repeated evacuation and gas filling on a day to day basis. This results in over-stretching of the microphone diaphragm. This problem is not expected to appear in sealed-off lasers. It was possible to use the microphone for at least two months with an average of three hours work per day before its sensitivity started to decay. This is not a major problem and it might be eliminated by having a more rugged crystal microphone or even other detection techniques (West et al. 1983) such as a thermistor, to monitor temperature changes in the cell directly. In conclusion the OA and OG signals share many characteristics and properties. However the OA method has the advantage over OG in that it is better in terms of signal to noise ratio.

For the completion of this work a lot more needs to be done to gain a better understanding of the OA laser signals. For example, resonant cell OA operation could be used for laser stabilization and then compared with the results of a non-resonant cell, as reported in this thesis. However, it would be difficult to excite the radial modes because of their high frequency values (see Section 5.4.2). Since the highest percentage in the gas mix is He gas, the velocity of propagation of sound in the laser medium is high, which places a limit on the lower resonant frequency of the OA cell. Different gas mixes could be studied taking into account cell and laser performance. The OA cell in this case could also be used to study the effect of different gases on the relaxation times of laser levels. The OA signals usually get stronger at lower temperatures which might be useful to control the cell temperature, or to study the OA behaviour.

Optoacoustic detection in a waveguide laser should be as successful as for a conventional laser. Preliminary attempts to apply the OA method to such a laser were faced with some problems. These are noted here for the benefit of future studies. Arcing from the laser electrode across to

the nearby microphone usually resulted in the destruction of the latter. Clearly it is very important that the electrode near the microphone is earthed. The discharge should be extremely stable, otherwise the OA signals will be very noisy. In the present work an A.L.E. ballastless double discharge supply model 30 KV DFH with negative polarity centre electrode is used. Audible signals from 'hot spots' on the laser electrodes have been obtained. These are picked up by the microphone as intermittent interference. Cleaning the electrodes, reducing the distance between the electrode and its associated hole drilled in the waveguide wall, or changing pressure and current have not so far overcome this problem. It is clearly necessary to eliminate this source of noise in OA detection of power in a waveguide laser, or else frequency stabilization with the method will not be possible.

Since the microphone in the conventional laser is approximately 10 cm from the laser anode, it would be of interest to place the microphone very close to the anode and compare the results with that obtained by Arimondo et al. (1984) concerning the existence of a critical discharge current for which the OA signal is zero. The only difference of the present experiment from that of Arimondo et al. is that in the latter work the distance between the microphone and discharge anode is very short.

Other techniques could also be applied to CO_2 laser stabilization using the OA method. For example Kavaya et al. (1983) used a second harmonic detected from an external OA cell to stabilize the laser away from the line centre without electronic offset. This idea can also be employed in the internal cell suggested in this work. Optoacoustic tracking of an SF_6 Lamb dip has been suggested by Souilhac et al. (1982) for CO_2 laser stabilization in an external cell. It is possible that the same approach can be used for intra OA frequency stabilization by the addition of a very small trace of SF_6, since Souilhac et al. (1982) claim

Lamb dip detection at a pressure of 20 torr in SF_6 gas. The addition of a trace gas to the laser mixture at a concentration insufficient to harm laser performance can be used in principle to stabilize the laser with enhanced performance at the absorption line resonances of the added gas. In this case the stabilized laser could be most useful for pollution studies of the same trace gas. (The possibility also exists of trace gas analysis by adding the sample under study to the laser gas mixture.) Moreover if the trace gas has a narrower pressure broadened spectral line than for CO_2, frequency stabilization will be further improved when the OA method is applied.

OA detection using Stark modulation (Kavaya et al. 1979) can be incorporated in the OA cell of the frequency stabilization system described in this thesis by the addition of a pair of parallel metallic plates to serve as Stark electrodes. If this method were to be successful, OA frequency stabilization could be achieved without frequency modulation of the laser beam which is clearly advantageous, since the coherence length of the laser would be improved. A preliminary trial was not successful. This was because a large electric field is required for the Stark cell, which for an electrode separation sufficient to avoid laser beam diffraction, the applied voltages were such as to cause electrical breakdown. If this problem could be overcome, the OA method of frequency stabilization would be improved further.

A bright prospect for the future is the implementation of the OA method for frequency stabilization of r.f. excited CO_2 lasers. Problems of discharge noise vanish for the OA technique since there is no electrical connection to the discharge region. This extension of the OA frequency control method is a particularly important one and offers much promise for the future.

References

Abrams A., Appl. Phys. Lett. 25, 304 (1974).

Abrams R., IEEE J. Quant. Electron. QE-8, 838 (1972).

A.L.E. Systems Inc., 150 Homer Avenue, Ashland, MA 01721, U.S.A.

Arimondo E., Vito M., Ernst K. and Inguscio M., Opt. Lett. 9, 530 (1984).

Bell A., Am. J. Sci. 20, 305 (1980).

Beverini N., Galli M., Inguscio M., Strumia F. and Bionducci G., Opt. Commun. 43, 261 (1982).

Bloom A., "Gas Lasers" [John Wiley and Sons Inc., 1968, U.S.A.].

Bordé Ch., Avrillier S., Lerberghe A., Salmon Ch., Bassi D. and Scoles G., "Third Symposium on Frequency Standards and Metrology", Colloque C8, Suppl. No.12, Vol.42, 15 (1981).

Boscolo I., Passaseo A. and Bernardini P., Infrared Phys. 26, 287 (1986).

Boyd G. and Kogelink H., Bell Syst. Tech. J., 41, 1347 (1962).

Bridges T., Burkhardt E. and Smith P., Appl. Phys. Lett. 20, 403 (1972).

Bridges T. and Chester A., Appl. Opt. 4, 573 (1965A).

Bridges T. and Patel C., Appl. Phys. Lett. 7, 244 (1965B).

Bridges T. and Patel C., Appl. Phys. Lett. 7, 21 (1965C).

Brooks Information Sheet (1984) [Brooks Instrument Division, Stuart Road Bredbury, Stockport SK6 2SR, U.K.]

Bruce C., Sojika B., Hurd B., Watkins W., White K. and Derzko Z., Appl. Opt. 15, 2970 (1976).

Busse G., Basel E. and Pfaller A., Appl. Phys. 12, 387 (1977).

Carswell A. and Wood J., J. Appl. Phys. 38, 3028 (1967).

Carter G. and Marcus S., Appl. Phys. Lett. 35, 129 (1979).

Clairon A., Lerberghe A., Breant C., Salmon C., Camy G. and Bordé C., "Third Symposium on Frequency Standards and Metrology", Colloque C8 Suppl. No. 12, Vol. 42, 127 (1981).

Claspy P., In "Optoacoustic Spectroscopy and Detection", Y-.H Pao (Ed.) [Academic Press, N.Y. 1977] pp.(133-166).

Crafer R., Gibson A., Kent M. and Kimmit M., Brit. J. Appl. Phys. Ser.(2) No.12, 183 (1969).

Crocker D., Clack C. and Butcher R., J. Phys. E : Sci. Instrum. 14, 121 (1981).

Deaton T., Depatie D. and Walker T., Appl. Phys. Lett. 26, 800 (1975).

Degnan J., Appl. Opt. 12, 1026 (1973).

Degnan J., Appl. Phys. 11, 1 (1976).

Degnan J. and Hall D., IEEE. J. Quantum Electron. QE-9, 901 (1973).

Dewey C.Jr., Kamm R. and Hackett C., Appl. Phys. Lett. 23, 633 (1973).

Doughty D. and Lawler J., Phys. Rev. A28, 773 (1983).

Duley W., "CO_2 Lasers; Effects and Applications", [Academic Press, London and N.Y. 1976].

EG and G Princeton Applied Research, PO Box 2565, Princeton. NJ 08540.

Edinburgh Instruments Ltd., Riccarton, Currie, Edinburgh, EH14 4AP.

Erez G., Lavi S. and Miron E., IEEE J. Quant. Electron. QE-15, 1328 (1979).

Fahlen T., Appl. Opt. 12, 2381 (1973).

Freed C., Bradley L. and O'Donnell R., IEEE J. Quant. Electron. QE-16, 1195 (1980).

Freed C. and Javan A., Appl. Phys. Lett. 17, 53 (1970).

Gould G., Appl. Opt. Suppl. II, 59 (1965).

Goldan P. and Goto K., J. Appl. Phys. 45, 4350 (1974).

Goldberg M. and Yusek R., Appl. Phys. Lett. 18, 135 (1971).

Goldsmith J. and Lawler J., Contemp. Phys. 22, 235 (1981).

Goldsmith J., Ferguson A., Lawler J. and Schawlow A., Opt. Lett. 4, 230 (1979).

Goldsborough J., In "Laser Handbook", Vol.1, F. Arecchi and E. Schultz (Eds.), [North Holland Publishing Company, Holland, 1972] p.598.

Green R., Keller R., Luther G., Schenck P. and Travis J., Appl. Phys. Lett. 29, 727 (1976).

Hall D., In "Laser, Advances and Applications", B.S. Wherrett (Ed.) [Proc. National Quantum Electronic Conference, 1979, Wiley (1980), U.K.] pp.(19-24).

Hall D., Gorton E. and Jenkins R., J. Appl. Phys. 48, 1212 (1977).

Hall D., Jenkins R. and Gorton E., J. Phys. D: Appl. Phys. 11, 859 (1978).

Hameau C., Arimondo E., Wascat J. and Glorieux P., Opt. Commun. 53, 375 (1985).

Hard T., Appl. Opt. 9, 1825 (1970).

Herzberg G., "Infrared and Raman Spectra", [van Nostrand, 1945, U.S.A.].

Hochuli V. and Sciacca T.Jr., IEEE J. Quant. Electron. QE-10, 239 (1974).

Hocker L., Kovacs M., Rodes C., Flynn C. and Javan A., Phys. Rev. Lett. 17, 233 (1966).

Hocker L., Sokoloff D., Daneu V., Szoke A. and Javan A., Appl. Phys. Lett. 12, 401 (1968).

Hotz D. and Austin J., Appl. Phys. Lett. 11, 60 (1967).

Howe J., Appl. Phys. Lett. 7, 21 (1965).

Ioli N., Maruzzi G. and Strumia F., Lett. Nuovo Cimento Vol.28, Ser.2, 257 (1980).

Kaiser R., Can. J. Phys. 37, 1499 (1959).

Kanstad S. and Nordal P., Phys. Technol. 11, 143 (1980).

Kavaya M., Margolis J. and Shumate M., Appl. Opt. 18, 2602 (1979).

Kavaya M., Menzies R. and Oppenheim U., IEEE J. Quant. Electron. QE-18, 19 (1982).

Kavaya M., Menzies R. and Oppenheim U., IEEE J. Quant. Electron. QE-19, 1234 (1983).

Keller R., Engleman R.Jr. and Zalewski E., J. Opt. Soc. Am. 69, 738 (1979).

Kerr E. and Atwood J., Appl. Opt. 7, 915 (1968).

King D. and Schenck P., Laser Focus, March (1978), p.50.

King D., Schenck P., Smyth K. and Travis J., Appl. Opt. 16, 2617 (1977).

Klimcak C. and Gelbwachs J., Appl. Opt. 24, 247 (1985).

Kompanets O., Kukudzhanov A., Letokhov V. and Michailov E., [Proc. 2nd Freq. Stand. Metro. Symposium, p.167, July 1976].

Kreuzer L., In "Optoacoustic Spectroscopy and Detection", Y-.H Pao (Ed.) [Academic Press, N.Y. 1977] pp.(1-25).

Kunikane T., Ohtsu M., Nakamura T. and Tako T., Jap. J. Appl. Phys. 23, 600 (1984).

Lawler J., Phys. Rev. A22, 1025 (1980).

Lawler J., Ferguson A., Goldsmith J., Jackson D. and Schawlow A., Phys. Rev. Lett. 42, 1046 (1979).

Lehmann K., Scherer G. and Klemperer W., J. Chem. Phys. 77, 2853 (1982).

Lengyel B., "Introduction to Lasers", [John Wiley 1971, U.S.A.].

Li T., Bell Syst. Tech. J. 45, 917 (1965).

Lobov G., Shtykov V., Bogatkin V. and Drugov V., Radio Eng. Electron. Phys. 17, 968 (1972).

Louis G., Lepoutre F. and Monchalin J., Can. J. Phys. 64, 1111 (1986).

Lund M., Cogan T. and Davis J., Rev. Sci. Instrum. 50, 971 (1979).

Lyszyk M., Herlemont F. and Lemair J., J. Phys. E : Sci, Instrum. 10, 1110 (1977).

Manes K. and Seguin H., J. Appl. Phys. 43, 5073 (1972).

Marcatili E. and Schmeltzer R., Bell Syst. Tech. J. 43, 1783 (1964).

Massig J., IEEE J. Quant. Electron. QE-13, 29 (1977).

Mingozzi P. and Tonelli M., J. Phys. E : Sci. Instrum. 10, 775 (1977).

Moeller G. and Rigden J., Appl. Phys. Lett. 7, 274 (1965).

Moeller G. and Rigden J., Appl. Phys. Lett. 8, 69 (1966).

Moffatt S. and Smith A., In "Lasers, Advances and Applications", B. Wherrett (Ed.), [Proc. Nat. Quantum Electron Conference 1979 (Wiley 1980, U.K.)] pp.(31-34).

Moffatt S. and Smith A., Opt. Commun. 37, 119 (1981).

Moffatt S. and Smith A., J. Phys. D : Appl. Phys. 17, 59 (1984).

Morse P., "Vibration and Sound" [McGraw-Hill, N.Y. 1948].

Muenchausen R., May R. and Hills G., Opt. Commun. 48, 317 (1984).

Nagai H., IEEE J. Quant. Electron. QE-8, 857 (1972).

Nowicki R. and Pienkoswki J., J. Phys. D : Appl. Phys. 15, 1165 (1982).

Nussmeir T. and Abrams R., Appl. Phys. Lett. 25, 615 (1974).

Okajima S., Yamanaka M., Nishizawa A., Makino S., Kondo M., Kon S. and Fujita J., Infrared Phys. 25, 569 (1985).

Olson H., "Elements of Acoustical Engineering", [van Nostrand, Reinhold, Princeton, N.Y. 1947] pp.(220-224).

Oriel Corp., 250 Long Beach Blvd., Stratford, CT 05497.

Ouhayoun M. and Bordé C., Metrologia 13, 149 (1977).

Papayoanou A., IEEE J. Quant. Electron. QE-13, 27 (1977).

Patel B., Ph.D. Thesis, Essex University (1971).

Patel C., Phys. Rev. Lett. 12, 588 (1964A).

Patel C., Phys. Rev. Lett. 13, 617 (1964B).

Patel C., Appl. Phys. Lett. 7, 15 (1965).

Patel C., Scient. Amer. August (1968) p.23.

Patel C., Tien P. and Mcfee T., Appl. Phys. Lett. 7, 290 (1965).

Penning F., Physica 8, 137 (1928).

Pepper D., IEEE J. Quant. Electron. 14, 971 (1971).

Physik Instrumente (PI) GmbH and Co., Siemensstrasse, D-7517, Waldbronn, West Germany.

Rettner C., Webster C. and Zare R., J. Phys. Chem. 85, 1105 (1981).

Rigden J. and Moeller G., IEEE J. Quant. Electron. QE-2, 365 (1966).

Rigrod W., J. Appl. Phys. 36, 2487 (1965).

Rosencwaig A., "Photoacoustics and photoacoustic spectroscopy", [John Wiley and Sons. N.Y. 1980].

Rosengren L., Max E. and Eng S., J. Phys. E : Sci. Instrum. 7, 125 (1974).

Rowley W. and Wilson D., Appl. Opt. 11, 475 (1972).

Sanderson R. and Streifer W., Appl. Opt. 8, 2241 (1969).

Sasnet M., "Lasers and Applications", Sept. 1984, p.85.

Sawartini T. and Kapany N., J. Opt. Soc. Am. 60, 132 (1970).

Schiffner G., IEEE J. Quant. Electron. QE-8, 877 (1972).

Scott M. and Myers G., Appl. Opt. 23, 2874 (1984).

Shanahan S. and Heckenberg N., J. Phys. E : Sci. Instrum. 17, 640 (1984).

Shotton K. and Rowley W., NPL. Rep. QU-28, (1975).

Shtrikman S. and Slatkine M., Appl. Phys. Lett. 31, 830 (1977).

Shy J-T. and Yen T-C., Opt. Commun. 60, 306 (1986).

Sinclair D., Appl. Opt. 3, 1067 (1964).

Skolnick M., IEEE J. Quant. Electron. QE-6, 139 (1970).

Smith A., Phys. Lett. A27, 432 (1968).

Smith A., Brit. J. Appl. Phys.: J. Phys. D. 2, 1129 (1969).

Smith A. and Brooks M., J. Phys. D: Appl. Phys. 12, 1237 (1979A).

Smith A. and Browne P., J. Phys. D: Appl. Phys. 7, 1652 (1974).

Smith A. and Moffatt S., Opt. Commun. 30, 213 (1979B).

Smith A. and Moffatt S., J. Phys. D: Appl. Phys. 17, 71 (1984).

Smith A., Shield H. and Webb A., IEEE J. Quant. Electron. QE-19, 815 (1983).

Smith P., Appl. Phys. Lett. 19, 132 (1971).

Snitzer E., J. Opt. Soc. Am. 51, 491 (1961).

Sofonea V. and Popescu I., Opt. Commun. 60, 302 (1986).

Souilhac D. and Gundjian A., Appl. Opt. 21, 1478 (1982).

Sobolev N. and Sokovikov V., Sov. Phys. USP. 10, 153 (1967).

Suzuki T., Jap. J. Appl. Phys. 9, 588 (1970).

Suzuki T., Opt. Commun. 38, 364 (1981).

Taylor F., Lombart A. and Eppers W., Appl. Phys. Lett. 11, 180 (1967).

Taylor R. and Bitterman S., Rev. Mod. Phys. 41, 26 (1969).

Thiebeux K., Delahaigue A., Courtois D. and Jouve P., Infrared Phys. 21, 41 (1981).

Thomas F., Horigan D. and Rudko R., Appl. Phys. Lett. 15, 88 (1969).

Thomason W. and Elbers D., Rev. Sci. Instrum. 46, 409 (1975)

Turk G., Travis J., Devoe J. and O'Haver T., Anal. Chem. 50, 817 (1978).

Tychinskii V., Sov. Phys. USP. 10, 131 (1967).

Tyte D., J. Phys. E.: Sci. Instrum. 3, 734 (1970).

University of Nijmegen, Holland, private communication.

Vasudev R. and Zare R., J. Chem. Phys. 76, 5267 (1982).

Wallard A., J. Phys. E: Sci. Instrum. 6, 793 (1973).

Walsh C., J. Phys. D: Appl. Phys. 18, 787 (1985).

Walsh C. and Brown N, Rev. Sci. Instrum. 56, 1582 (1985).

Webster C. and Menzies R., J. Chem. Phys. 78, 2121 (1983A).

Webster C. and Rettner C., Laser Focus, Feb. 1983B, p.41.

West G., Barrett J., Seibert D. and Reddy, K., Rev. Sci. Instrum. 54, 797 (1983).

Willetts D. and Harwright C., J. Phys. D: Appl. Phys. 11, 111 (1978).

Witteman W., IEEE J. Quant. Electron. QE-2, 375 (1966).

White A., IEEE. J. Quant. Electron. QE-1, 349 (1965).

White A. and Gordon E., Appl. Phys. Lett. 3, 197 (1963).

Woods P. and Jolliffe B., J. Phys. E: Sci. Instrum. 9, 395 (1976).

Zalewski E., Keller R. and Apel C., Appl. Opt. 20, 1584 (1981).